UNIVERSITÀ
DEGLI STUDI
DI PADOVA

Sede Amministrativa: Università degli Studi di Padova

Dipartimento di *Ingegneria Industriale*

SCUOLA DI DOTTORATO DI RICERCA IN: Ingegneria Industriale
INDIRIZZO: Ingegneria dell'Energia
CICLO: XXVI

EXPERIMENTAL CHARACTERIZATION OF NANOFLUIDS AS HEAT TRANSFER MEDIA

Direttore della Scuola: Ch.mo Prof. Paolo Colombo
Coordinatore d'indirizzo: Ch.mo Prof. Luisa Rossetto
Supervisore: Prof. Claudio Zilio

Dottorando: Laura Colla

EXPERIMENTAL CHARACTERIZATION OF NANOFLUIDS AS HEAT TRANSFER MEDIA

Contents

Chapter 1

Introduction

Several solutions have been proposed to enhance the thermal performance of the heat transfer devices. The most common technique consists in maximizing the heat transfer area in heat exchangers, and, at the moment, it seems no further improvement could be achieved. Another possibility could be given by increasing the heat transfer coefficient that, for an imposed flux, depends on the thermal properties of the fluid. Aiming to improve the characteristics of the traditional working fluids (as water, glycol, oil and refrigerants), a new generation of thermal vectors, called *nanofluids*, has been proposed. Nanofluids are suspensions of nano-sized solid particles (1-200 nm) in liquids. These new suspensions may be utilized in several applications, *i.e.* engine cooling, engine transmission oil, cooling electronics, refrigeration, drilling, lubrications, thermal storage, solar water heating etc. [1].

1.1 Thesis objectives and outline

The objective of this work is the analysis of the nanofluids behaviour, with the purpose to apply these new fluids in energy, mechanical and tribological fields.

Different nanoparticles can be prepared with different methods and also different nanofluids derive from different preparation techniques. A description of the most common methods is provided in the next chapter. The stability of the suspension will be evaluated considering the mean size distribution of nanoparticles in suspension, the ζ potential end the pH of the nanofluids.

The following chapter is dedicated to the description of the experimental apparatus for the measurements of thermal conductivity and dynamic viscosity of nanofluids. In that chapter, instruments and procedures are explained in detail.

The convective heat transfer will be considered in chapter 4. Here the description of a specifically built experimental apparatus is provided.

Chapters from 5 to 12 relate to nanofluids characterization. Nine nanofluids have been studied at different mass fractions and different temperatures, in order to evaluate whether it is convenient to replace the base fluids. For almost all the nanofluids, firstly, the stability was evaluated, and then their properties were measured, considering the variation on thermal conductivity and dynamic viscosity when adding nanoparticles and when changing temperature. For the most promising nanofluids heat transfer measurements were performed.

In the last chapter a final comment on the potentiality of studied nanofluids will be made, relating to the properties here investigated.

1.2 Background and literature review

Nanofluids have been introduced by Steve Choi of Argonne's Energy Technology Division and Jeff Eastman of the Materials Science Division on Argonne National Laboratory in 1995 [2].

It is well known thermal conductivity of solids is order of magnitude higher than that of common liquids. The idea of increasing the conductivity of fluids by mixing solid particles dates back to 1873 [3]. The first attempt to insert particles of micrometric size showed several problems, including abrasion, obstruction of channels and settling of the particles. Modern nanotechnology provides the opportunity to produce nanoparticles, which remain in suspension almost indefinitely, under certain conditions.

Nanoparticles move under Brownian motion, which is the random motion of particles suspended in a fluid resulting from their collision with the quick atoms or molecules in the gas or liquid. The direction of the force of atomic bombardment is constantly changing, and at different times, the particle is hit more on one side than another, leading to the seemingly random nature of the motion.

Brownian motion is a stochastic (or probabilistic) processes and it is a limit of both simpler and more complicated stochastic processes. It is closely linked to the normal distribution.

In the last years, an exponential increase of publications on nanofluid is occurred. As analyzed in Buschmann 2013 [4], the number of publications layer has been considered to compare its trend, from 2000 to 2012, in the field of nanofluids, heat transfer, turbulence and turbulent boundary, as shown in Figure 1.1. Normalization is carried out taking 2011 values as reference, which are 485 publications for nanofluids, 8950 for heat transfer, 5918 for turbulence and 1036 for turbulent boundary layer. The exponential increase of publications for nanofluid is clearly visible.

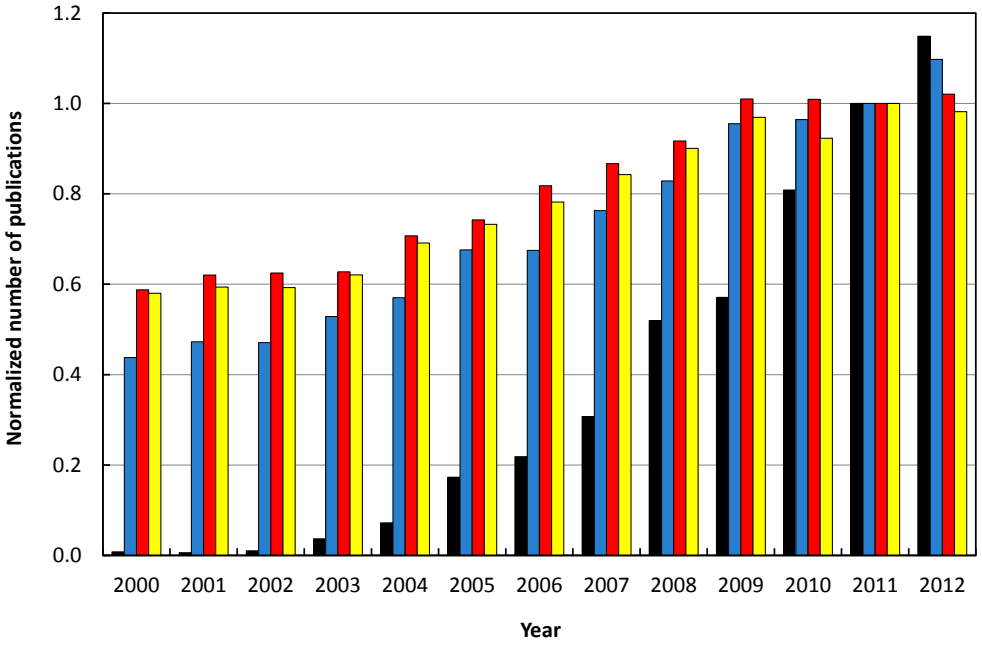

Figure 1.1: Normalized number of publications, from 2000 and 2012, in the fields of ■ nanofluids, ■ heat transfer, ■ turbulence and ■ turbulent boundary layer. Normalization is carried out taking 2011 values as reference. Data taken at 25-09-2013 from ISI WEB of KNOWLEDGE.

Two main methods are used to prepare stable nanofluids, *i.e.* the single-step method and the two-steps method. The single-step method implies the synthesis of nanoparticles directly into the fluid. Tuning the synthesis parameters and adding some chelating agents, a good control of the particles nucleation and growth can be obtained. The two-step method consists in the dispersion of previously obtained nanopowders in a fluid. Physical treatments (ultrasonication, mechanical mixing, etc.) are used to disperse the nanoparticles and chemical additives (surfactants or tensioactives) and to avoid particles aggregation, which is a common problem of nanopowders, due to their high surface reactivity. Generally, single-step method permits to avoid the dispersion and the mixing steps, ensuring a better control over particles size and dispersion than the two-steps route.

Dispersion methods and chemical synthesis can still be done in different ways. Therefore, it is very difficult to obtain the same nanofluid in two different laboratories if the procedure is not planned exactly in the same mode. For this reason, a comparison between nanofluids is very difficult to execute.

Thermal conductivity is the most studied property for nanofluids. In literature, many works have been published on the influence of temperature, concentration, shape and size of nanoparticles or use of surfactants on the thermal conductivity of nanofluids. In general, the conductivity of nanofluids is higher than that of the base fluid [5-10], but in some papers different results have been published [11,12]. It should be noted that small nanoparticles have large surface to volume ratio, providing higher thermal conductivity to nanofluid than that of conventional heat transfer fluids. However, the heat transfer mechanism in nanofluids is not completely understood, since some contradictions have been found in literature, as in [13], where large particles seam to improve thermal conductivity respect to smaller ones. Many parameters are affecting the thermal conductivity of nanofluids and for this reason models must be supported by experimental data.

However, the addition of nanoparticles in the conventional fluids affects the dynamic viscosity of the nanofluid and could penalize the pressure drop in a pumping flow system. Literature models can not accurately predict this property and nanofluids behaviour is not always Newtonian, since, over a certain concentration of nanoparticles and dispersant, the nanofluid behaviour could become non-Newtonian. For these reasons, it is fundamental to measure the nanofluids dynamic viscosity.

On the contrary, density and heat capacity of nanofluids can be generally calculated as weighted averages, knowing the properties of base fluid and nanoparticle material.

In order to obtain higher energy efficiency, better devices performance and lower operating costs, the study of the heat transfer coefficient of nanofluids is very promising. Many works relate to heat transfer enhancement using nanofluids. Numerous studies have shown that heat transfer of nanofluids is higher than that of base fluids [14-16]. However, contradictory results on nanofluids behaviour have been also reported. For example, Pak and Cho [17] results showed that the Nusselt number of alumina–water and titania–water nanofluids increased with increasing Reynolds number in turbulent flow and increasing the volume concentration. However, they found that the convective heat transfer coefficient of the nanofluids with 3 vol% nanoparticles was 12% smaller than that of pure water at a given condition.

Nanofluids are complex fluids, they can be obtained using different methods of preparation, different amount of nanoparticles of different material and morphology. Experiments should be carried out in order to investigate properties of each interesting new nanofluid.

1.2.1 Why nanofluids are studied

Nanofluids attract scientific community and industries for their potentiality in improving properties of the base fluid, such as heat transfer capability. The general expectation is that the higher thermal conductivity of the solid particles leads to an effectively increased thermal conductivity which in turn should enhances heat transfer. Several papers have been published showing a considerable increase of the heat transfer coefficient relative to the base fluids. Enhancements of up to 60% in the thermal conductivity of water-based nanofluids were found in the literature [18, 19]. However, many publications indicate controversial results.

Moreover, new and innovative strategies to save, transfer and store thermal energy involve nanofluids.

1.2.2 Uses of nanofluids

Nanotechnology offers an extremely broad range of potential applications from electronics to new materials. Many possible applications have been explored and many devices and systems have been studied. In particular, many are the potential uses for nanofluids in heat transfer applications. Nanofluids are considered as potential working fluids to be used in high heat flux systems such as electronic cooling systems, solar applications [20], heat pipes, and nuclear reactors. As secondary fluids, they can be applied in commercial refrigeration, chiller, solar panels in absorption systems.

The use of nanofluids as working fluids in the refrigeration systems is truly considered in the recent years. Many investigations have been proposed on nanoparticles used in both the refrigerant and in the lubricant oil of a vapour compression system [21-24]. Nanofluids could also be employed in chillers exploiting their enhanced cooling capacity with respect to the base fluids [25].

As nanolubricants, they can improve thermal dissipation, anti-wear and extreme pressure properties of compressors lubricants. The dispersion of nanoparticles directly in the refrigerant can improve the thermodynamic performance of refrigerating machines.

Moreover, adding nanoparticles to lubricants can significantly improve, beyond their thermal properties, also their tribological properties, with benefits to the life cycle of machines with moving parts (*i.e.* refrigeration compressors).

Nanofluids can be used for a wide variety of industries, ranging from transportation to energy production and in electronics systems like microprocessors, Micro-Electro-Mechanical Systems (MEMS) and in the field of biotechnology. Other applications are in the

fields of drilling, cooling of welding, defence, space, high-power lasers, biomedical applications, drag reductions and so forth.

Several studies have been done to search suitable nanofluids to be used in high heat flux systems such as electronic cooling systems, solar collectors, heat pipes, and nuclear reactors to reduce the peak temperatures on the cooled wall, generate uniform temperature distributions, and assure better compactness of heat transfer systems without or with less pumping power increases penalty, as described in [26].

1.2.3 Challenges of nanofluids

It is interesting to note that the applications of nanotechnology in different fields have distinctly different demands, and thus face very different challenges. For the fabrication and processing of nanomaterials, some challenges must to be met: overcome the huge surface energy, a result of enormous surface area or large surface to volume ratio; ensure all nanomaterial with desired size, uniform size distribution, morphology, chemical composition and microstructure, that altogether result in desired physical properties.

Challenges also arise in the lack of agreement of results obtained by different researchers and in the lack of theoretical understanding of the mechanisms responsible for changes in properties. The characterization of suspensions is still poor and the stability of nanoparticles dispersion must to be better analysed.

Other challenges include high cost of nanofluids and difficulties in production process.

1.2.4 Open questions on nanofluids

Much remains unknown about nanoparticles. Materials made from nanoparticles differ from their larger counterparts. Different branches of science must collaborate to the study of nanofluids, because it requires skills in different fields.

Despite an exponential increase in experimental and theoretical investigations on nanofluids, a lot of research is still needed to fully understand their behaviour. A big issue concerns the production of stable and reliable fluids, by developing more suitable methods of production and nanoparticles dispersion. Experimental data are still scarce for some properties (*e.g.* viscosity and heat transfer coefficient) and frequently incongruent among the various laboratory. Much higher repeatability must be achieved. The influence of size, shape, concentration and material of nanoparticles from both the experimental and theoretical point of view must be deeply explored. Moreover, the application of nanofluids to industrial systems require experimental tests on real plants to evaluate long term behaviour of

nanofluids in terms of stability, wearing, material compatibility, energy efficiency, fouling *etc*.

References

[1] R. Saidur, K.Y. Leong, H.A. Mohammad, "A review on applications and challenges of nanofluids", *Renewable and Sustainable Energy Reviews*, 15, 3, 1646–1668 (2011).

[2] S.U.S. Choi, J.A. Eastman, "Enhancing thermal conductivity of fluids with nanoparticles", *ASME International Mechanical Engineering Congress & Exposition*, November 12-17, 1995, San Francisco, CA.

[3] J.C. Maxwell, *Electricity and Magnetism*, 1st Ed., Clarendon Press, Oxford, England, (1873).

[4] M.H. Buschmann, "Nanofluisd in thermosyphons and heat pipe: Overview of recent experiments and modeling approaches", *International Journal of Thermal Sciences*, 1-17 (2013).

[5] S.M. Abbasi, A. Rashidi, A. Nemati, K. Arzani, "The effect of functionalisation method on the stability and the thermal conductivity of nanofluid hybrids of carbon nanotubes/gamma alumina", *Ceramics International*, 39, 3885-3891 (2013).

[6] A. Nasiri, M. Shariaty-Niasar, A. M. Rashidi, R. Khodafarin, "Effect of CNT structures on thermal conductivity and stability of nanofluid", *International Journal of Heat and Mass Transfer*, 55, 1529–1535 (2012).

[7] S. K. Das, N. Putra, P. Thiesen, W. Roetzel, "Temperature dependence of thermal conductivity enhancement for nanofluids", *Journal of Heat Transfer*, 125, 4, 567-574 (2003).

[8] S.M.S. Murshed, K.C. Leong, C. Yang, "Enhanced thermal conductivity of TiO_2-water based nanofluids", *International Journal of Thermal Sciences*, 44, 4, 367-373 (2005).

[9] R. Prasher, P. Bhattacharya, P.E. Phelan, "Thermal conductivity of nanoscale colloidal solutions (nanofluids)", *Physical Review Letters*, 94, 2, 25901 (2005).

[10] T.K. Hong, H.S. Yang, C.J. Choi, "Study of the enhanced thermal conductivity of Fe nanofluids", *Journal of Applied Physics*, 97, 6, 064311 (2005).

[11] J. Buongiorno, D. Venerus, N. Prabhat, T. McKrell, J. Townsend, R. Christianson, Y. Tolmachev, P. Keblinski, L. Hu, J. Alvarado, I. Bang, S. Bishnoi, M. Bonetti, F. Botz, A. Cecere, Y. Chang, G. Chen, H. Chen, S. Chung, M. Chyu, S. Das, R. Di Paola, Y. Ding, F. Dubois, G. Dzido, J. Eapen, W. Escher, D. Funfschilling, Q. Galand, J. Gao, P. Gharagozloo, K. Goodson, J. Gutierrez, H. Hong, M. Horton, K. Hwang, C. Iorio, S. Jang, A. Jarzebski, Y. Jiang, L. Jin, S. Kabelac, A. Kamath, M. Kedzierski, L. Kieng, C. Kim, J. Kim, S. Kim, S. Lee, K. Leong, I. Manna, B. Michel, R. Ni, H. Patel, J. Philip, D. Poulikakos, C. Reynaud, R. Savino, P. Singh, P. Song, T. Sundararajan, E. Timofeeva, T. Tritcak, A. Turanov, S. Van Vaerenbergh, D. Wen, S. Witharana, C. Yang, W. Yeh, X. Zhao, S. Zhou, "A benchmark study on the thermal conductivity of nanofluids", *Journal of Applied Physics*, 106, 094312 (2009).

[12] A.T. Utomo, H. Poth, P.T. Robbins, A.W. Pacek, "Experimental and theoretical studies of thermal conductivity, viscosity and heat transfer coefficient of titania and alumina nanofluids", *International Journal of Heat and Mass Transfer*, 55, 7772-7781 (2012).

[13] P. Warrier, A. Teja, "Effect of particle size on the thermal conductivity of nanofluids containing metallic nanoparticles", *Nanoscale Research Letters*, 6, 247 (2011).

[14] P. Garg, J.L. Alvarado, C. Marsh, T.A. Carlso, D.A. Kessler, K. Annamalai, "An experimental study on the effect of ultrasonication on viscosity and heat transfer performance of multi-wall carbon nanotube-based aqueous nanofluids", *International Journal of Heat and Mass Transfer*, 52, 5090-5101 (2009).

[15] V. Kumaresan, S. Mohaideen Abdul Khader, S. Karthikeyan, R. Velraj, "Convective heat transfer characteristics of CNT nanofluids in a tubular heat exchanger of various lengths for energy efficient cooling/heating system", *International Journal of Heat and Mass Transfer*, 60, 413-421 (2013).

[16] M.M. Heyhat, F. Kowsary, A.M. Rashidi, M.H. Momenpour, A. Amrollahi, "Experimental investigation of laminar convective heat transfer and pressure drop of water-based Al_2O_3 nanofluids in fully developed flow regime", *Experimental Thermal and Fluid Science*, 44 483-489 (2013).

[17] B.C. Pak, Y.I. Cho, "Hydrodynamic and heat transfer study of dispersed fluids with submicron metallic oxide particles", *Experimental Heat Transfer*, 11, 2, 151–170, (1998).

[18] P. Keblinski, R. Prasher, J. Eapen, "Thermal conductance of nanofluids: is the controversy over?", *Journal of Nanoparticles Research*, 10, 1089 (2008).

[19] W. Yu, D.M. France, J.L. Routbort, S.U.S. Choi "Review and Comparison of Nanofluid Thermal Conductivity and Heat Transfer Enhancements", *Heat Transfer Engineering*, 29, 432 (2008).

[20] H. Tyagi, P.E. Phelan, R.S. Prasher, "Predicted efficiency of a nanofluid-based direct absorption solar receiver", *ASME 2007 energy sustainability conference*, 729-736 (2007).

[21] E.V. Clancy, *United States Patent Application Publication*, Pub. No. US 2012/0017614 A1 (2012).

[22] J.U. Ahamed, R. Saidur, H.H. Masjuki, "A review on exergy analysis of vapor compression refrigeration system", *Renewable and Sustainable Energy Reviews*, 15, 3, 1593-1600 (2011).

[23] D.S. Kumar, R. Elansezhian "Experimental Study on Al2O3-R134a Nano Refrigerant in Refrigeration System", *International Journal of Modern Engineering Research*, 2, 5, 3927-3929 (2012).

[24] C.G. Lee, S.W. Cho, Y. Hwang, J.K. Lee, B.C. Lee, J.S. Park, J.S. Jung, "Effects of nanolubricants on the friction and wear characteristics at thrurst slide bearing of scroll compressor", *International Proceeding of the 22nd International Congress of Refrigeration*, Bejijng (China) (2007).

[25] S. Wu, D. Zhu, X. Li, H. Li, J. Lei, "Thermal energy storage behavior of Al_2O_3–H_2O nanofluids", *Thermochimica Acta*, 483, 73-77 (2009).

[26] J.M. Wu, J. Zhao, "A review of nanofluid heat transfer and critical heat flux enhancement-Research gap to engineering application", *Progress in Nuclear Energy*, 66, 13-24 (2013).

Chapter 2

Preparation and characterization of nanofluids

Nanoparticles are extremely interesting because the physical behaviour of the materials is different at nanometer scale compared to larger scales, and then the thermal, optical, mechanical, electrical and magnetic properties are often superior to those of bulk materials. The main parameter that determines these special properties is the high surface to volume ratio of nanoparticles. In the follow chapter, an investigation on the common method of preparation of nanoparticles and nanofluids is provided. In addition, nanofluids stability characterization is presented.

2.1 How to prepare nanoparticles

One nanometer is approximately the length equivalent to 10 hydrogen or 5 silicon atoms aligned in a line. Small features permit more functionality in a given space, but nanotechnology is not only a simple continuation of miniaturization from micronmeter scale to nanometer scale. Materials in the micrometer scale mostly exhibit physical properties the same as that of bulk form, while materials in the nanometer scale may exhibit physical properties distinctively different from that bulk. In general, nanotechnology can be considered as a technology for the design, fabrication and applications of nanostructures and nanomaterials. Many technologies have been explored to fabricate nanoparticles. The following are some of the most frequently used methods.

High-energy **ball milling** is one nanofabrication process of mayor industrial importance. It is a physical method also known as mechanical attrition or mechanical alloying. Coarse-grained materials in the form of powders are crushed mechanically in rotating drums by hard steel or tungsten carbide balls, usually under controlled atmospheric conditions to prevent unwanted reactions such as oxidation. This technique can be operated at a large scale and therefore it can be employed in industrial fields.

Chemical synthesis may be carried out in either the solid, liquid or gaseous state. In solid-state synthesis, solid reaction precursors are brought into intimate contact by mixing and grinding. Then heat treatment at high temperatures promotes atomic diffusion processes to form a reaction product. Liquid-state and gas-state synthesis can be implemented in much lower temperatures, thus unwanted grain growth can be inhibited and the result is a true nanoscale system. In fact, diffusion in the liquid and gas phases is typically many orders of magnitude greater than in the solid phase.

Vapour phase deposition can be used to fabricate thin films, multilayers, nanotubes, nanofilaments or nanometer-sized particles.

The general techniques can be classified in **physical vapour deposition** (PVD) or **chemical vapour deposition** (CVD).

In **PVD,** solid materials are converted into a gaseous phase by physical processes. Then, solid materials are cooled and re-deposited on a substrate. Examples of PVD conversion processes include **thermal evaporation** (such as resistive or electron beam heating or even flame synthesis), **laser ablation** or **pulsed laser deposition** (where a short nanosecond pulse from a laser is focused on the surface of a bulk target), **spark erosion** and **sputtering** (the removal of a target material by bombardment with atoms or ions).

CVD involves the reaction or thermal decomposition of gas phase species at elevated temperatures (typically 500−1000°C) and subsequent deposition on a substrate. Several CVD processes employ catalysts to enhance the rates of certain chemical reactions.

The use of plasmas (*i.e*., ionized gases) during vapour deposition allow access to substantially different chemical and physical processes and also higher-purity final materials relative to the conventional PVD and CVD processes described above. There are several different types of plasma deposition reactor for plasma-assisted PVD (**DC glow discharge**, **magnetron sputtering**, **vacuum arc deposition**).

A variant of many of the PVD processes described above are thermal spraying techniques, in which a spray of molten or semi-molten solid particles generated by either an electrical thermal source (*e.g*., plasma spraying) or by chemical combustion (*e.g*., flame spraying or high-velocity oxygen fuel spraying) are deposited on a substrate and undergo rapid solidification. This is extensively used to produce nanocrystalline powder, wire or rod feedstocks, previously fabricated by the mechanical milling or precipitation routes.

Sol-gel methods involve a set of chemical reactions which irreversibly convert a homogeneous solution of molecular reactant precursor (a sol) into an infinite molecular weight three-dimensional polymer (a gel) forming an elastic solid filling the same volume as

the solution. Typically, this involves a hydrolysis reaction followed by condensation polymerization.

Electrochemical deposition, also known as electrodeposition, is a special electrolysis resulting in the deposition of solid material on an electrode. Electrochemical deposition is widely used in making metallic coatings, then the process is also known as electroplating. When deposition is confined inside the pores of template membranes, nanocomposites are produced. If the template is removed, nanorods or nanowires are prepared.

2.1.1 Carbon structures

Carbon is a particular material that can be a good metallic conductor in the form of graphite, a wide band gap semiconductor in form of diamond, or a polymer when bonded with hydrogen. Carbon provides examples of materials covering the entire range of nanometer scaled structures from fullerenes, which are zero-dimensional nanoparticles, to carbon nanotubes, one-dimensional nanowires to graphite, a two-dimensional layered anisotropic material, to solid fullerene, a three-dimensional bulk materials with the fullerene molecules as the fundamental building block of the crystalline phase.

Carbon fullerene commonly refers to a molecule with 60 carbon atoms, C_{60}, as shown in Figure 2.1, and with an icosahedral symmetry, but also includes larger molecular fullerenes C_n (n>60).

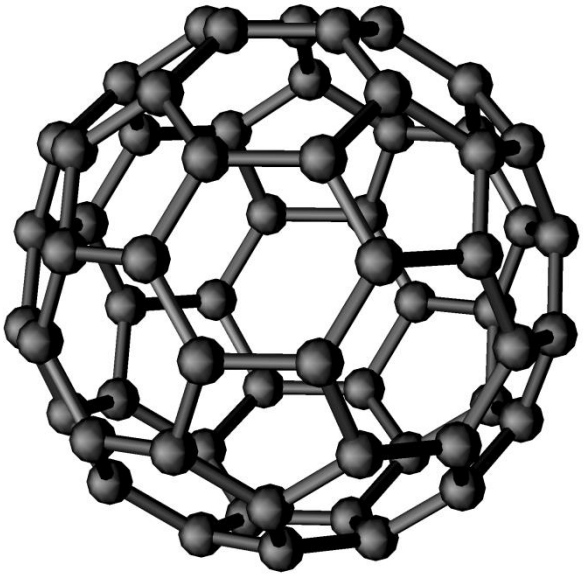

Figure 2.1: Fullerene C_{60}.

A nanotube is a variation of fullerene that has become elongated in its structural patterning due to its molecular arrangements. Nanotubes are extremely strong and cannot be broken. The only way to destroy them is to break a bond at the molecular scale.

They can be considered as the result of folding graphite layers into carbon cylinders and may be composed of a single shell–single wall nanotubes (SWNTs), or of several shells—multi-wall nanotubes (MWNTs). Depending on the folding angle and the diameter, nanotubes can be metallic or semiconducting.

Carbon nanotubes can be prepared by arc evaporation [1], laser ablation [2], pyrolysis [3] and electrochemical methods [4,5]. Carbon nanotubes were firstly synthetized by Iijima in 1991 in the carbon cathode by arc discharge [6]. However, the experimental discovery of single-wall carbon nanotubes came in 1993 [7,8], whereas the discovery in 1996 of a much more efficient synthesis route, involving laser vaporization of graphite to prepare arrays of ordered single-wall nanotubes [9], offered major new opportunities for quantitative experimental studies of carbon nanotubes.

In chapter 6 nanofluid formed by single-wall carbon nanohorns (SWCNHs) in water will be characterized. SWCNHs are roughly spherical aggregates of carbon nanostructures. More exhaustive explanation and figures can be found in chapter 6.

2.1.2 Core-shell structures

Another particular type of nanostructure is the core-shell nanoparticle. In that nanostructure, the chemical compositions of the core and the shell are different. Core and shell can often have totally different crystal structure and physical properties. For example, one can be metallic and another dielectric. Metal-oxide, metal-polymer and oxide-polymer structures can be synthetized. Core-shell nanoparticles could have potential applications in medical field, *e.g.* in catalysis and as precursors for making property-tunable nanoparticles.

2.2 How to prepare nanofluids

It is fundamental to obtain a stable and homogenous colloidal solution for successful reproduction of properties and interpretation of experimental data. The techniques applied to this purpose are the two-step method and the single-step method.

Two-step method

Nanoparticles powder is put into the base fluids and physically dispersed by strong mechanical stirring, low or high energy ultrasounds, ball milling, high pressure homogenisation [10], thus obtaining nanofluids with different particle/fluid combinations. In

Figure 2.2 and Figure 2.3, the VCX130 Sonicator, Sonics Materials and the NS1001L PANDA Homogenizer, GEA Niro Soavi, supplied in the IENI-CNR laboratories, are shown, respectively.

The two-step technique is suitable for the dispersion of oxide nanoparticles, while it is less effective for metal nanoparticles, because of their greater tendency to create agglomerates with negative effects on the physical properties and because of their tendency to form oxides in water.

Figure 2.2: VCX130 Sonicator, Sonics Materials, supplied in the IENI-CNR laboratories.

Figure 2.3: NS1001L PANDA Homogenizer, GEA Niro Soavi, supplied in the IENI-CNR laboratories.

Single-step methods

In this case, synthesis and dispersion of nanoparticles into the fluid take place simultaneously. Various techniques are available for such purpose: direct dispersion of nanoscale vapour from metallic source material into fluids [11]; physical process set up by wet grinding technology with bead mills [12]; chemical reduction method for producing metallic nanofluids [13]; optical laser ablation in liquid [14].

Both for the two-step method and for the single-step method, dispersants (with steric or ionic effects) and optimization of parameters, such as pH and Zeta potential, could be necessary to ensure stable solutions [15].

2.3 Parameters affecting nanofluids properties

Nanosized particles have high-energy surface. For example, in 4 nm diameter particle roughly 50% of the atoms are on the surface. Therefore, surface properties and chemistry control the nanoparticle behaviour [16]. In aqueous environments, there is a tendency for nanoparticles to aggregate, *i.e*. they mix creating clusters, reducing the particle surface energy. It depends on a number of factors, including surface functionalization, pH, and ionic strength.

Forces of different nature, which interact amongst particles, lead to the aggregation and to the settling of aggregates. These two phenomena may occur independently or can be interlinked. Anyway, they involve a reduction of stability of the nanofluids and, consequently, a poor reproducibility of fluid properties.

The suspension stability can be controlled through the pH control and optimization [17], the size and shape nanoparticles control, the selection of the proper dispersant and surfactant that can be added to the nanofluids [18]. Moreover, different methods of nanoparticles dispersion into the base fluid (ball milling, ultrasonication, homogenization) can lead to a different stability [10, 19].

2.4 Mean dimension of nanoparticles

As explained in the previous paragraph, nanoparticles size is one of the most important parameter to determine the possible aggregation of the nanoparticles when they are dispersed in the fluid. There are various techniques for the measurement of the average size of the solid nanoparticles and some for the measurement in the fluid of interest.

For the measurement of solid nanoparticles the scanning or transmission electron microscopy are typically used. The electron microscope is a type of microscope that does not use light as the radiation source but an electron beam. The resolving power of a microscope is inversely proportional to the wavelength of the using radiation, therefore using electrons the resolution typically reaches up to a few tens of nm or a few nm for scanning microscopy and less than 1 nm or 10 nm for microscopy in transmission, depending on the equipment. In the **Scanning Electron Microscopy, SEM**, an electron beam hits the sample that you want to observe. Numerous particles are emitted from the sample between which the secondary electrons. These electrons are detected by a special detector and converted into electrical impulses. In a **Transmission Electron Microscopy, TEM**, the electrons forming the beam pass through a section where a minimum quantity of sample is deposited. The thickness of the sample must be sufficiently thin to allow some of the incident electrons are able to cross it; during this crossing many electrons are absorbed and others, in correspondence to non-uniformity of the atomic arrangement of the crystal, are irregularly deflected. After the beam has passed through the sample, it is focused by a lens, and then expanded and analysed.

To determine the average size of the nanoparticles in solution, the **Dynamic Light Scattering, DLS**, technique is the proper method [20]. The size of a particle is related to its speed due to Brownian motion, as shown by the Stokes-Einstein equation (2.1)

$$D = \frac{kT}{6\pi\mu r} \tag{2.1}$$

in which D is the diffusion coefficient, k is the Boltzmann constant, T is the absolute temperature, r is the radius of a particle in a continuum medium of dynamic viscosity μ.

When a light source (laser), with a known frequency, is directed against the particles, undergoes a scattering whose fluctuation in time depends on the moving speed (smaller particles will be faster), this variation is then put in relation with the size of the particle. On the base of this physical behaviour, the Zetasizer Nano ZS measures the Brownian motion of the particles in the sample and relates this to a size based on established theories [21, 22]. A complete description of this technique is provided in chapter 2.5.

Another technique, useful to determine qualitatively the presence and the size of the nanoparticles, is based on the optical absorption in the UV-Visible. The metallic nanoparticles are, in fact, characterized by very intense absorptions in the region of UV-Vis-NIR. This often results in intense coloration. This phenomenon is due to the interaction between the incident electromagnetic radiation and the electrons of the conduction band that, at certain wavelengths of electromagnetic radiation are in resonance each other, resulting in

absorption of the radiation. In the case of spherical particles, there is a linear relationship between the position of the peak, the absorption band, and size of the nanoparticles, from which the average size can be estimated.

2.5 Nanofluids stability characterization

The nanofluids are suspensions of nanoparticles in liquid, but often the particles, once dispersed, tend to form aggregates, which can settle and penalize the fluid properties. For this reason, the study of the stability of nanofluids is crucial in their characterization.

2.5.1 DLS measurements

In order to evaluate the tendency of nanoparticles to aggregate and eventually settle, the nanoparticle size distribution in the fluid over time was selected as control parameter. A Zetasizer Nano ZS (Malvern) was used for measuring the average dimension of the nanoparticles in solution. This instrument can detect the size from 0.6 nm to 6 μm using a DLS process. The declared accuracy is better than +/-2%. The main components of this instrument are a laser, which illuminates the sample particles within the sample cell, and a detector to acquire the intensity of the scattered light. In Figure 2.4 the Zetasizer Nano ZS is shown.

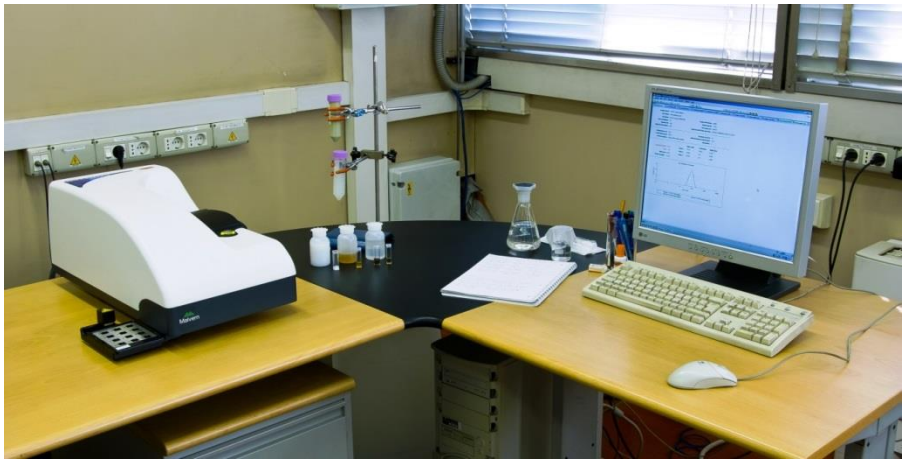

Figure 2.4: Zetasizer Nano ZS (Malvern).

Due to the Brownian motion, a nanoparticle moves randomly in a space. It receives a random displacement, caused for example by other particles hitting it or by an external force and the displacements are assumed to be independent.

An important feature of the Brownian motion is that, at equal temperature and viscosity, the small particles move quickly, creating rapid changes in the intensity of scattering, while the big particles move more slowly, by creating variations of intensity lens. Thanks to an auto-correlator, the speed of changes in intensity is measured, and the diffusion coefficient of the particles is calculated from a correlation function, which depends on several factors, including temperature, viscosity of the fluid, refractive index of the base fluid and radius of the particles considered as spheres (equation 2.1). On the basis of these results, the program returns a graph representing the intensity of the signal as a function of the particles diameter, from which we can estimate an average diameter.

The particle size measured in a DLS instrument is the diameter of the ideal sphere that diffuses at the same rate of the particle being measured. All the size measurements were performed at 25°C with a scattering angle of 173°. The DLS measurements provide the size distribution using a correlation which can separate three different populations existing in the sample, showing one peak for each population. If, by a measurement, only one peak is found, it means that a large majority of the particles have a diameter around the common average value.

For each nanofluid studied in this work, the DLS technique was used with the aim to verify the dependency of the nanoparticle diameter size from the concentration of the solution.

The following analysis was made to determine the tendency of the particles in suspension to settle down along time. Two samples of the fluid were put in two different measurement cuvettes. The first sample was measured almost every day for thirty-five days, without shaking the fluid, to evaluate the changes in size distribution due to natural sedimentation. The second sample was measured almost every day for thirty-five days after sonication of the fluid to evaluate the changes in size distribution after mechanically removing the sedimentation.

2.5.2 ζ potential measurements

Another important parameter to consider for the stability evaluation is the ζ potential. Most of the particles or nanoparticles dispersed in water have a surface charge, originated by ionization phenomena or absorption of charged species. The charged particles in solution are surrounded by several ionic layers. In solution, the particles move along with a double layer ion. The Zeta potential is the potential at the level of this double layer, also called sliding plane. A high potential gives greater stability to colloidal systems, rising the electrostatic repulsions, which prevent the aggregation of dispersed particles. Instead, if Zeta potential is

low, the attractive forces prevail over repulsion and, therefore, aggregation and precipitation phenomena are more probably.

The Zeta potential of nanoparticles was also measured using the Zetasizer Nano (Malvern). This instrument uses a combination of two-measurement techniques, *i.e.* electrophoresis and laser Doppler velocimetry. This combination method measures the velocity of a particle in a liquid when an electrical field is applied. Then, Henry equation (2.2) can be applied, knowing the viscosity and the dielectric constant ε of the sample.

$$U_E = \frac{2\varepsilon\zeta\, f(Ka)}{3\mu} \tag{2.2}$$

The velocity of a particle in an electric field is commonly referred to as its Eloctrophoretic mobility U_E, ζ is the Zeta potential and *f(Ka)* is the Henry's function (two values are generally used as approximations for the *f(Ka)* determination: either 1.5 or 1.0).

The Smoluchowski equation (2.3) is used to obtain the ζ potential from the measured mobility of the particles in aqueous media (for high ionic strengths).

Smoluchowski equation:

$$U_E = 4\pi\varepsilon_0\varepsilon_r \frac{\zeta}{6\pi\mu}(1+k\,r) \tag{2.3}$$

where ε_0 and ε_r are the relative dielectric constant and the electrical permittivity of a vacuum respectively, μ is the solution viscosity, r is the particle radius and κ is the Debye–Hückel parameter, which considers the bulk ionic concentration, the valence of the ion, the charge of an electron, the Boltzmann constant and the absolute temperature.

The Zeta potential value of 30 mV is considered as the limit above which the stability of the suspension is to be considered satisfactory.

Obviously, Zeta potential can be measured only for electrically conductive liquids.

The declared accuracy in the Zeta potential measurements is around ±10%.

2.5.3 pH measurements

The pH of a colloidal solution is one of the main parameters influencing the particle aggregation and the stability of the suspension, therefore the pH of each nanofluid here considered has been measured using a pocket-sized pH meter with replaceable electrode (HANNA Instruments) (Italy). The declared uncertainty is lower than 0.1.

The particular condition at which the negative and positive charges are electrically equivalent is called isoelectric point (IEP).

The pH at which the surface of nanoparticles is electrically neutral identifies the zero point of charge. When the solution is more basic than the IEP, negative ions prevail at the interface and the surface is negatively charged. Similarly, when the solution pH is more acidic than the IEP, positive species predominate and the surface is positively charged.

The nanofluid is much more stable as its pH is far from that of IEP.

References

[1] T.W. Ebbesen, "Carbon Nanotubes", *Annual Review of Materials Research*, 24, 235 (1994).

[2] T. Guo, P. Nikolaev, A. Thess, D.T. Colbert, R.E. Smalley, "Self-Assembly of Tubular Fullerenes", *Journal of Physical Chemistry*, 99, 10694–10697 (1995).

[3] M. Endo, K. Takeuchi, S. Igarashi, K. Kobori, M. Shiraishi, H.W. Kroto, "The production and structure of pyrolytic carbon nanotubes (PCNTs)", *Journal of Physics and Chemistry of Solids*, 54, 1841-1848 (1993).

[4] W.K. Hsu, J.P. Hare, M. Terrones, H.W. Kroto, D.R.M. Walton, P.J.F. Harris, "Condensed-phase nanotubes", *Nature*, 377, 687 (1995).

[5] W.K. Hsu, M. Terrones, J.P. Hare, H. Terrones, H.W. Kroto, D.R.M. Walton, "Electrolytic formation of carbon nanostructures", *Chemical Physics Letters*, 262, 161 (1996).

[6] S. Jijima, "Helical microtubules of graphitic carbon", *Nature*, 354, 56 (1991).

[7] S. Jijima, T. Ichihashi, "Single-shell carbon nanotubes of lnm diameter", *Nature*, 363, 603 (1993).

[8] D.S. Bethune, C.H. Kiang, M.S. de Vries, G. Gorman, R. Savoy, J. Vazquez, R. Beyers, "Cobalt-catalysed growth of carbon nanotubes with single-atomic-layer walls", *Nature*, 363, 605 (1993).

[9] A. Thess, R. Lee, P. Nikolaev, H. Dai, P. Petit, J. Robert, C. Xu, Y.H. Lee, S.G. Kim, A.G. Rinzler, D.T. Colbert, G.E. Scuseria, D. Tomanek, J.E. Fischer, R.E. Smalley, "Crystalline Ropes of Metallic Carbon Nanotubes", *Science*, 273, 483 (1996).

[10] L. Fedele, L. Colla, S. Bobbo, S. Barison, F. Agresti, "Experimental stability analysis of different water-based nanofluids", *Nanoscale Research Letters*, 6, 300 (2011).

[11] J.A. Eastman, S.U.S. Choi, S. Li, W. Yu, L.J. Thomson, "Anomalously Increased Effective Thermal Conductivities of Ethylene Glycol Based Nanofluids Containing Copper Nanoparticles", *Applied Physics Letters*, 78, 718–720 (2001).

[12] M. Chopkar, P.K. Das, I. Manna, "Synthesis and Characterization of Nanofluid for Advanced Heat Transfer Applications", *Scripta Materialia*, 55, 549–552 (2006).

[13] H. Zhu, C. Zhang, S. Liu, Y. Tang, "Effects of Nanoparticle Clustering and Alignment on Thermal Conductivities of Fe_3O_4 Aqueous Nano-fluids", *Applied Physics Letters*, 89, 023123 (2006).

[14] T.X. Phuoc, Y. Soong, M.K. Chyu, "Synthesis of Ag-Deionized Water Nanofluids Using Multi-Beam Laser Ablation in Liquids", *Optics and Lasers in Engineering*, 45, 1099–1106 (2007).

[15] L. Xinfang, Z. Dongsheng, W. Xianju, "Evaluation on dispersion behavior of the aqueous copper nano-suspensions", *Journal of Colloid and Interface Science*, 310, 456-463 (2007).

[16] V.H. Grassian, "When Size Really Matters: Size-Dependent Properties and Surface Chemistry of Metal and Metal Oxide. Nanoparticles in Gas and Liquid Phase Environments", *Journal of Physical Chemistry C*, 112, 47, 18303-18313 (2008).

[17] X. Wang, D. Zhu, S. Yang, "Investigation of pH and SDBS on enhancement of thermal conductivity in nanofluids", *Chemical Physics Letters*, 470, 107-111 (2009).

[18] A. Ghadimi, R. Saidur, H.S.C. Metselaar, "A review of nanofluid stability properties and characterization in stationary conditions", *International Journal of Heat and Mass Transfer*, 54, 17-18, 4051–4068 (2011).

[19] Y. Hwang, J. K. Lee, J. K. Lee, Y.M. Jeong, S. Cheong, Y.C. Ahn, S.H. Kim, "Production and dispersion stability of nanoparticles in nanofluids", *Powder Technology*, 186, 2, 145–153 (2008).

[20] B.J. Berne, R. Pecora, "Dynamic Light Scattering", Courier Dover Publications (2000).

[21] R. Pecora, "Dynamic Light Scattering: Applications of Photon Correlation Spectroscopy", Plenum Press (1985).

[22] C. Washington, "Particle Size Analysis in Pharmaceutics and other Industries: Theory and Practice", Ellis Horwood, England (1992).

Chapter 3

Experimental apparatus and procedures

The study of the thermophysical properties of nanofluids is necessary to understand their energy behaviour. Main properties are dynamic viscosity, thermal conductivity, density and heat capacity. An increase in thermal conductivity can lead to an increase in the convective heat transfer. However, nanofluids can be actually applied in technological systems only if the addition of nanoparticles does not determine a significant viscosity enhancement, because the increase of the required energy to pump the nanofluid could nullify the advantages obtained in terms of thermal properties. With the aim to evaluate the nanofluids potentialities, in this work dynamic viscosity and thermal conductivity will be determined experimentally, while density and heat capacity are calculated from weighted averaging.

3.1 Experimental dynamic viscosity measurements

Viscosity is a significant property and must be taken into consideration for heat transfer performances studies. In fact, the pumping power is related to the viscosity of a fluid. When a fluid flows through a pipe, both in laminar and turbulent flow, the pressure drop is related to the stress at the wall and therefore to the viscosity. In particular, in laminar flow, the pressure drop is directly proportional to the viscosity. The heat transfer coefficient is also influenced by viscosity, in fact it is related to Reynolds number, which strongly depends on the dynamic viscosity.

The measurement methods of the rheological properties, such as viscosity, depend on the type of fluid. For a Newtonian fluid the viscosity is not dependent on the flow conditions, *i.e.* the shear stress or the shear rate, but, in the case of non-Newtonian fluids, the measurements are more complex for the dependence of viscosity on the type and intensity of the imposed flow. For this reason, when studying non-Newtonian fluids, a rheometer is the instrument required, because it consents to impose the shear rate or the shear stress during the viscosity measurement.

In this thesis, dynamic viscosity was measured using a rotational rheometer, AR-G2 (TA Instruments), shown in Figure 3.1. The viscosity measurement is made by means of the equation related to the specific rheometer, which describes its functioning. The equation is obtained by a balance of torques in the case of rotational rheometer.

AR-G2 rheometer, using magnetic bearings, allows to obtain ultra-low nano-torque control which is fundamental for measuring low viscosity fluids such as water-based fluids.

Among the different geometries, plate-cone geometry was chosen because suitable for low viscosity fluids. The relative viscosity equation is:

$$\mu = \frac{3M\Theta}{2\pi R^3 \Omega} \tag{3.1}$$

Where Θ is the cone angle, R is the cone radius, Ω is the angular velocity and M is the torque defined as:

$$M = \int_0^R \sigma r \, 2\pi r \, dr = \eta\dot{\gamma}\frac{2\pi R^3}{3} \tag{3.2}$$

σ is the shear stress, r is the radial coordinate and γ is the shear rate.

In order to stabilize the measurement temperature, an Upper Heated Plate (UHP), shown in Figure 3.2, was used, combined to a geometry with 1° cone and 40 mm diameter. The plate is thermostated by the Peltier effect, the temperature can vary in the range between -20°C and 200°C. A second sensor reads and controls the temperature within the cone. Figure 3.3 represents a schematic of the plate-cone geometry, while in Figure 3.4 a Peltier cover, installed to homogenize the sample temperature, is shown.

A critical point in this measurement is the sample loading. After some trials with water, a constant quantity of about 0.34 ml was considered optimal for the analysis. The sample was deposited using a pipette, taking care no air bubbles were inside.

Before the measurements, the rheometer was carefully calibrated at each temperature, *i.e.* the non-zero moment of inertia of the rheometer spindle, the non–zero moment of inertia of the measurement geometry and the instrument friction were calibrated. Then, due to thermal expansion, zero reference point at the experimental temperature had to be found. Finally, the rotational mapping of the instrument allowed finding the small variations in behaviour around one revolution of the shaft, monitoring the torque required to maintain this speed through a full 360° rotation.

The viscosity measurement is performed by reading the corresponding shear stress to shear rate imposed. All the measurements were performed at atmospheric pressure, at a constant temperature.

The declared instrument uncertainty is 5%.

Figure 3.1: Rotational rheometer, AR G2, TA Instruments.

Figure 3.2: UHP system.

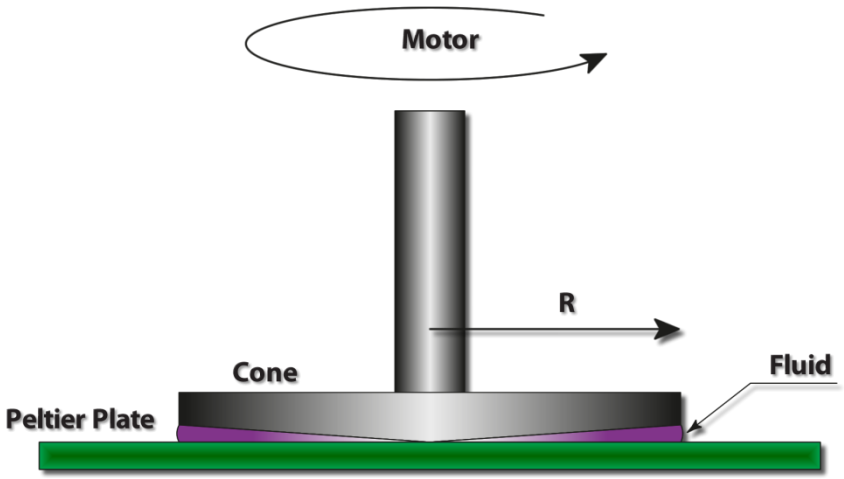

Figure 3.3: Cone-plate geometry.

Figura 3.4: Peltier cover installed to homogenize the sample temperature.

3.1.1 Viscosity of suspensions

In the case of nanofluids, nanoparticles dispersed into the fluid often cause the viscosity to be different than that of the base fluid. Hydrodynamic interactions and particles-particles interaction lead to increased viscous dissipation even at low concentration.

In literature, several theoretical models have been proposed to correlate viscosity data of nanofluids. In general, they derived from the Einstein model [1],

$$\mu_{nf} = \mu_f \left(1 + 2.5\varphi\right) \tag{3.3}$$

based on the assumption of a viscous fluid containing spherical particles. Here, φ is the particle volume fraction (vol%) and μ_{nf} and μ_f are the dynamic viscosity of the nanofluid and

the base fluid, respectively. In general, this formula is applicable when φ is lower than 0.02 and there are not nanoparticle interactions.

Starting from the Einstein's formula, Brinkman suggested an equation applicable to moderate particle volume concentration, roughly 4% [2], in the form

$$\mu_{nf} = \mu_f \frac{1}{(1-\varphi)^{2.5}} \tag{3.4}$$

In [3], Batchelor considered the nanoparticle Brownian motion and their interaction, proposing the formula

$$\mu_{nf} = \mu_f \left(1 + 2.5\varphi + 6.5\varphi^2\right) \tag{3.5}$$

These entire equations base on the assumptions that the viscosity of the nanofluid is only a function of the base fluid viscosity and the particle concentration and that the nanoparticles can be modelled as rigid spherical particles.

Other equations have been proposed with second and third order corrections, as for example

$$\mu_{nf} / \mu_f = 1 + k_1\varphi + k_2\varphi^2 + k_3\varphi^3 + ... \tag{3.6}$$

where k_1, k_2 are coefficients always different, depending on fitting parameters.

However, when the fluids exhibit strongly non-Newtonian behavior, more complex equations should be used to describe their rheological behavior.

Additional correlations are temperature dependent or consider aspect ratio of nanoparticles or particle-particle and particle-fluid interactions. If nanoparticles are rod-like shape, as carbon nanotubes, the value of *k* coefficients is different.

Actually, none model is able to predict the viscosity of nanofluids precisely in a broad range of nanoparticle volume fraction. Moreover, most nanofluids have particles of varying shapes, sizes, size distributions, with different particle-particle and particle-fluid interactions.

For this reason, dynamic viscosity of nanofluids studied in this work will be determined experimentally.

3.1.2 Measurements of water dynamic viscosity

All the measurements were performed at constant temperature and variable shear rate, generally starting from 80 1/s to 1200 1/s, at constant step of about 124 1/s (except for temperatures higher than 60°C, at which faster measurements must be performed due to the water evaporation). A conditioning step of 10 seconds and at pre-shear rate at 80 1/s was

applied before the measurements. Each experimental point is the average of three values of viscosity, sampled under constant shear rate. The experimental temperature uncertainty during the viscosity measurements is about 0.1°C, the torque resolution is 0.1 nNm and the displacement resolution is 25 nrad.

In order to evaluate the rheometer uncertainty, a well-known fluid, such as water, was analysed at each experimental temperature and the viscosity data were compared with Refprop 9.0 database [4].

As shown by Figure 3.5 (and in Table 3.1), all the measured data are quite close to the literature data in the shear rate range between 200 1/s and 1200 1/s, being the percentage absolute average deviation (AAD%) within 1.5%. As shown in figure 3.6, the deviations at low shear rates should be due to difficulties in the torque control by the rheometer, while at high shear rate to changes in the fluid laminar flow.

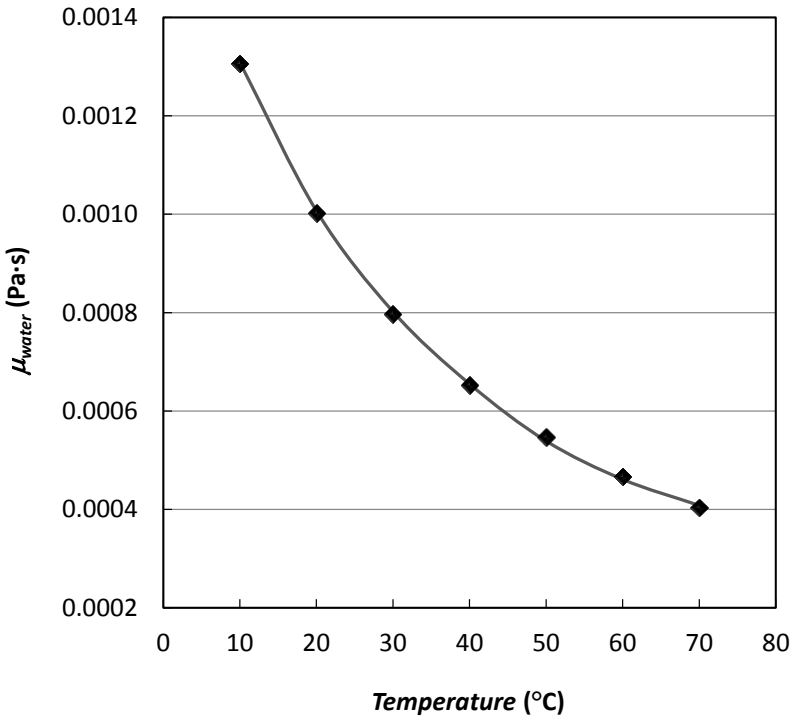

Figure 3.5: Experimental dynamic viscosity of water at 827 1/s, (♦), and Refprop 9.0 trend [4] (—).

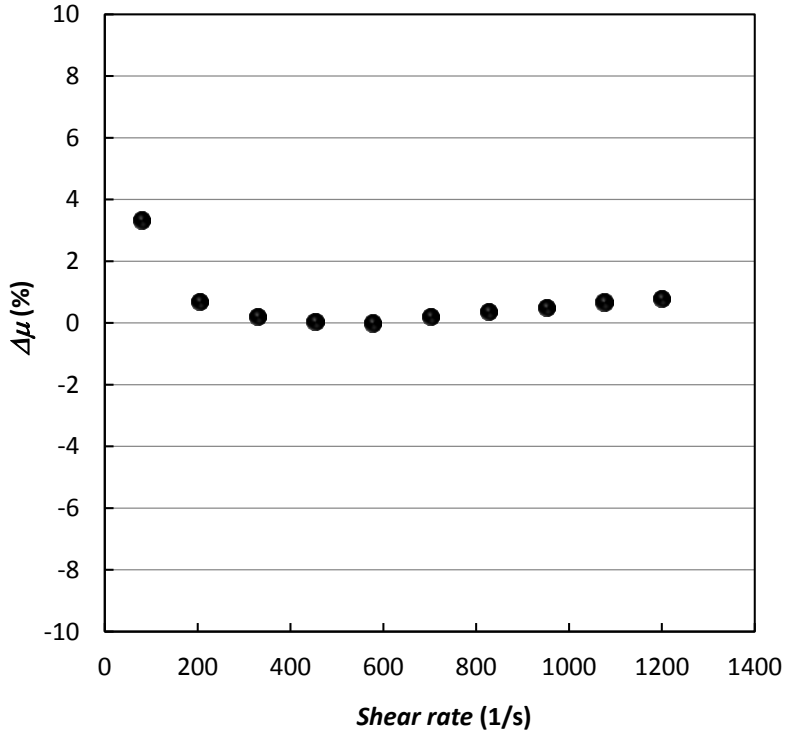

Figure 3.6: Deviations between experimental viscosity data and literature [4] data as a function of shear rate at 50°C.

Table 3.1: Experimental dynamic viscosity for water at 827 1/s.

$$\Delta\mu\% = 100 \cdot \frac{\left(\mu_{\exp} - \mu_{water[4]}\right)}{\mu_{water[4]}}$$

T (°C)	μ_{exp} (Pa·s)	$\mu_{water\,[4]}$ (Pa·s)	$\Delta\mu\%$
10.0	0.001309	0.001306	0.23
20.0	0.001007	0.001002	0.50
30.0	0.000802	0.000797	0.63
40.0	0.000655	0.000653	0.31
50.0	0.000539	0.000547	-1.46
60.0	0.000461	0.000466	-1.07
70.0	0.000408	0.000404	0.99

3.2 Thermal conductivity measurements

Up today numerous techniques have been used for the measurement of nanofluids thermal conductivity: transient techniques such as hot-wire (transient hot-wire), or hot-disk

(transient plane source), the 3ω method, that is based on fluctuations of the temperature and the laser flash thermal diffusivity, as well as stationary techniques such as parallel plates technique. In this work the thermal conductivity measurements were performed using a TPS 2500 S (Hot Disk), shown in Figure 3.7, an instrument based on the hot disk technique which can measure thermal conductivity and thermal diffusivity of several materials. The main parts of the instrument are the sensor, shown in Figure 3.8, made of a double spiral of thin nickel wire that works as a continuous plane heat source and also serves as a temperature sensor, a proper box containing the sensor and the fluid and a thermostatic bath to reach the test temperature.

The continuous double spiral of a nickel metal sensor is immersed in the fluid and small constant current is supplied to the sensor. During the measurements, the power input provided by the sensor creates an increase in temperature. The sensor records the temperature versus time response, accurately determined through resistance measurement, operating both as a heat source and a thermometer. This temperature increase is highly dependent on the thermal transport properties of the material surrounding the sensor, therefore the instrument can calculate the thermal transport characteristics, as follow.

The differential equation of heat conduction in an isotropic material whose thermal conductivity is dependent from temperature is given by [5]:

$$\frac{\partial^2 T}{\partial x^2}+\frac{\partial^2 T}{\partial y^2}+\frac{\partial^2 T}{\partial z^2}=\frac{1}{a}\frac{\partial T}{\partial t} \tag{3.7}$$

where $T(x, y, z, t)$ is the temperature at point (x, y, z) and time t, and

$$a=\frac{k}{\rho c_p} \tag{3.8}$$

a is the thermal diffusivity, k the thermal conductivity, ρ the density, and c_p is the specific heat of the conducting material at temperature T. $\rho \cdot c_p$ is sometimes called the volumetric specific heat of the material. Both ρ and c_p are assumed temperature independent for a small change in temperature.

When a heat source of strength Q is switched on at t=0 in the studied material, equation (3.7) can be modified to include the effect of the heat source [5], as follows

$$a\nabla^2 T+\frac{Q}{\rho c_p}=\frac{\partial T}{\partial t} \tag{3.9}$$

Usually $Q = Q(r, t)$ is a function of position and time. Q is the amount of heat released at (x, y, z, t) per unit time, per unit volume, or power dissipation per unit volume.

The fundamental solution (for Q=0) of equation (3.7) is given by

$$T = T_0 + \frac{1}{(4\pi a t)^{3/2}} \exp\left(-\frac{r^2}{4at}\right), \quad (t > 0) \tag{3.10}$$

where T_0 is the initial temperature. In the case a source of strength Q exists in the material, the general solution to equation (3.9) is given by the convolution of the function $Q/\rho c_p$ with the fundamental solution expressed in equation (3.10), as described in [6], and the instantaneous point source solution is obtained as

$$T(r,t) = T_0 + \frac{Q_0 / \rho c_p}{(4\pi a t)^{3/2}} \exp\left(-\frac{(r - r_0)^2}{4at}\right) \tag{3.11}$$

A hot disk sensor composed of a double spiral nickel wire can be treated as a disk consisting of a certain number (m) of concentric rings, which are equally spaced, since the sensor is designed to have uniform power density throughout the disk. Assume that b is the radius of the largest ring, then the smallest ring has a radius of b/m.

Again, Q_0 is the heat released per unit length per unit time of the sensor coil, and $\pi b(m+1)Q_0 = P_0$ is the power output of the hot disk sensor.

Considering a dimensionless parameter called the *characteristic time ratio*

$$\tau = \frac{\sqrt{at}}{b} \tag{3.12}$$

The average temperature increase in the sensor surface can be expressed as

$$\Delta\overline{T}(\tau) = \frac{P_0}{\pi^{3/2} bk} D(\tau) \tag{3.13}$$

where $D(\tau)$ is a dimensionless time which expression is given in [6].

Knowing the relationship between t and τ, ΔT can be plotted as a function of $D(\tau)$, and a straight line should be obtained. From the slope of this line, thermal conductivity k can be calculated.

However, the proper value of τ is generally unknown, since the thermal diffusivity is unknown. The correct value of a will yield a straight line for the ΔT versus $D(\tau)$ plot. An optimization process can be done by the software, plotting ΔT versus $D(\tau)$ for a range of a values. This optimization process can be done by the software until an optimized value of a is found. Density (ρ) and the specific heat (Cp) of the material are known separately and between k and a there is only one independent parameter, being $a = k/\rho \cdot Cp$. Therefore, both

thermal conductivity and thermal diffusivity of the sample can be obtained from the above procedure based on the transient measurement using a hot disk sensor.

With the hot disk technique, a wide range of materials can be measured, after suitable sample preparation and choosing the proper sensor diameter. The range of thermal conductivity which can be detected is from 0.005 W/(m K) to 500 W/(m K) over a wide temperature range.

The declared instrument uncertainty is 5%.

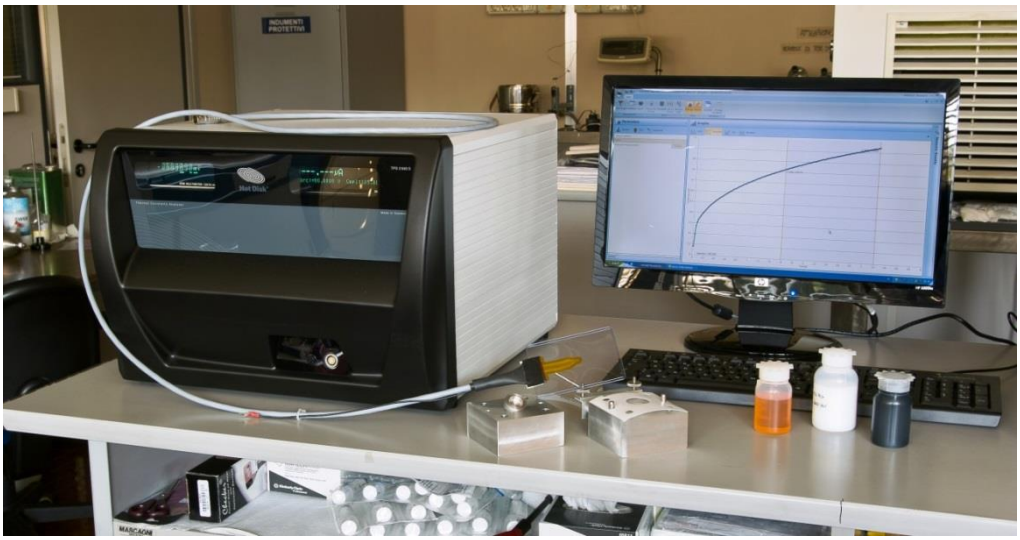

Figure 3.7: TPS 2500 S, Hot Disk.

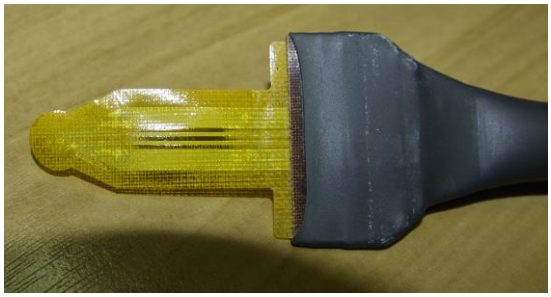

Figure 3.8: TPS 2500 S sensor.

3.2.1 Thermal conductivity of suspensions

Thermal conductivity is the most studied property in the literature. Many works have been published on the influence of temperature, concentration, shape and size of nanoparticles or use of surfactants on the thermal conductivity of nanofluids. In general, the conductivity of nanofluids is higher than that of the base fluid [7-12], but some papers do not

find this enhancement [13, 14]. It should be noted that small nanoparticles have large surface to volume ratio, providing higher thermal conductivity to nanofluid than that of conventional heat transfer fluids. However, the heat transfer mechanism in nanofluids is not completely understood, since some contradictions have been found in literature, as in [15], where large particles seam to improve thermal conductivity respect to smaller ones. Many parameters are affecting the thermal conductivity of nanofluids and for this reason models must be supported by experimental data.

Theoretical modelling of the effective conductivity of a composite material dates back to Maxwell [16], who derived the expression for the electrical conductivity of a two component mixture. Nevertheless, all the considerations could be easily applied to the thermal conductivity as well, since the governing equations are similar. The Maxwell equation for thermal conductivity of composite materials k is:

$$k = k_b\left(1+\frac{3\varphi(\delta-1)}{\delta+2-\varphi(\delta-1)}\right) \tag{3.14}$$

Here, k_b is the thermal conductivities of base fluid, φ is the volume concentration of nanoparticles, δ is defined as ratio of thermal conductivities of particle and base medium k_p/k_b. The above equation is derived under the following assumptions: the suspended particles are spherical, particles are non-interacting and the interfacial resistance between the liquid and solid phases is negligible.

The Maxwell model for thermal conductivity of composites has some limitations. Above all, the volume fraction of nanoparticles suspended in liquid must be small enough to assume none interaction between them. At high volume fractions, the particles can not be considered isolated from each other, or they even can form a percolated network. However, there is a considerable experimental evidence of the validity of the Maxwell model for thermal conductivities of non-nanoscale particulate suspensions.

Moreover, thermal conductivity of suspensions also depends on size and shape of particles. Therefore the Hamilton and Crosser model [17] was considered for comparison:

$$k_{nf} = k_b\frac{k_p+(n-1)k_b+(n-1)\phi(k_b-k_p)}{k_p+(n-1)k_b+\phi(k_b-k_p)} \tag{3.15}$$

k_p represents the thermal conductivity of the added solid particles, k_w is the thermal conductivity of water (the bulk liquid), φ is the particle volume fraction of the suspension, n is the empirical shape factor given by $n=3/\psi$ and ψ is the sphericity. For a spherical shape particle, the sphericity (ψ) is 1.

In this work a comparison with the predictions of the Hamilton and Crosser (H-C) model will be given for the measured nanofluids. Other models chosen for comparison are presented below.

Bruggeman model [18] is based on the differential effective medium theory in order to estimate the effective thermal conductivity of composites at high particle concentrations

$$k_{nf} = k_b \frac{(3\varphi - 1)\frac{k_p}{k_b} + [3(1-\varphi) - 1] + \sqrt{\Delta}}{4} \qquad (3.16)$$

$$\Delta = \left\{ (3\varphi - 1)\frac{k_p}{k_b} + [3(1-\varphi) - 1] \right\}^2 + 8\frac{k_p}{k_b}$$

Lu and Lin model [19] is used for spherical and non-spherical particles. The effective conductivity of composites containing aligned spheroids of finite conductivity was modelled with the pair interaction.

$$k_{nf} = k_b(1 + a\varphi + b\varphi^2) \qquad (3.17)$$

In the case of spherical particles, the values of the coefficients *a* and *b* are 2.25 and 2.27, respectively.

Xuan *et al*. model [20] is based on the Maxwell model and includes the effects of random motion, particle size, concentration and temperature.

$$k_{nf} = k_b \left[\frac{k_p + 2k_b + 2\varphi(k_b - k_p)}{k_p + 2k_b + \varphi(k_b - k_p)} + \frac{\rho_p \cdot \varphi \cdot c_{p,p}}{2k_b} \sqrt{\frac{k_B \cdot T}{3 \cdot \pi \cdot \mu \cdot r_c}} \right] \qquad (3.18)$$

where T is the temperature, ρ_p is the density of particles, $c_{p,p}$ represents the specific heat capacity of particles, k_B is the Boltzmann constant, r_c is the radius of the clusters and μ is the viscosity.

3.2.2 Measurements of water thermal conductivity

All the measurements of thermal conductivity were performed using the TPS 2500 S (Hot Disk). The power supplied by the sensor for each measurement was 40 mW and the time of the power input was 4 s. The experimental temperature uncertainty during the measurements is about 0.1°C.

Before measuring nanofluids, pure water thermal conductivity was measured at ambient pressure in the temperature range between 10.7°C and 68.5°C to test the sensor of the instrument and to evaluate the instrument accuracy. The data obtained were compared with

Refprop 9.0 database [4], as reported in Table 3.2 and shown in Figure 3.9. The absolute average deviation is less than 1%, well within the 5% accuracy declared by the constructor.

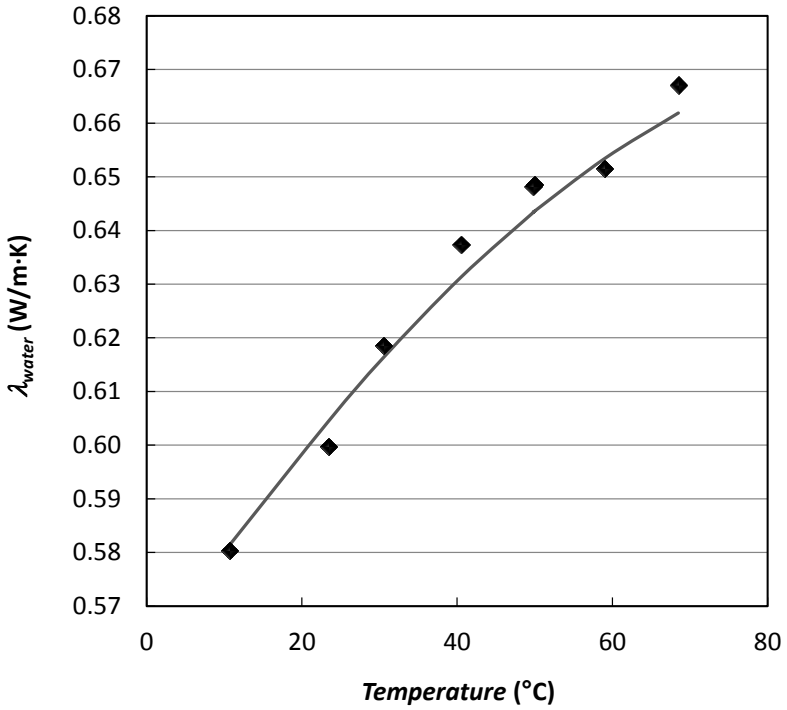

Figure 3.9: Experimental thermal conductivity of water, (♦), and Refprop 9.0 [4] (—).

Table 3.2: Experimental thermal conductivity data.

$$\Delta\lambda\% = 100 \cdot \frac{\left(\lambda_{\exp} - \lambda_{water[4]}\right)}{\lambda_{water[4]}}$$

T (°C)	$\lambda_{exp.}$ (W/m·K)	$\lambda_{water\ [4]}$ (W/m·K)	$\Delta\lambda\%$
10.7	0.5803	0.5814	-0.19
23.4	0.5997	0.6044	-0.78
30.5	0.6186	0.6163	0.37
40.5	0.6374	0.6313	0.97
50.0	0.6486	0.6436	0.78
49.8	0.6482	0.6434	0.75
59.0	0.6516	0.6534	-0.28
68.5	0.6671	0.6619	0.79

3.3 Conclusions

Many parameters are affecting thermophysical properties of nanofluids. For this reason models must be supported by experimental data.

Thermal conductivity was measured by means of the hot disk technique, while dynamic viscosity was measured using a rotational rheometer, both at different temperatures and ambient pressure, since there are no models able to correctly predict these properties for nanofluids.

On the contrary, density and heat capacity of nanofluids can be generally calculated as weighted averages, knowing the properties of base fluid and nanoparticle material.

Density of nanofluid (ρ_{nf}) was calculated knowing density of nanoparticles (ρ_{np}) and density of base fluid (ρ_f) at each temperature and volume fraction (φ):

$$\rho_{nf} = (1-\varphi)\rho_f + \varphi\rho_{np} \tag{3.19}$$

Heat capacity of nanofluid (Cp_{nf}) was calculated knowing heat capacity of nanoparticles (Cp_{np}) and heat capacity of base fluid (Cp_f) at each temperature and mass fraction (ω):

$$Cp_{nf} = (1-\omega)Cp_f + \omega Cp_{np} \tag{3.20}$$

References

[1] A. Einstein, *Annalen der Physik*, 19, 289–306 (1906).

[2] H.C. Brinkman, "The viscosity of concentrated suspensions and solutions", *Journal of Chemical Physics*, 20, 4, 571-581 (1952).

[3] G.K. Batchelor, "The effect of Brownian motion on the bulk stress in a suspension of spherical particles", *Journal of Fluid Mechanics*, 83, 97-117(1977).

[4] E.W. Lemmon, M.L. Huber, M.O. McLinden, NIST Standard Reference Database 23, Reference Fluid Thermodynamic and Transport Properties (REFPROP), version 9.0; National Institute of Standards and Technology (2010).

[5] H.S. Carslaw and J.C. Jaeger, "Conduction of Heat in Solids, second ed., Oxford Science Publications", New York (2000).

[6] J. He, "The Rapid thermal conductivity measurement with a hot disk sensor Part 1. Theoretical considerations", *Thermochimica Acta*, 436, 122-129 (2005).

[7] S. M. Abbasi, A. Rashidi, A. Nemati, K. Arzani, "The effect of functionalisation method on the stability and the thermal conductivity of nanofluid hybrids of carbon nanotubes/gamma alumina", *Ceramics International*, 39, 3885-3891 (2013).

[8] A. Nasiri, M. Shariaty-Niasar, A. M. Rashidi, R. Khodafarin, "Effect of CNT structures on thermal conductivity and stability of nanofluid", *International Journal of Heat and Mass Transfer*, 55 1529–1535 (2012).

[9] S. K. Das, N. Putra, P. Thiesen, W. Roetzel, "Temperature dependence of thermal conductivity enhancement for nanofluids*", Journal of Heat Transfer*, 125, 4 567-574 (2003).

[10] S. M. S. Murshed, K. C. Leong, C. Yang, "Enhanced thermal conductivity of TiO_2-water based nanofluids", *International Journal of Thermal Sciences*, 44, 4 367-373 (2005).

[11] R. Prasher, P. Bhattacharya, P. E. Phelan, "Thermal conductivity of nanoscale colloidal solutions (nanofluids)", *Physical Review Letters*, 94, 2 (2005).

[12] T. K. Hong, H. S. Yang, and C. J. Choi, "Study of the enhanced thermal conductivity of Fe nanofluids", *Journal of Applied Physics*, 97, 6 (2005).

[13] J. Buongiorno, D. C. Venerus, N. Prabhat, T. McKrell, J. Townsenddi et al., "A benchmark study on the thermal conductivity of nanofluids conduttività", *Journal of Applied Physics*, 106 (2009).

[14] A. T. Utomo, H. Poth, P. T. Robbins, A. W. Pacek, "Experimental and theoretical studies of thermal conductivity, viscosity and heat transfer coefficient of titania and alumina nanofluids", *International Journal of Heat and Mass Transfer*, 55 (2012).

[15] P. Warrier and A. Teja, "Effect of particle size on the thermal conductivity of nanofluids containing metallic nanoparticles", *Nanoscale Research Letters*, 247, 6 (2011).

[16] J.C. Maxwell, A Treatise on Electricity and Magnetism, Dover Publications, Inc. (1954).

[17] R.L. Hamilton and O.K. Crosser, "Thermal conductivity of heterogeneous two-component systems", *Industrial & Engineering Chemistry Fundamentals*, 1 182-191 (1962).

[18] D.A.G. Bruggeman, "Berechnung Berechnung verschiedener physikalischer Konstanten von heterogenen Substanzen. I. Dielektrizitätskonstanten und Leitfähigkeiten der Mischkörper aus isotropen Substanzen", *Annalen der Physik*, 416, 7, 636-664 (1935).

[19] S. Lu and H. Lin, "Effective Effective conductivity of composites containing aligned spheroidal inclusions of finite conductivity", *Journal of Applied Physics*, 79, 9, 6761-6769 (1996).

[20] Y. Xuan, Q. Li and W. Hu, "Aggregation structure and thermal conductivity of nanofluids", *AlChE Journal*, 49, 4 1038-1043 (2003).

Chapter 4

Convective heat transfer

The final objective of this work is to investigate the convective heat transfer capabilities of nanofluids. For this purpose, a convective heat transfer experimental loop has been designed and constructed. In this chapter, the design, calibration of instrumentation, the water testing and the uncertainty analysis are described.

4.1 State of the art

The number of publications dealing with heat transfer properties of nanofluids is exponentially growing from ten years ago to today. However, many publications indicate controversial results. Many authors prove an enhancement of heat transfer coefficient of nanofluids on respect to the base fluid heat transfer coefficient. For example, Hwang *et al.* [1] reported improvement in convective heat transfer coefficient in the thermally fully developed regime, through experimental investigation of flow and convective heat transfer characteristics of Al_2O_3/water nanofluid in laminar flow. In addition, Wen and Ding [2] found that heat transfer enhancement for Al_2O_3 in water increases with increasing particle volume concentration up to 40%, while the thermal conductivity enhancement is below 15%. Heat transfer coefficient of CNT nanofluids can enhance up to a 150% and increases with the non-dimensional axial distance x/D, while decreases with concentration in the range from 1.1 vol% to 4.4 vol% [3]. In turbulent flow, in general, metal and CNT nanoparticles are much more promising in terms of heat transfer with respect to oxides. *E.g.*, Pak and Cho [4] investigated some oxide nanofluids, for which turbulent heat transfer coefficient actually decreased by 3–12%, even though the Nusselt number increased. Vice-versa, Xuan and Li [5] obtained for Cu-water nanofluids at 2 vol % an increase of ~40% in turbulent heat transfer coefficient, while Faulkner *et al.* [3] reported max heat transfer enhancement by 350% for aqueous solution with 0.5 wt% MCNT. Nguyen *et al.* [6] showed size-dependent heat transfer coefficients in turbulent forced convection.

Other studies describe a quantitatively not specified enhancement and further authors are hostile to an enhancement of heat transfer [7]. Interesting reviews on nanofluids heat transfer investigations in the past decade may be found in [8-11].

4.2 Apparatus design and construction

A hydraulic circuit was specifically designed and built to measure the heat transfer coefficient of nanofluids. The design of the experimental section was carried out with particular attention to each detail.

The measurement section is composed of two parts: an initial developing section and a developed region. It is a straight copper pipe with 8 mm inner diameter (D) and 2 mm thickness.

The developing section, 0.5 m long, is important to permit the formation of fully developed flow. In this first region (the entrance section), distinct boundary layers coexist with *core* fluid that is not yet disturbed by the walls. In the second region, the core has disappeared and the boundary layers are no longer distinct. The velocity profile is constant in axial direction. Entrance length for laminar flow can be calculated as

$$X \approx 0.06 \cdot \mathrm{Re} \cdot D \tag{4.1}$$

whereas in turbulent flow it is calculated as

$$X \approx 4.4 \cdot \mathrm{Re}^{1/6} \cdot D \tag{4.2}$$

Reynolds number is

$$\mathrm{Re} = \frac{\rho \cdot D \cdot v}{\mu} \tag{4.3}$$

in which ρ is the density, v is the velocity and μ is the dynamic viscosity.

In turbulent flow, the developing section ensures the fully developed region, whereas in laminar flow it is ensured for Re lower than 1000. For Re between 1000 and 2300, the fully development of the flow starts within the subsequent part of the tube.

The following region, 2 m long, is divided in 8 subsections. Every 0.25 m, 4 thermocouples are placed in circumferential way as shown in Figure 4.1. They are inserted into 1.5 mm deep cavities, which are dug in the tube to enable the sensors to be as close as possible to the internal pipe surface. Figure 4.2 represents the inlet part of the measurement section.

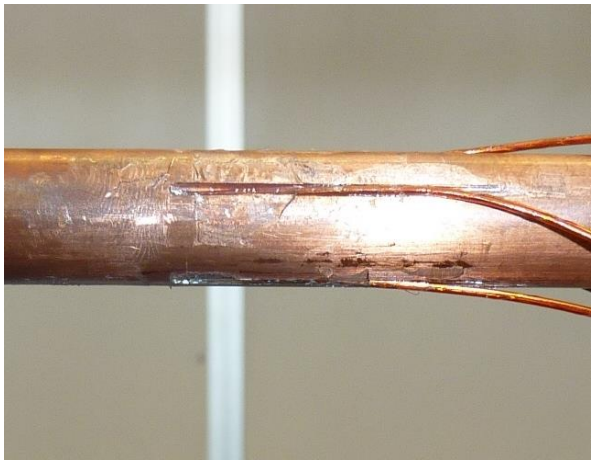

Figure 4.1: Thermocouples inserted into 1.5 mm deep cavities.

Preliminary tests were performed in order to choose the appropriate method to fix the sensors in the cavity base, trying welding and glues. The best solution seemed to be bonding and the cavity was then filled with aluminium to ensure the continuity of the pipe thickness. The influence of the conductive heat transfer through the copper thickness will be discussed in chapter 4.2.1.32 thermocouples measure the wall temperature (T_w) along the heated pipe. For each subsection, the wall temperature is the mean value of the 4 acquisitions.

However, the possibility of measuring the temperature at the highest and the lowest point, in the same axial position, is useful to verify if the temperature varies transversely.

Through the developed region, a specific heat flux (q) is generated by heating electrical resistance wires winded continuously around the pipe, as shown in Figures 4.3 and 4.4. Therefore, a constant heat flux condition is imposed through the wall of the pipe in which the measured fluid flows. The 8 heating electrical resistance wires have been tested to verify the declared values of specific electrical resistance (*er*). Measured values are listed in Table 4.1. Then they are winded around the pipe, each one carefully paced with the central part of the winding above the point of acquisition of the wall temperature. Each wire covers the pipe 0.125 m before and after the acquisition point.

The initial and final parts of the wire, that are not in contact with the pipe, were measured in order to calculate the real electrical power transferred to the pipe. The 8 heating electrical resistance wires are switched in parallel and linked to a System DC Power Supply N5700, Agilent Thecnologies. Imposing the voltage and the current intensity uniquely, the power supplied to the heating elements is known. Therefore, the power is adjustable and its maximum value is 900 W.

Figure 4.5 represents the model of the measurement section.

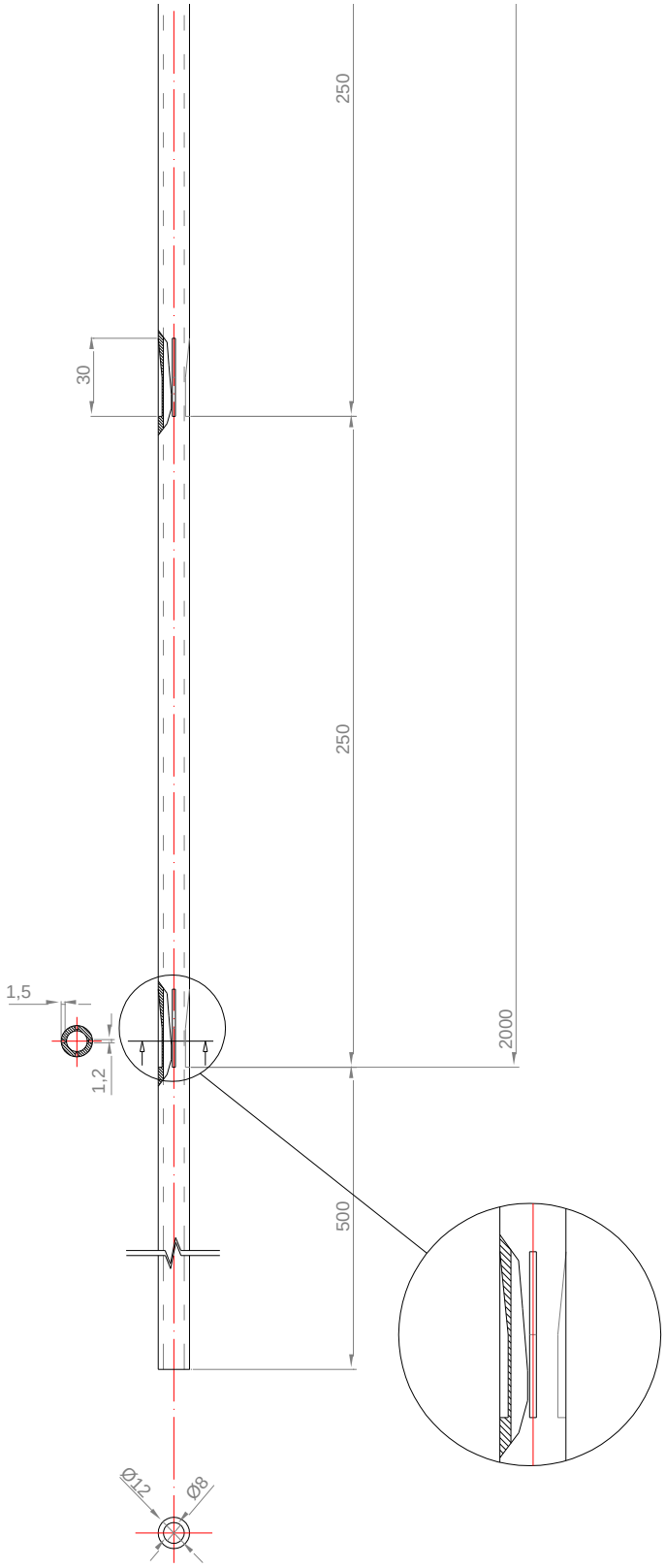

Figure 4.2: Schematic of inlet part of the measurement section.

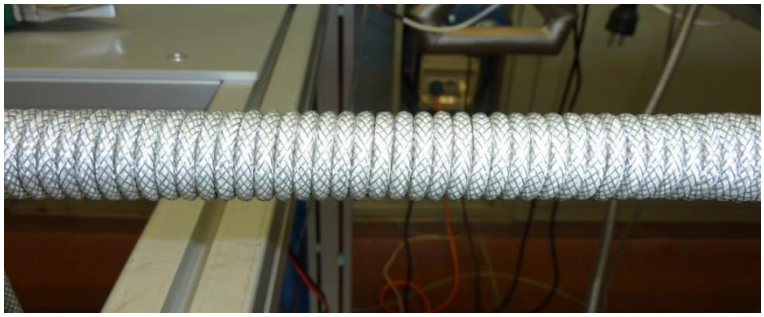

Figure 4.3: Heating electrical resistance wires winded continuously around the pipe.

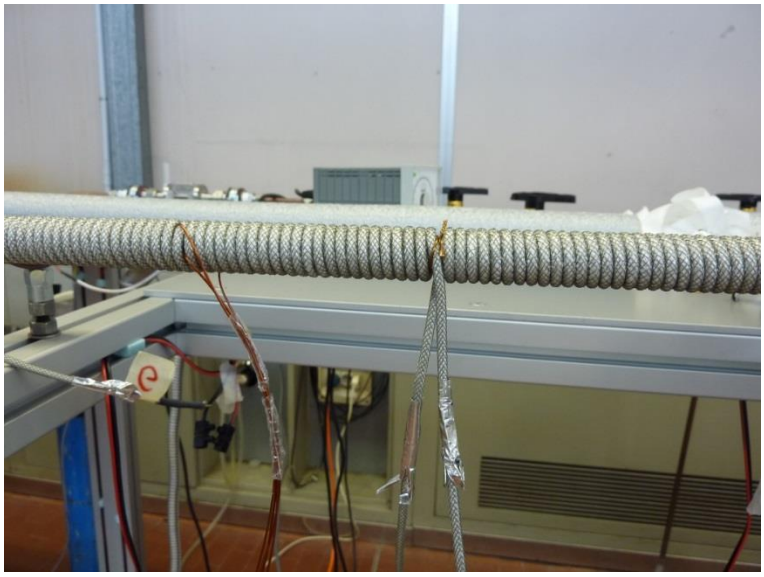

Figure 4.4: Heating electrical resistance wires. Thermocouples wires are shown.

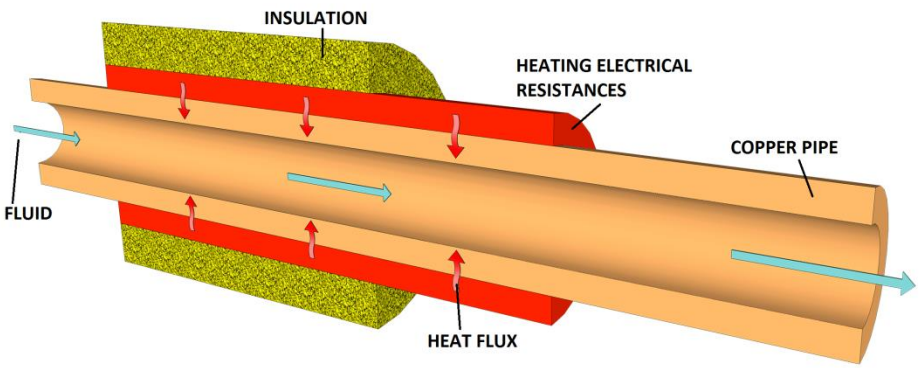

Fig. 4.5: Model of the measurement section.

At the inlet and outlet of the measurement section 2, platinum resistance thermometers (Pt100) measure fluid bulk temperatures (T_{in} and T_{out}). They are placed after a mixer device in order to measure the adiabatic mixing temperature.

With the aim of interrupting the axial thermal flow, two pipes having very low conductivity were added to the extremities of the experimental section, as shown in Figure 4.6. They are 50 mm long and their inner diameter is 8 mm.

Aluminium foils cover the electrical resistance wires to avoid the radiant flux to the outside as shown in Figure 4.7. Pipe and electrical resistances are insulated to minimize the power loss and to obtain a constant heat flux condition along the test section. For this purpose, 25 mm thickness polyurethane material was used, having low thermal conductivity, 0.029 W/(m·K).

Table 4.1: Heating electrical resistance wires characteristics.

name	*electrical resistance* (Ω)	*wire lenght* (m)	*er* (Ω/m)
A	346.9	3.462	100.2
B	347.0	3.463	100.2
C	347.2	3.462	100.3
D	346.7	3.462	100.1
E	347.6	3.464	100.3
F	346.6	3.462	100.1
G	347.0	3.461	100.3
H	347.7	3.462	100.4

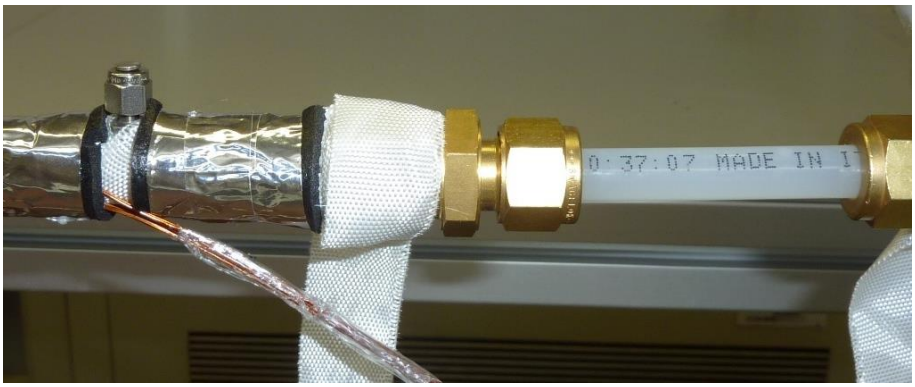

Figure 4.6: Pipe added to avoid the axial thermal flow.

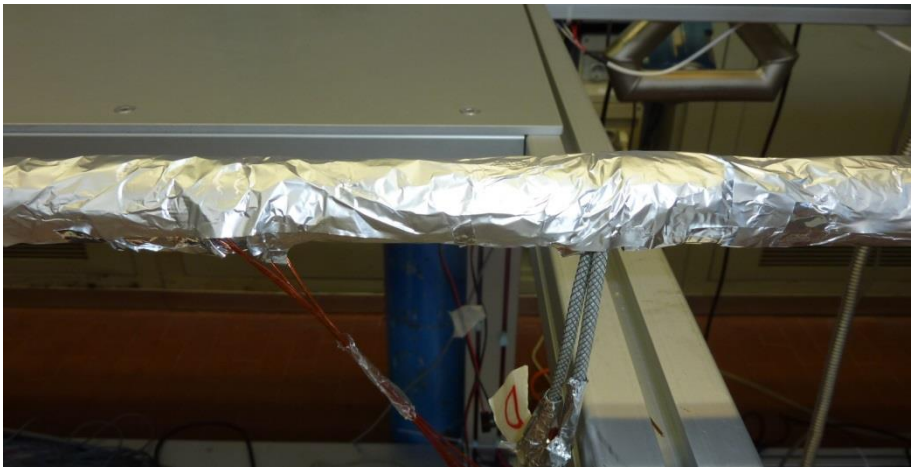

Figure 4.7: Aluminium foils covering the electrical resistance wires.

A magnetic gear pump (Ismatec MCP-Z, Figure 4.8) allows adjusting the mass flow rate from 0.261 ml/min to 6318 ml/min, which is equivalent to the range0.005 kg/s - 0.105 kg/s for water. Corresponding speeds for water are 0.05 m/s - 2.10 m/s and the Reynolds number can vary from 400 to 16000. After and before the magnetic drive gear pump, flexible pipes for vacuum use are inserted to minimize the mechanical vibrations.

A Coriolis mass flow meter (Emerson Process, Micromotion Elite model; 1/4-inch; 316L SS, Figure 4.9) measures the flow rate with a very low declared instrument uncertainty of 0.05%.

Figure 4.8: Magnetic gear pump.

Figure 4.9: Coriolis mass flow meter.

A cooling machine with turbine pump (Polyscience 5106T model, Figure 4.10) is connected to a plate heat exchanger, inside of which the fluid flows. The plate heat exchanger is placed downline of the measurement section and work upstream in order to cool down the fluid and keep always the same temperature at the inlet of the measuring section. In fact, the coefficient heat transfer measurements were performed at constant heat flux, mass flow rate and inlet temperature. In order to accurately control the inlet temperature, a proportional-integral-derivative controller (PID controller) was positioned upline of the measurement section, as shown in Figure 4.11. The controller minimize the difference between the measured process variable, inlet temperature, and the set point value, by adjusting the process control input. It actuates an additional heating electrical resistance wire. The proportional, integral and derivative terms were determined and adjusted as a function of the flow rate.

Figure 4.10: Cooling machine with turbine pump (Polyscience 5106T model).

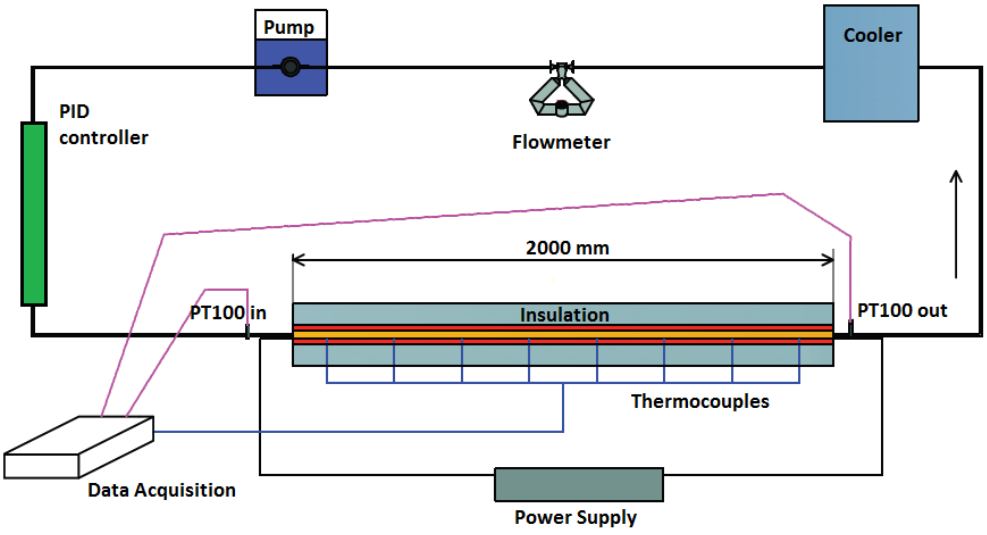

Figure 4.11: Schematic of the circuit.

The digital multimeter, Agilent Thecnologies, was used in this experiment as shown in Figure 4.12. It acquires several data: thermocouple signals, voltage and Pt100 resistance. Acquired data were implemented into a LabVIEW user interface, as shown in Figure 4.13. In the figure, parts “A” and “F” indicate the power control, parts “B” and “C” indicate the

temperature acquisition, part “D” indicates the flow rate acquisition and part “E” shows the wall temperature as a function of the axial position.

Before filling the circuit with liquid, it is put under vacuum using a vacuum pump, as shown in Figure 4.14.

Figure 4.12: Digital Multimeter.

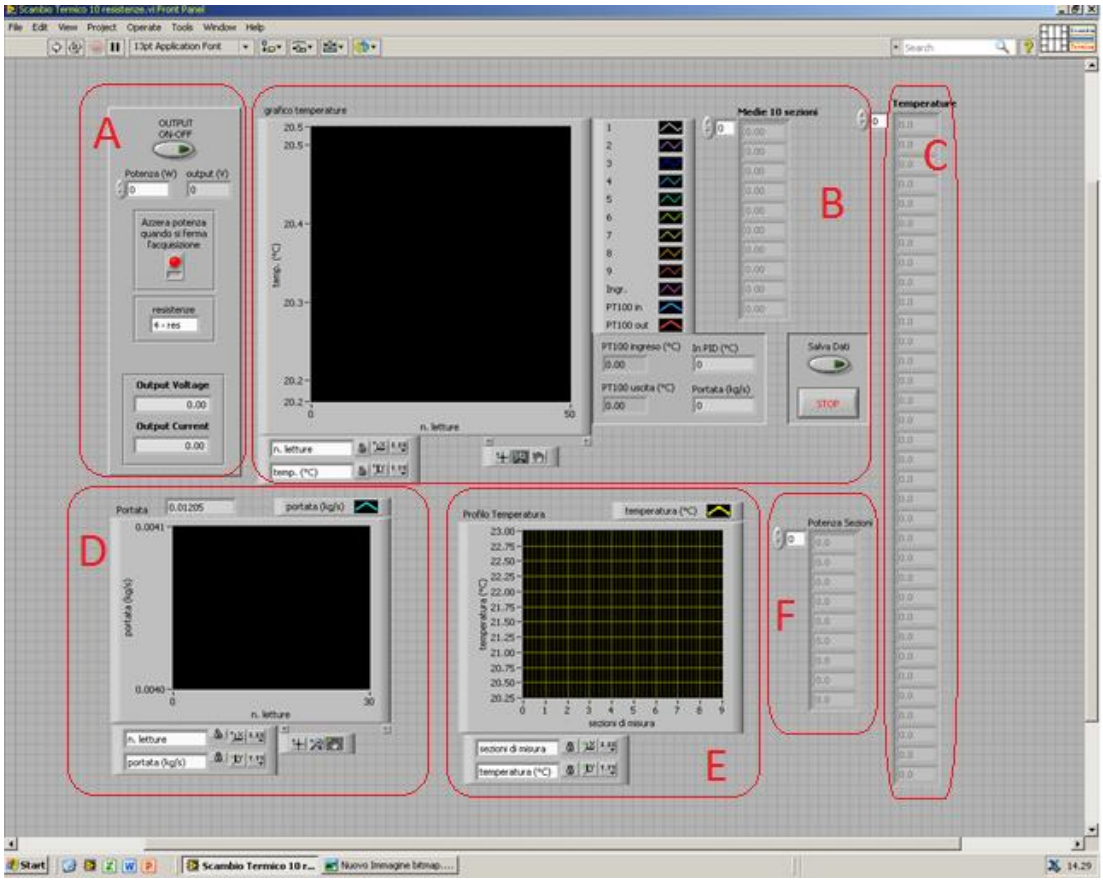

Figure 4.13: LabVIEW user interface.

Figure 4.14: Vacuum pump.

4.2.1 Radial conduction through the pipe

Between the inner pipe surface and the thermocouple sensors, which measure the wall temperature, there is 0.5 mm of cylindrical copper layer. The follow analysis is done to verify if the radial conduction along the copper layer causes a variation in temperature between the reading value and the wall value.

The solution of the general equation of heat transfer conduction in cylindrical coordinate is

$$t = c_1 \ln r + c_2 \tag{4.4}$$

Determining the constants c_1 and c_2, due to the boundary conditions, the temperature radial distribution (t) is

$$t = t_1 - \frac{t_1 - t_2}{\ln \frac{r_2}{r_1}} \ln \frac{r}{r_1} \tag{4.5}$$

The temperature varies logarithmically in the thickness of the layer. The temperature gradient is inversely proportional to the radius r. In Figure 4.15, symbols are displayed.

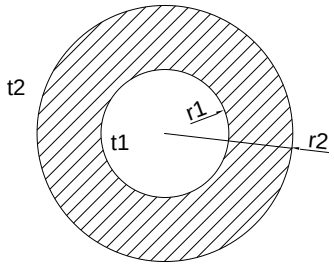

Figure 4.15: Cylindrical copper layer.

Heat flux is obtained from the Fourier low

$$Q = -\lambda A \frac{dt}{dr} = -\lambda 2\pi r l \frac{dt}{dr} \tag{4.6}$$

Considering r_1 = 0.004 m, r_2 = 0.06m, r = 0.0045 m and, for example, Q = 75 W, t = 44.47°C, l = 0.25 m and λ_{Cu} = 386 W/(mK), the difference between the temperature measured by the thermocouple t and the calculated wall temperature t_1 is 0.01°C. Therefore, the radial conduction through the pipe was neglected.

4.3 Calibration

The power supplied to the heating electrical resistances was verified using a wattmeter connected in parallel to each resistance wire at a time. The results were the same for each wire and the power supplied value has been confirmed.

In order to verify the electrical resistance of the wires as a function of the temperature, one wire was immersed in a thermostatic bath and the electrical resistance has been measured from 22°C and 80°C. As shown in Figure 4.16, the maximum difference in the electrical resistance values is 1.3 Ω. Therefore, the electrical resistance was considered independent from the temperature.

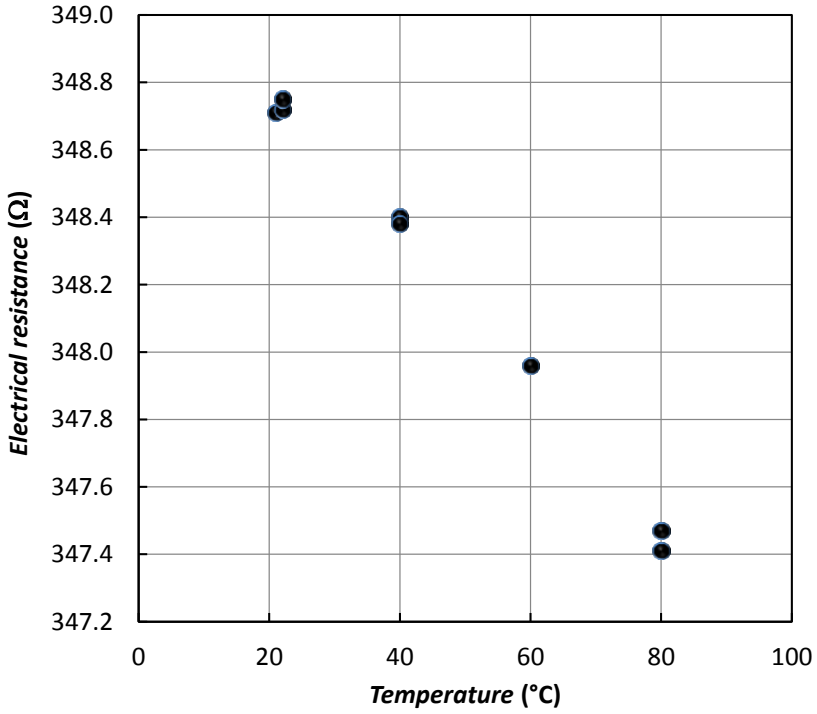

Figure 4.16: Electrical resistance of the wires as a function of the temperature.

4.3.1 Thermocouples calibration

40 thermocouples were created in order to measure the wall temperature. They are made by two different wires joined at one end, called thermoelements or legs of the thermocouple. Type T (copper – constantan) thermocouples, suited for measurements in the −200°C - 350°C range are chosen. All the sensors were calibrated in a temperature range from 10°C to 70°C. The calibration consists on measuring the thermocouple electromotive force at a series of approximately uniformly spaced temperatures. The temperature versus electromotive force points were interpolated and the coefficients of a polynomial equation were determined, for each sensor. The temperature values derived from Pt100 measurements, which was immersed in a thermostatic bath together with the thermocouples. The two Pt100 used in this work are platinum resistance thermometers with a resistance of 100 ohm at 0°C. They were produced by Fasinternational and the declared uncertainty is 0.05°C, which comprises the entire measurement chain uncertainty.

A third order polynomial equation has been determined for each thermocouple and the following Table 4.2 and Figure 4.17 is an example.

Table 4.2: Temperature and electromotive force for one sensor.

Pt100 temperature (°C)	*Thermocouple* ΔV (V)
8.33	0.000329
17.64	0.000698
27.62	0.001108
37.53	0.001519
47.18	0.001930
57.49	0.002376
67.75	0.002825

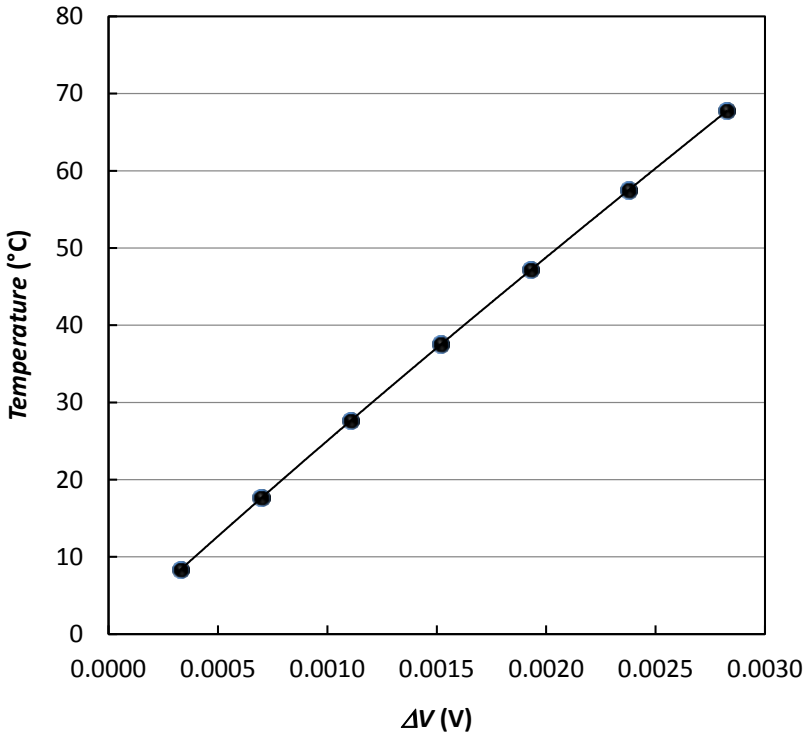

Figure. 4.17: Temperature versus electromotive force. Third order polynomial curve.

Resulting equation is:

$T = 93061070.2321777000000000 \cdot (\Delta V)^3 - 980376.2076685500000000 \cdot (\Delta V)^2 + 26048.7942541273000000 \cdot \Delta V - 0.1205620187126560$

As a zero-point reference, a 50 channels ice-point was used, as shown in Figure 4.18, which is comprised in the calibration system.

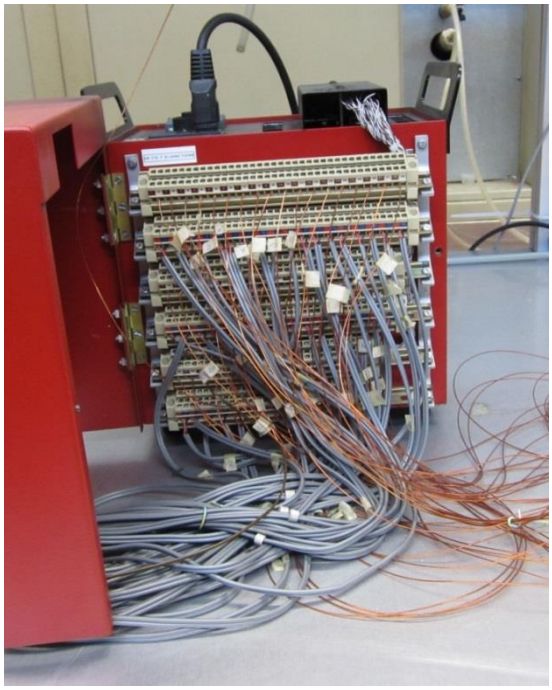

Figure 4.18: Ice-point.

4.4 Water convection testing

The circuit was tested with water in order to verify the operation using a fluid of known properties. Moreover, most of the nanofluids measured in this work are water-based fluids, therefore measurements on water were used for comparison between nanofluid and base-fluid.

Along the experimental section, the bulk temperature of each subsection i ($T_{f,i}$) was calculated in consecutive steps, knowing the supplied power and using the energy balance.

For i=1:

$$T_{f,1} = T_{in} + \frac{qSx_1}{\rho C_p v A} \tag{4.7}$$

For i=2 to i=8:

$$T_{f,i} = T_{f,i-1} + \frac{qS\left(x_i - x_{i-1}\right)}{\rho C_p v A} \tag{4.8}$$

where T_{in} is the inlet bulk temperature (°C), q the specific heat flux (W/m^2), S the perimeter of the internal pipe section (m), x the axial distance (m), ρ the fluid density (kg/m^3), C_p the specific heat capacity of the fluid (J/kg·K), v the fluid velocity (m/s) and A is the transversal area (m^2).

Nusselt number (Nu) and heat transfer coefficient (α) of fluids were calculated with the equations:

$$\mathrm{Nu}_{f,i} = \frac{\alpha_{f,i} D}{\lambda_f} \tag{4.9}$$

$$\alpha_{f,i} = \frac{q}{\left(T_{w,i} - T_{f,i}\right)} \tag{4.10}$$

where the subscripts *f,i* and *w,i* stand for fluid at subsection *i* and wall at subsection *i*, respectively.

Measurements on water were performed both in laminar and in turbulent flow, with Re up to 16000. Inlet temperature have been set to about 20°C, 30°C and 40°C. Heat flux varied from 1991 W/m^2 to 15915 W/m^2. Figures 4.19 and 4.20 show an example of temperature profiles and Nu for water in laminar flow. Figures 4.21 and 4.22 show an example of temperature profiles and Nu for water in turbulent flow.

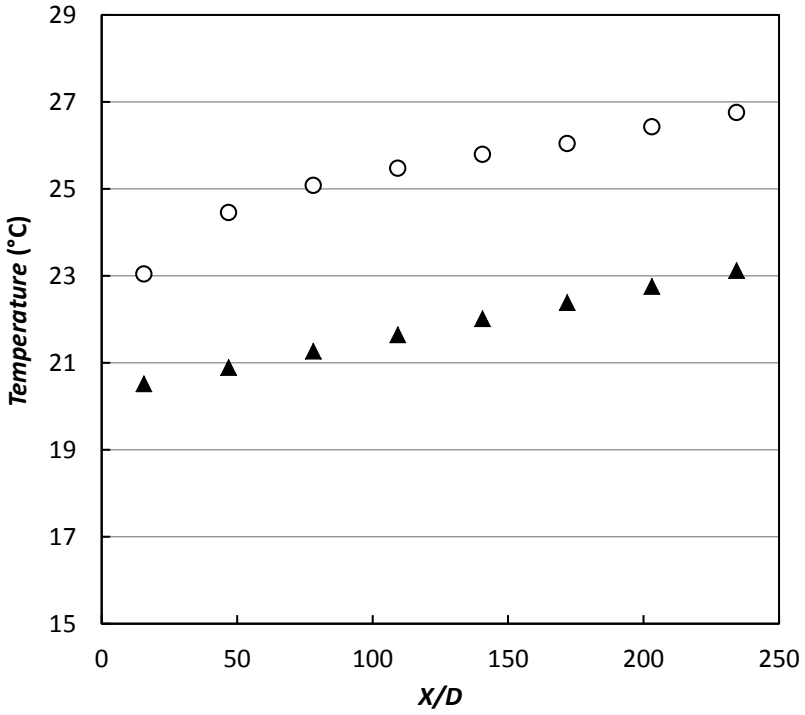

Figure 4.19: Water in laminar flow, Re=1334, T_{in}=20.3°C, q=1991 W/m^2. ○ wall temperature, ▲ bulk temperature.

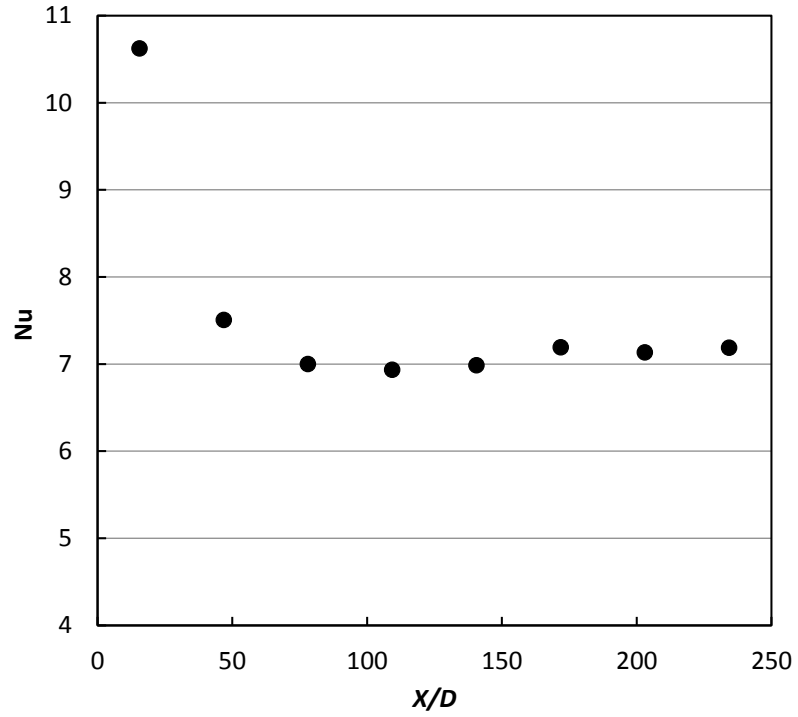

Figure 4.20: Water in laminar flow, Re=1334, T_{in}=20.3°C, q=1991 W/m^2. Nusselt number.

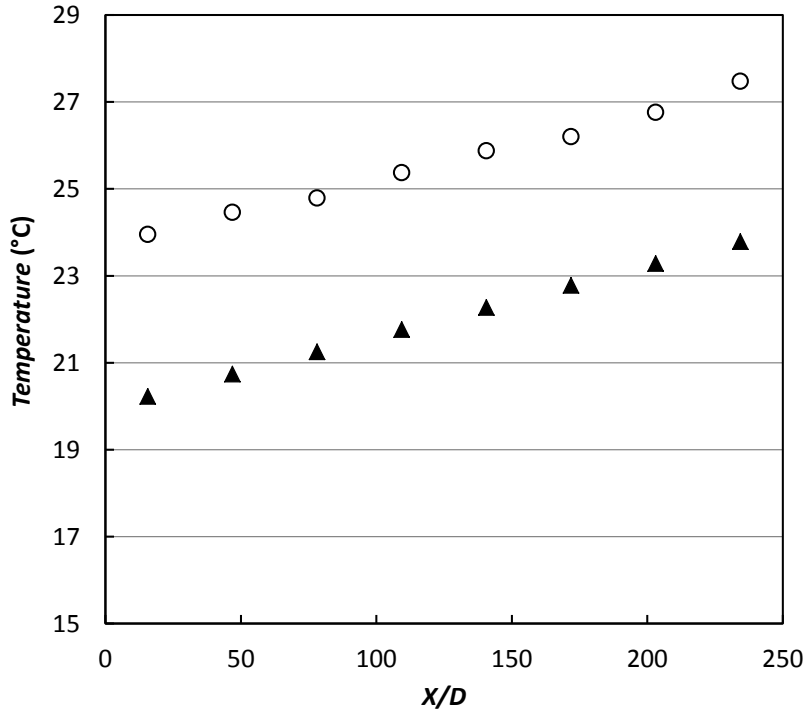

Figure 4.21: Water in turbulent flow, Re=4730, T_{in}=19.4°C, q=11947 W/m^2. ○ wall temperature, ▲ bulk temperature.

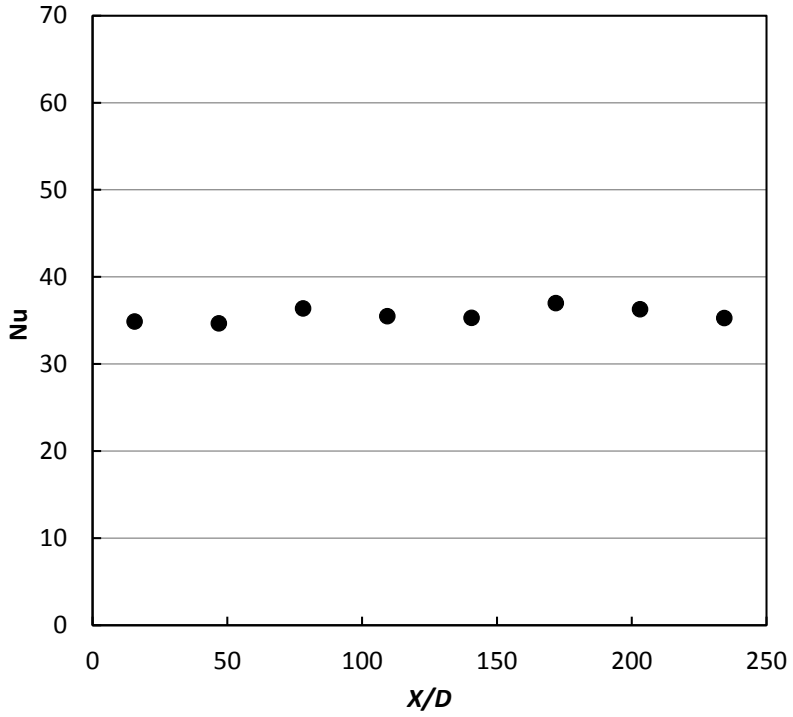

Figure 4.22: Water in turbulent flow, Re=4730, T_{in}=19.4°C, q=11947 W/m^2. Nusselt number.

The thermal balance is within 4% for all the measurements.

The experimental values from the measurements with water were compared with the following equations.

Gnielinski equation [12] valid for liquids (1.5<Pr<500) and Re>2300:

$$\mathrm{Nu} = 0.012\left(\mathrm{Re}^{0.87} - 280\right)\mathrm{Pr}^{0.4} \tag{4.11}$$

Petukhov equation [13] valid for 4000<Re<50000 and 0.7<Pr<60:

$$\mathrm{Nu} = \frac{(\xi/8)\,\mathrm{Re}\,\mathrm{Pr}}{1.07 + 12.7\sqrt{\xi/8}\left(\mathrm{Pr}^{2/3} - 1\right)} \tag{4.12}$$

with the pressure loss coefficient according to [14]:

$$\xi = \left[1.82\log_{10}\left(\mathrm{Re}\right) - 1.64\right]^{-2} \tag{4.13}$$

Gnielinski equation [15] valid for 10^4<Re<10^6 and 0.1<Pr<1000:

$$\mathrm{Nu} = \frac{(\xi/8)\,\mathrm{Re}\,\mathrm{Pr}}{1 + 12.7\sqrt{\xi/8}\left(\mathrm{Pr}^{2/3} - 1\right)}\left\{1 + \left(\frac{D}{L}\right)^{2/3}\right\} \tag{4.14}$$

with the pressure loss coefficient [16]:

$$\xi = \left[1.8\log_{10}\left(\mathrm{Re}\right) - 1.5\right]^{-2} \tag{4.15}$$

Churchill equation [17] valid for 2100<Re<10^4:

$$\mathrm{Nu} = \left(\frac{1}{Nu_t^2} + \frac{1}{Nu_{tr}^2} \right)^{-1/2} \tag{4.16}$$

where $\mathrm{Nu_t}$ indicates the Nusselt number for turbulent flow and $\mathrm{Nu_{tr}}$ for transition region [17]:

$$\mathrm{Nu}_t = 8 + \frac{0.079\,\mathrm{Re}\sqrt{\xi}\,\mathrm{Pr}}{\left(1+\mathrm{Pr}^{4/5}\right)^{5/6}} \tag{4.17}$$

with the pressure loss coefficient given by

$$\frac{1}{\xi} = \left(\frac{1}{\left[\left(\frac{8}{\mathrm{Re}} \right)^{10} + \left(\frac{\mathrm{Re}}{36500} \right)^{20} \right]^{1/2}} + \left(2.21 \ln\left\{ \frac{\mathrm{Re}}{7} \right\} \right)^{10} \right)^{1/5} \tag{4.18}$$

$$\mathrm{Nu_{tr}} = 4.364 \exp\left(\frac{\mathrm{Re} - 2200}{730} \right) \tag{4.19}$$

The maximum, the mean and the minimum deviations of the experimental values from the equations are as follows:

- Gnielinski equation [12] : -14%, -5%, -0.1%,
- Petukhov equation [13]: -23%, -21%, -16%,
- Gnielinski equation [15]: -26%, -24%, -21%,
- Churchill equation [17]: -25%, -22%, -18%.

Deviations are calculated as $\Delta\mathrm{Nu}\% = 100 \cdot (\mathrm{Nu_{experimental}} - \mathrm{Nu_{calculated}}) / \mathrm{Nu_{calculated}}$.

Cited correlations are based on experimental values and high deviations, around 20%, are frequently observed, *e.g.* in Huber and Walter [18].

In Figure 4.23 an example of experimental and calculated Nu is shown.

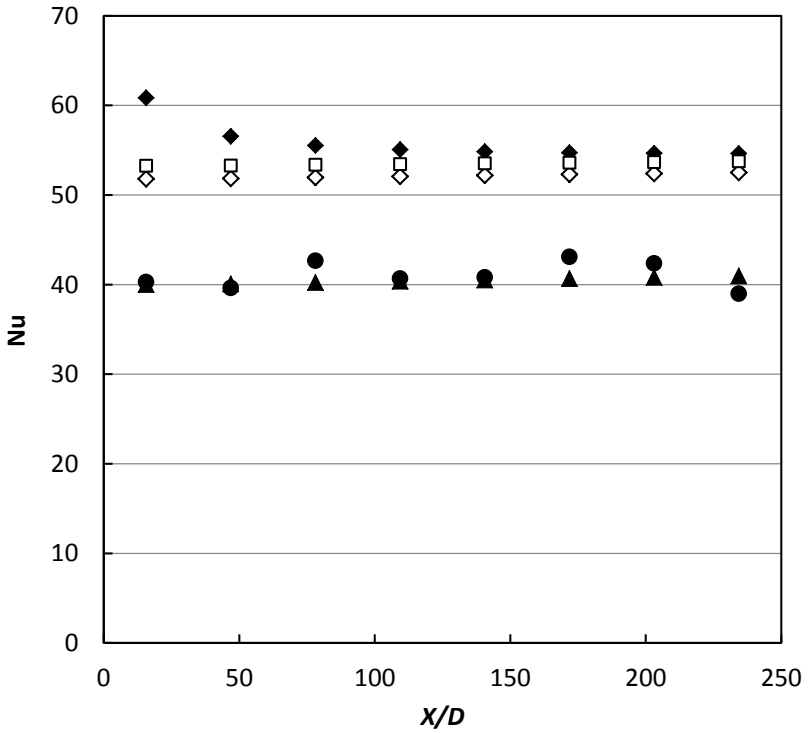

Figure 4.23: Water in turbulent flow, Re=6960, T_{in}=40.6°C, q=7964 W/m^2. Nusselt number as a function of the ratio distance from the tube inlet / inner diameter. ● experimental, ▲ Gnielinski equation (4.11), ◊ Petukhov equation (4.12), ♦ Gnielinski equation (4.14), □ Churchill equation (4.16).

4.5 Uncertainty analysis

The experimental uncertainty was analysed for each parameter.

In the case of water, the uncertainties on the calculated properties as c_p, ρ, λ and μ are 0.1%, 0.0001%, 0.01% and 1% respectively, as declared in Refprop 9.0, relatively to the model employed for the estimation [19].

The measurements uncertainty for the wall temperature was calculated considering the uncertainty of the thermocouples calibration, the uncertainty of the Pt100 sensor and the uncertainty of the acquisition system. Resulting value is 0.1°C.

The uncertainty of the bulk inlet temperature is the uncertainty of the Pt100 sensor, 0.05°C. The other bulk temperatures have an uncertainty value calculated by propagating the uncertainties on the individual input parameters in equations 4.7 and 4.8, where T_{in} is Pt100 temperature, the mass flow rate $m=\rho vA$ and the power supplied $Q=qSx_1$.

For uncertainties propagation, the standard methodology applicable to normal distributions was used. For any generic function y =f (x_1, x_2,…,x_n), the composed uncertainty for x_i non correlated was calculated as follows:

$$i_c = \sqrt{\sum_{i=1}^{n}\left(\left(\frac{\partial f}{\partial x_i}\right)\cdot i_{x_i}\right)^2} \qquad (4.20)$$

In turn, the uncertainty of mass flow rate m is 0.05%, as declared by the Coriolis mass flowmeter constructor, considering negligible the uncertainty of the acquisition (0.00000176 kg/s).

The uncertainty of the heat flux is calculated knowing the accuracy of voltage and current supplied by the System DC Power Supply N5771A, which are 0.1% of reading value + 300 mV and 0.1% of reading value + 15 mA. They are acquired directly by a LabVIEW data acquisition, using a GPIB controller. The power experimental uncertainty is 0.56%.

The uncertainty on the value of the predicted heat transfer coefficient was calculated by propagating the uncertainties on the individual input parameters in equation 4.10, assuming negligible the uncertainty of the area.

In the case of nanofluids, the uncertainty analysis is more complex, due to other variables, which must be taken into account. If the nanofluid is commercial and the mass fraction constant, the uncertainty on the mass or volume fraction is declared by the manufacturer. If the mass fraction varies, because of adding of water, the mass fraction contains an additional uncertainty caused by the error done in the weighing. The uncertainty on the volume fraction considers the uncertainty on the density of water and nanoparticles. The uncertainties on c_p and ρ, considers the uncertainty on c_p and ρ of water and nanoparticles. The uncertainties on λ and μ are 1% and 1.5% respectively.

The uncertainty on the heat transfer coefficient is particularly affected by the temperature difference in equation 4.10. Increasing the difference between wall temperature and bulk temperature, the uncertainty diminishes.

4.6 Conclusions

An experimental apparatus was built in order to measure the convective, single phase heat transfer coefficient of nanofluids, at constant wall heat flux. The circuit was tested with water in order to verify the operation using a fluid of known properties. Results confirm that the circuit is suitable for heat transfer coefficient measurements.

References

[1] K.S. Hwang, S.P. Jang, S.U.S. Choi, "Flow and convective heat transfer characteristics of water based Al_2O_3 nanofluids in fully developed laminar flow regime", *International Journal of Heat and Mass Transfer*, 52, 193–9 (2009).

[2] D.S. Wen, Y.L. Ding, "Experimental investigation into convective heat transfer of nanofluid at the entrance region under laminar flow conditions", *International Journal of Heat and Mass Transfer*, 47, 5181–5188 (2004).

[3] D.J. Faulkner, D.R. Rector, J.J. Davidson, R. Shekarriz, "Enhanced Heat Transfer Through the Use of Nanofluids in Forced Convection", ASME Paper No. IMECE2004-62147 (2004).

[4] B. Pak, Y.I. Cho, "Hydrodynamic and Heat Transfer Study of Dispersed Fluids With Submicron Metallic Oxide Particle", *Experimental Heat Transfer*, 11, 151–170 (1998).

[5] Y. Xuan, Q. Li, "Investigation on Convective Heat Transfer and Flow Features of Nanofluids", *ASME Journal of Heat Transfer*, 125, 151–155 (2003).

[6] C.T. Nguyen, G. Roy, C. Gauthier, N. Galanis, "Heat Transfer Enhancement Using Al_2O_3-Water Nanofluid for an Electronic Liquid Cooling System", *Applied Thermal Engineering*, 27, 1501–1506 (2007).

[7] N. Prabhat, J. Buongiorno, L.W. Hu, "Convective Heat Transfer Enhancement in Nanofluids: Real Anomaly or Analysis Artifact?", *Journal of Nanofluids*, T10070-T10070 (2011).

[8] Y. Ding, H. Chen, L. Wang, C.Y. Yang, Y. He, W. Yang, W.P. Lee, L. Zhang, R. Huo, "Heat Transfer Intensification Using Nanofluids", *KONA Powder and Particle*, 25, 23–38 (2007).

[9] X.Q. Wang and A.S. Mujumdar, "Heat Transfer Characteristics of Nanofluids: A Review", *International Journal of Thermal Sciences*, 46, 1, 55–62 (2007).

[10] W. Yu, D.M. France, E.V. Timofeeva, D. Singh, J.L. Routbort, "Comparative Review of Turbulent Heat Transfer of Nanofluids", *International Journal of Heat Transfer*, 55, 5380–5396 (2012).

[11] V. Bianco, O. Manca, S. Nardini, "Numerical Simulation of Water/Al2O3 Nanofluid Turbulent Convection", *Advances in Mechanical Engineering*, 976254 (2010).

[12] V. Gnielinski, "New equations for heat and mass transfer in turbulent pipe and channel flow", *International Journal of Chemical Engineering*, 16, 359-368 (1976).

[13] B. S. Petukhov, V. V. Kirillov, "To the question of heat transfer in turbulent pipe flow of liquids in tubes (Zur Frage des Wärmeübergangs bei turbulenter Strömung von Flüssigkeiten in Rohren)", Teploenergetika, 4, 63 (1958).

[14] G. K. Filonenko, Hydraulic resistance of pipes (Hydraulischer Widerstand von Rohrleitungen), Teploenergetika, 1, 40 (1954).

[15] V. Gnielinski, "A new calculation procedure for the heat transfer in the transition region between laminar and turbulent pipe flow (Ein neues Berechnungsverfahren für die Wärmeübertragung im Übergangsbereich zwischen laminarer und turbulenter Rohrströmung)", Forschung im Ingenieurwesen, 61, 9, 240 (1995).

[16] P. K. Konakov, "A new equation for the friction coefficient for smooth tubes (Eine neue Formel für den Reibungskoeffizienten glatter Rohre)", Report of the academic society for science of the UDSSR, LI51, 7, 503 (1946).

[17] S. W. Churchill, "Comprehensive correlating equations for heat, mass and momentum transfer in fully developed flow in smooth tubes", *Industrial & Engineering Chemistry*, 16, 109 (1977).

[18] D. Huber, H. Walter, *Proceedings of the 2010 international conference on theoretical and applied mechanics, and 2010 international conference on Fluid mechanics and heat & mass transfer*, 132 (2010).

[19] E.W. Lemmon, M.L. Huber, M.O. McLinden, NIST Standard Reference Database 23, Reference Fluid Thermodynamic and Transport Properties (REFPROP), version 9.0; National Institute of Standards and Technology (2010).

Chapter 5

Water based TiO_2 nanofluid characterization

Titanium oxide (TiO_2) nanoparticles are commonly used in applications ranging from cosmetics to paints. These nanoparticles production is consolidated and therefore a large scale production of TiO_2 water-based nanofluid is possible. In literature, TiO_2 water-based nanofluids are some of the most studied nanofluids.

In this chapter, the characterization of TiO_2 water-based nanofluids in concentrations ranging between 1 and 35 % in mass is presented.

5.1 Nanofluid preparation

Water-based nanofluid with TiO_2 at 35 wt% was purchased by Sigma-Aldrich. Acetic acid was present as dispersant at 1-5 wt%.

Bidistilled water (CARLO ERBA, Bidistilled water, CAS Nr 7732-18-5) was used to dilute the 35% wt nanofluid and obtain the other desired nanofluid compositions (1 wt%, 10 wt% and 20 wt%). In fact, starting from the fluid at 35 wt%, the other mass fractions were prepared taking the nanofluid after one hour sonication and adding bidistilled water in a weighed amount, measured by an analytical balance (Gibertini E42S 240 g FS), with an uncertainty of 0.0002 g. The four nanofluids were further sonicated in order to improve the dispersion of nanoparticles in the water.

5.2 Nanofluids stability characterization

The DLS was used to analyse the average dimension of the nanoparticles in solution. All size measurements were made at 25°C with a scattering angle of 173°. One set of measurements was made to verify the dependency of the nanoparticles size from the concentration of the solution. After sonication, the TiO_2 mean particle diameter, measured 3 times for each sample, was 76 nm at 1 wt%, 72 nm at 10 wt% and 73 nm at 20 wt%. Figure

5.1 shows the particle size distribution, according to the intensity detected by the Zetasizer, for the water-TiO_2 nanofluids at these compositions. The absence of particle micrometer-sized aggregates confirmed the good stability of the obtained dispersions. The forth solution (35 wt%) could not be measured since this concentration is too high, giving a not transparent fluid to the light and problem of multiple scattering. However, considering the measured values for the other concentrations, nanoparticle size is assumed to be independent from concentration.

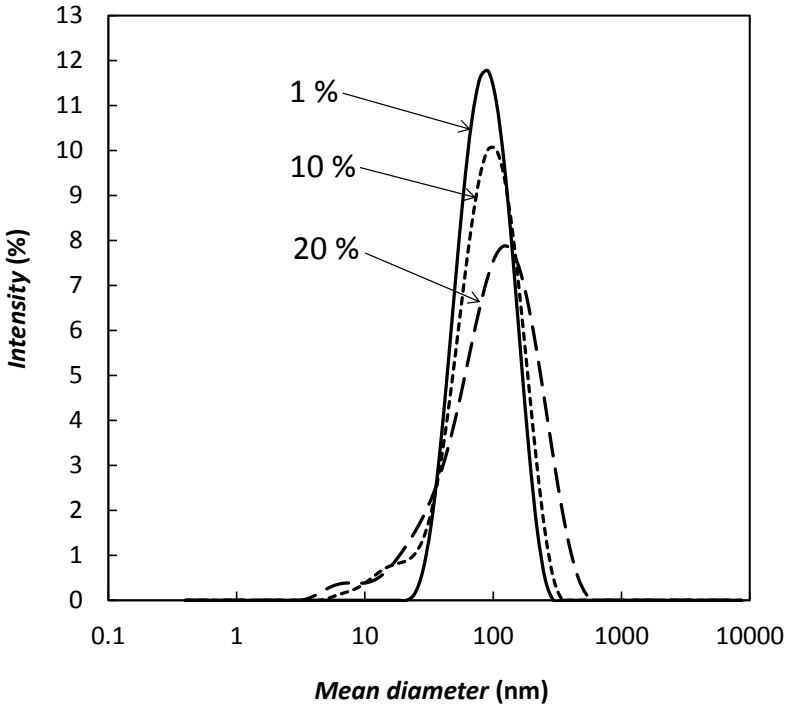

Figure 5.1: Nanoparticles size distribution for water containing TiO_2 at 1 wt% (—), 10 wt% (---), 20 wt% (− · −).

The analysis, already described in chapter 2.5.2, was made to determine the tendency of the particles in suspension to settle down along time. Since the mean diameter was found to be the same for all the compositions, only the solution at 1 wt% was investigated with this method. The variation along time of TiO_2 nanoparticle mean diameters, with TiO_2 at 1 wt%, is shown in Figure 5.2.

In the case of static solutions the mean size slightly decreased to around 51 nm after 35 days, indicating a partial precipitation. However, after sonication for one hour, a mean particle size centred on 76 nm was always recovered, suggesting the absence of further

aggregation phenomena. This result is interesting because it suggests a possible application of these fluids in devices where they are frequently or continuously stirred, *e.g.* in plants with forced circulation.

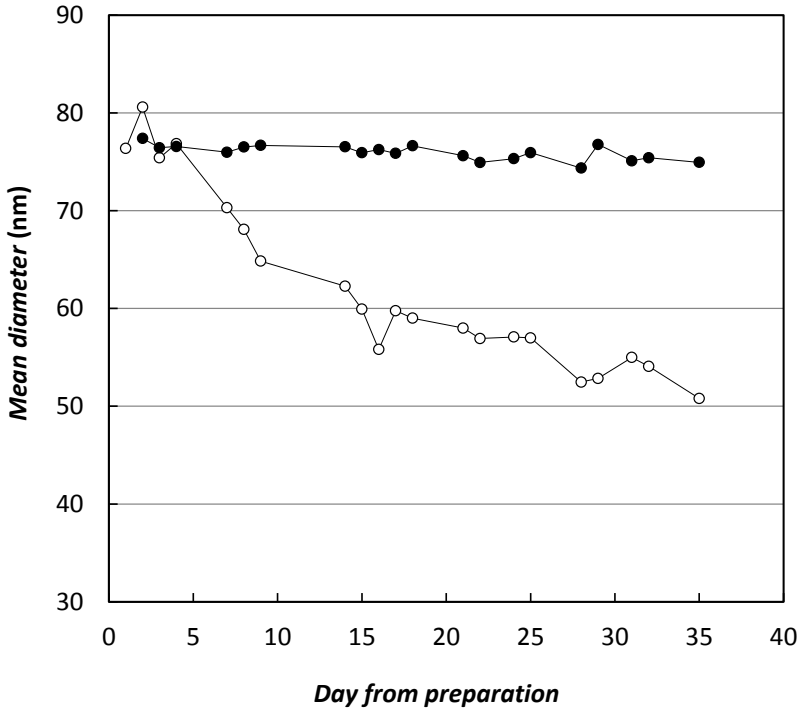

Figure 5.2: Nanoparticles mean diameter in relation to the time elapsed from the day of preparation in water-based nanofluids containing TiO_2 at 1 wt%. (○) static and (●) stirred samples at the DLS.

ζ potential and pH of each nanofluid of TiO_2-water nanofluids has been measured as described in paragraphs 2.5.2 and 2.5.3. ζ potential was around 55 mV, higher than the empirical limit of 30 mV over which a colloidal solution should be stable. The pH increases with dilution and the values were 3.1 for the 1 wt% solution, 2.4 for 10 wt%, 2.2 for 20 wt% and 1.9 for 35 wt%.

5.3 Thermal conductivity

Thermal conductivity of TiO_2-water nanofluids was measured, in order to evaluate its possible enhancement as a function of temperature and nanoparticle concentration.

Table 5.1 presents the thermal conductivity of the nanofluids and the thermal conductivity ratio in relation to pure water.

Thermal conductivity increases with temperature and with increasing nanoparticles concentration. For the 1 wt% nanofluid, the measured enhancement is, within the experimental uncertainty, negligible at temperatures lower than 50°C, while at higher temperatures a significant increase in thermal conductivity is observed. For all the nanofluids, the enhancement on thermal conductivity raises with temperature.

Table 5.1: Thermal conductivity and thermal conductivity ratio, related to pure water from Refprop 9.0 database [1] for 1 wt%, 10 wt%, 20 wt% and 35 wt% TiO_2 water-based nanofluids at different temperatures.

Mass fraction	1 wt%		10 wt%		
Vol. fraction	0.24 vol%		2.54 vol%		
***T* (°C)**	**λ (W/mK)**	$\lambda_{exp}/\lambda_{water}$	***T* (°C)**	**λ (W/mK)**	$\lambda_{exp}/\lambda_{water}$
20.7	0.6063	1.012	21.2	0.6191	1.031
30.7	0.6220	1.039	30.6	0.6368	1.034
40.5	0.6456	1.023	40.5	0.6586	1.044
50.2	0.6891	1.071	50.3	0.6937	1.078
59.5	0.7097	1.086	57.4	0.7132	1.095
69.5	0.7308	1.103	68.8	0.7738	1.169
79.4	0.7880	1.177	79.4	0.8351	1.247
Mass fraction	20 wt%		35 wt%		
Vol. fraction	5.54 vol%		11.22 vol%		
***T* (°C)**	**λ (W/mK)**	$\lambda_{exp}/\lambda_{water}$	***T* (°C)**	**λ (W/mK)**	$\lambda_{exp}/\lambda_{water}$
21.8	0.6514	1.083	21.2	0.7279	1.213
30.7	0.6773	1.099	30.6	0.7554	1.226
40.4	0.7162	1.135	40.7	0.7790	1.234
50.0	0.7249	1.127	50.2	0.8028	1.247
60.0	0.7548	1.154	59.7	0.8577	1.312
68.2	0.7938	1.200	68.9	0.8811	1.331
79.3	0.8675	1.296	79.8	0.8921	1.332

In Figure 5.3 the thermal conductivity ratio is reported in relation to the mass fraction of the nanoparticles at different temperatures. Linear interpolation lines are introduced to highlight the trends. The graph is divided in two parts by a diagonal which represent the proportional increase of the conductivity ratio with the mass fraction.

Thermal conductivity increases less than proportionally at any temperature with increasing nanoparticles concentration. At a given mass fraction, in the very dilute region (ω_{TiO2} = 1%) the enhancement is more than proportional to the mass fraction at any temperature, e.g., at 80°C almost 20% enhancement is achieved. At intermediate mass fractions, the enhancement is more than proportional to the mass fraction only at high temperatures. At 35 % mass fraction, the enhancement is less than proportional to the mass fraction at any temperature (from 20% to 33%). In any case, the enhancement increases at increasing temperatures, the maximum value being 38.1% for 35 wt% nanofluid at 70°C. At a given temperature, the enhancement is less than proportional to TiO_2 mass fraction for the low temperatures, while it is more than proportional at temperatures over 70°C.

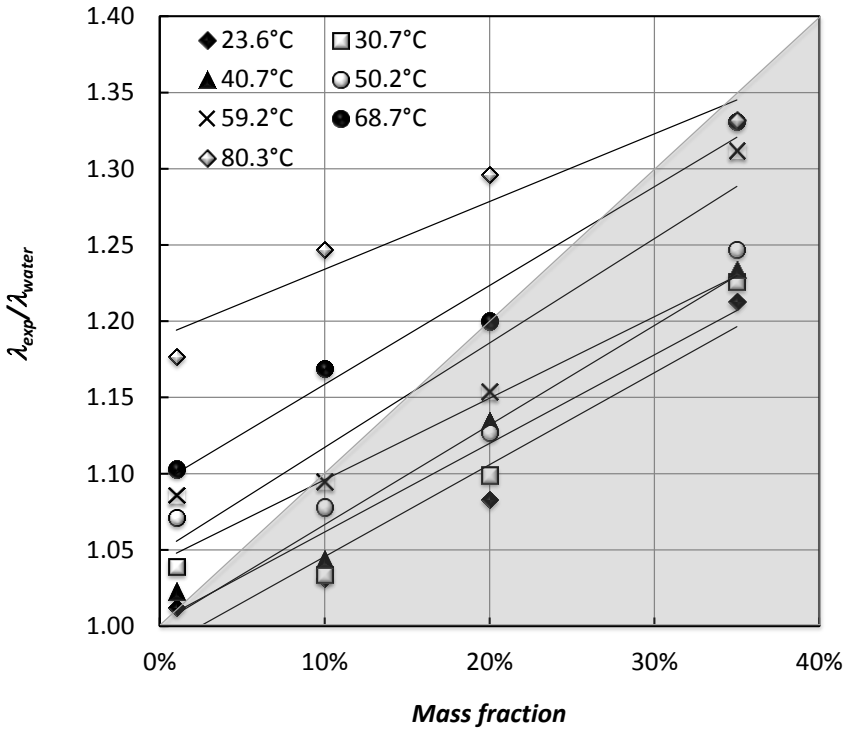

Figure 5.3: Thermal conductivity ratio, related to pure water from Refprop 9.0 database [1], for 1 wt%, 10 wt%, 20 wt% and 35 wt% TiO_2 water-based nanofluids at different temperatures. (♦) 23.6, (□) 30.7, (▲) 40.7, (○) 50.2, (x) 59.2, (●) 341.7, and (◊) 80.3°C.

It is worth noting some troubles have been encountered on measurements at temperatures above 50°C. At high temperature the fluid tends to evaporate, but bubbles start to appear at different temperature depending on the nanoparticles concentration. The higher the particles mass fraction, the lower the temperature at which the bubbles become visible.

5.4 Dynamic Viscosity

Table 5.2 shows the experimental viscosity values (μ_{exp}) for all the nanofluids at constant shear rate (about 755 1/s) and the enhancement on viscosity (μ_{exp}/μ_{water}) related to pure water from Refprop 9.0 database [1] (μ_{water}).

Table 5.2: Viscosity and viscosity ratio, related to pure water from Refprop 9.0 database [1] for 1 wt%, 10 wt%, 20 wt% and 35 wt% TiO_2 water-based nanofluids at different temperatures, at a shear rate of about 755 1/s.

Mass fraction	1 wt%		10 wt%	
Vol. fraction	0.24 vol%		2.54 vol%	
***T* (°C)**	μ_{exp} **(Pa s)**	μ_{exp}/μ_{water}	μ_{exp} **(Pa s)**	μ_{exp}/μ_{water}
10	0.00132	1.0108	0.001577	1.2076
20	0.001023	1.0214	0.001235	1.233
30	0.000793	0.9947	0.000921	1.1546
40	0.000645	0.9881	0.000792	1.2134
50	0.000533	0.9758	0.000666	1.2172
60	0.000491	1.0519	0.00056	1.2013
70	0.000412	1.0201	0.000481	1.1909

Mass fraction	20 wt%		35 wt%	
Vol. fraction	5.54 vol%		11.22 vol%	
***T* (°C)**	μ_{exp} **(Pa s)**	μ_{exp}/μ_{water}	μ_{exp} **(Pa s)**	μ_{exp}/μ_{water}
10	0.002165	1.6579	0.004058	3.1074
20	0.001625	1.6224	0.003091	3.0861
30	0.001323	1.6592	0.002516	3.1555
40	0.001046	1.6019	0.00212	3.2467
50	0.000857	1.5668	0.001765	3.2276
60	0.000759	1.6276	0.001521	3.2611
70	0.000669	1.6564	0.001382	3.4217

The deviations between nanofluid and water viscosity are about 20%, 60% and 215% at 10 wt%, 20 wt% and 35 wt% TiO_2 concentration, respectively. It can be noted that the viscosity enhancement is almost independent from temperature for all the concentrations

here analyzed. The nanofluid at 1 wt% shows a water-like behaviour and a variation, with respect to water, within the experimental error, but at the higher concentrations the viscosity enhancement becomes unproportional and quite elevated.

Nanofluid behaviour is always Newtonian, as can be deduced by Figure 5.4, where shear stress is represented as a function of shear rate for the 35 wt% nanofluid. All isotherms are linear and converge to the origin of the diagram.

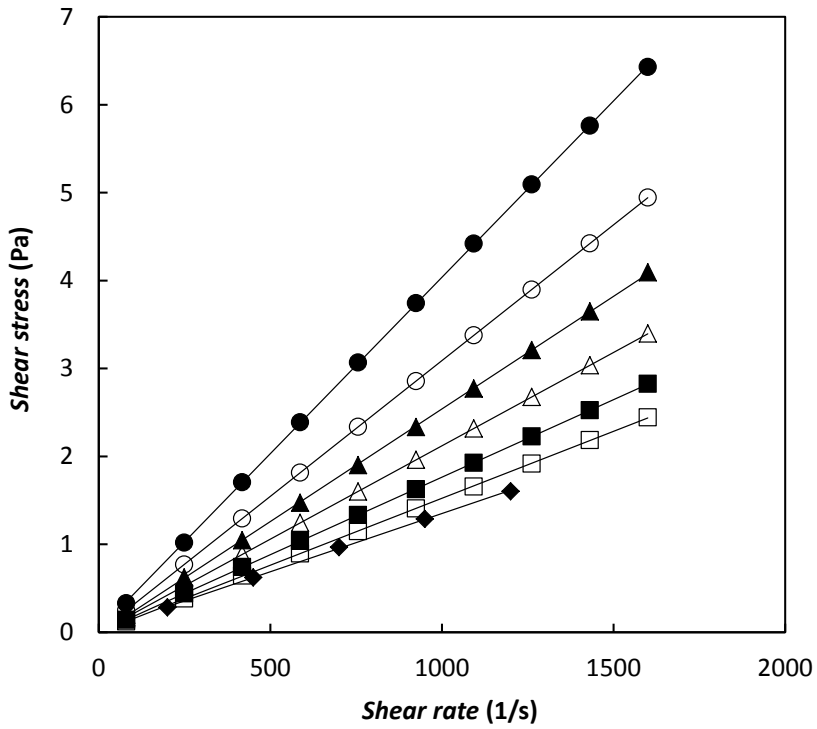

Figure 5.4: Shear stress as a function of shear rate for water-TiO_2 nanofluid at 35 wt% at (●) 10, (○) 20, (▲) 30, (Δ) 40, (■) 50, (□) 60 and (♦) 70°C.

5.5 Comparison with published literature

In Figure 5.5, a comparison with some experimental data is also proposed.

Murshed *et al*. [2] measured thermal conductivity of TiO_2-water nanofluids with cetyltrimethtlammoniumbromide (CTAB) surfactant at ambient temperature and revealed very higher conductivity values, if compared with our results at the same temperature and on respect to the Hamilton and Crosser model.

Zhang *et al*. [3] performed conductivity measurement on TiO_2-water nanofluids at 10°C, 30°C and 40°C at low concentrations and their results are in good agreement with data here reported.

Duangthongsuk and Wongwises [4, 5] studied thermal conductivity of TiO_2-water nanofluids at temperatures ranging between 15°C and 35°C. Their values are higher than data here described for the same compositions and temperatures.

However a comparison with literature data is not easy because many parameters affecting nanofluid behavior are not available in the papers, as the employed preparation method or pH value. For this reason, fluids containing the same particles can exhibit different behaviours.

In literature, only two papers on viscosity measurements for TiO_2-water nanofluid at the same shear rates here considered have been found, but no numerical values are available. Chen *et al.* [6] found a Newtonian behaviour at room temperature for particle volume concentration less than 1.5%. Only one volume concentration is comparable with our concentrations and no discordance has been found. Tseng and Lin [7] observed a pseudoplastic flow behaviour in the compositions range between 5% and 12% by volume. They found viscosity values higher than those observed for our nanofluids, for all the volume concentrations.

5.5.1 Thermal conductivity

The Maxwell model, equation 3.14, was used to predict the thermal conductivity of the suspensions, assuming they contain spherical particles and considering only the dependency on the particle volume fraction. However, thermal conductivity of suspensions also depends on size and shape of particles. Therefore, the Hamilton and Crosser model, equation 3.15, was also considered for comparison.

Figure 5.5 shows the experimental thermal conductivity ratio in relation to the mass fraction of the nanoparticles, at different temperatures, for the present measurements and some literature data sets (chapter 5.5) in comparison with the predictions of the Hamilton and Crosser (H-C) model.

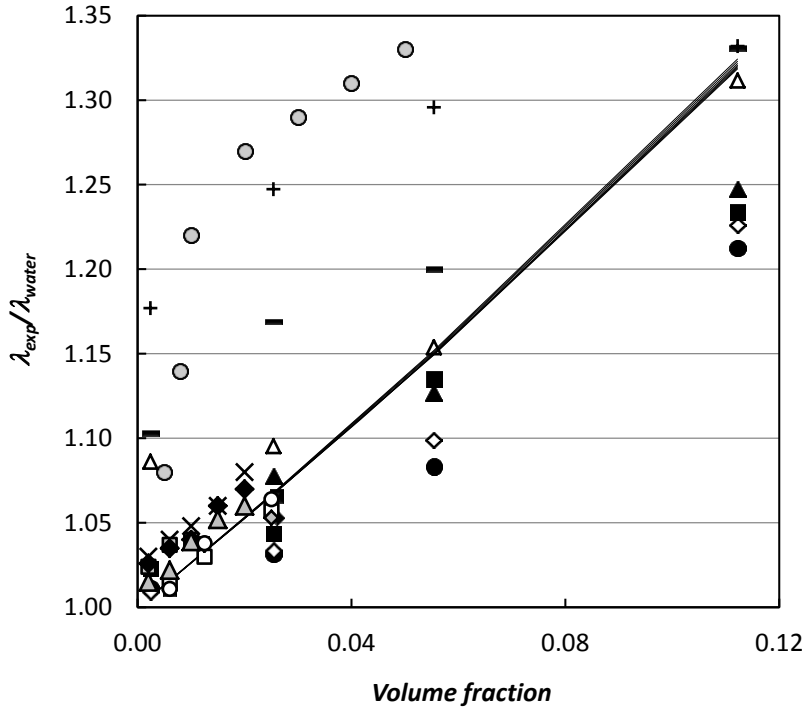

Figure 5.5: Comparison between literature data on TiO_2-water- nanofluids of $\lambda_{exp}/\lambda_{water}$ at (●) 23.6, (◊) 30.7, (■) 40.7, (▲) 50.2, (Δ) 59.2, (-) 68.7, and (+) 80.3 °C (this work); (□) 10, (♦) 30, and (○) 40°C (Zang *et al.* [3]); (x) 15, (♦) 25, (▲) 35 K (Duangthongsuk *et al.* [4]), and (■) ambient temperature (Duangthongsuk *et al.* [5]); (●) ambient temperature (Murshed *et al.* [2]).

The lines represent the Hamilton and Crosser model at different temperatures.

The Hamilton and Crosser model, equation 3.15, always overestimates the thermal conductivity enhancement with respect to experimental data at temperatures between 23°C and 50°C, while overestimates the enhancement at temperatures between 59°C to 80°C.

5.5.2 Dynamic viscosity

A comparison between the Batchelor predictive model, equation 3.5, and the experimental data was made.

Figure 5.6 shows the experimental and the calculated viscosities with respect to temperature, for the different particle concentrations. The model is in agreement with the experimental values for the fluid at 1 wt%, while at higher nanoparticles mass fractions the model underestimates the viscosity behaviour.

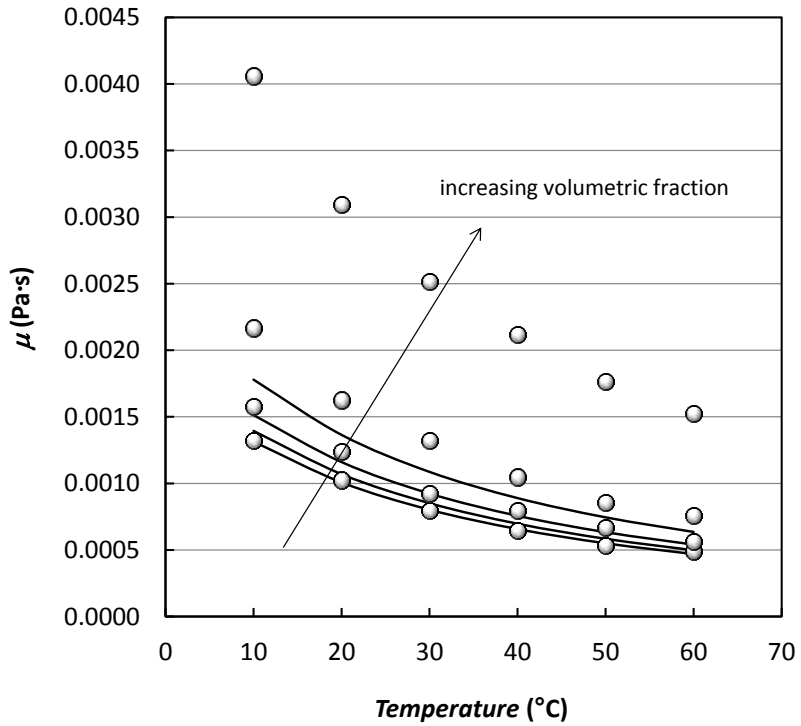

Figure 5.6. Experimental viscosity (○) of nanofluids as a function of temperature. Comparison with Batchelor model (—).

5.6 Conclusions

Water-based nanofluids containing TiO_2 nanoparticles has been studied at four different nanoparticle concentrations (1 wt%, 10 wt%, 20 wt% and 35 wt%), at experimental temperatures ranging between 10°C and 70°C and between 20°C and 80°C for viscosity and conductivity measurements, respectively, with steps of 10°C. All the fluids resulted quite stable in a static situation and completely stable after sonication for one hour. The average particle diameter was 76 nm and no aggregations were found.

The measured thermal conductivity of TiO_2-water nanofluids increases with mass concentration and with temperature. The effect of increasing conductivity is more evident at higher temperatures.

All the nanofluids exhibited a Newtonian rheological behaviour. The viscosity enhancement, related to pure water, was independent from temperature for all the concentrations here analysed. The nanofluid at 1 wt% shows a water like behaviour and a variation, with respect to water, within the experimental error, but at the higher concentrations the viscosity enhancement is not proportional and surprisingly excessive (+243% for 35 wt% at 70°C).

References

[1] E.W. Lemmon, M.L. Huber, M.O. McLinden, NIST Standard Reference Database 23, Reference Fluid Thermodynamic and Transport Properties (REFPROP), version 9.0; National Institute of Standards and Technology (2010).

[2] S.M.S. Murshed, K.C. Leong, C. Yang, "Enhanced thermal conductivity of TiO_2 – water based nanofluids", *International Journal of Thermal Sciences 44, 367-373 (*2005).

[3] X. Zhang, H. Gu, M. Fujii, "Experimental Study on the Effective Thermal Conductivity and Thermal Diffusivity of Nanofluids", *International Journal of Thermophysics, 27, 2, 569-580 (*2006).

[4] W. Duangthongsuk and S. Wongwises, "Effect of thermophysical properties models on the predicting of the convective heat transfer coefficient for low concentration nanofluid", *International Communications in Heat and Mass Transfer*, 35, 1320-1326 (2009).

[5] W. Duangthongsuk and S. Wongwises, "Comparison of the effects of measured and computed thermophysical properties of nanofluids on heat transfer performance", *Experimental Thermal and Fluid Science*, 34, 616-624 (2010).

[6] H. Chen, S. Witharana, Y. Jin, C. Kim, Y. Ding, "Predicting thermal conductivity of liquid suspensions of nanoparticles (nanofluids) based on rheology", *Particuology*, 7, 151-157 (2009).

[7] W.J. Tseng and K.C. Lin, "Rheology and colloidal structure of aqueous TiO_2 nanoparticle suspensions", *Materials Science and Engineering*, A355 186-192. 2765 (2003).

Chapter 6

Water based SWCNH nanofluid characterization

Carbon nanostructures (single or multi-wall carbon nanotubes (SWCNT, MWCNT), carbon nanohorns (CNH), fullerene, graphene), amorphous carbon (Carbon-black, labeled as CB and Thermax Cancarb N99) are very promising materials in terms of heat transfer, because of their high thermal conductivity. However, they are expensive and difficult to produce on a large scale and their effects on environment and health are not well known till now. In order to understand the SWCNH-water nanofluid properties, the viscosity was measured at ambient pressure and in the temperature range between 10°C and 80°C. Using the rheometer, the Newtonian behaviour should be evaluated and the data were regressed by viscosity correlations. Thermal conductivity was measured for the nanofluid at 0.1 wt%.

6.1 Nanofluid preparation

Deionised water (Millipore, Billerica MA, USA, 18.2 Ω) was used as base fluid. The SWCNHs used in this work were produced and provided by Carbonium Srl. The SWCNHs are roughly spherical aggregates of nanohorns consisting in a single layer of a graphene sheet wrapped into an irregular tubule with a variable diameter of generally 2-5 nm and a length of 30-50 nm, with their tips cone-shaped. The SWCNHs are mainly of three types: dahlias, buds and seeds [1, 2]. The critical point that differentiates SWCNHs from carbon nanotubes (CNTs), that showed important thermal conductivity increase [2], is their much lower toxicity [3], due to both the lack of fibril-like structure and the absence of any metal nanoparticles used to catalyse nanotube growth during their production. Moreover, their heterogeneous surface structure favours their dispersion in water.

The morphological characterization of nanoparticles was performed by field emission scanning electron microscopy (FE-SEM) with a SIGMA Zeiss instrument (Carl Zeiss SMT Ltd, UK). A SEM picture of SWCNHs is shown in Figure 6.1, where the actual dimensions of nanoparticles can be deduced to be 60 nm.

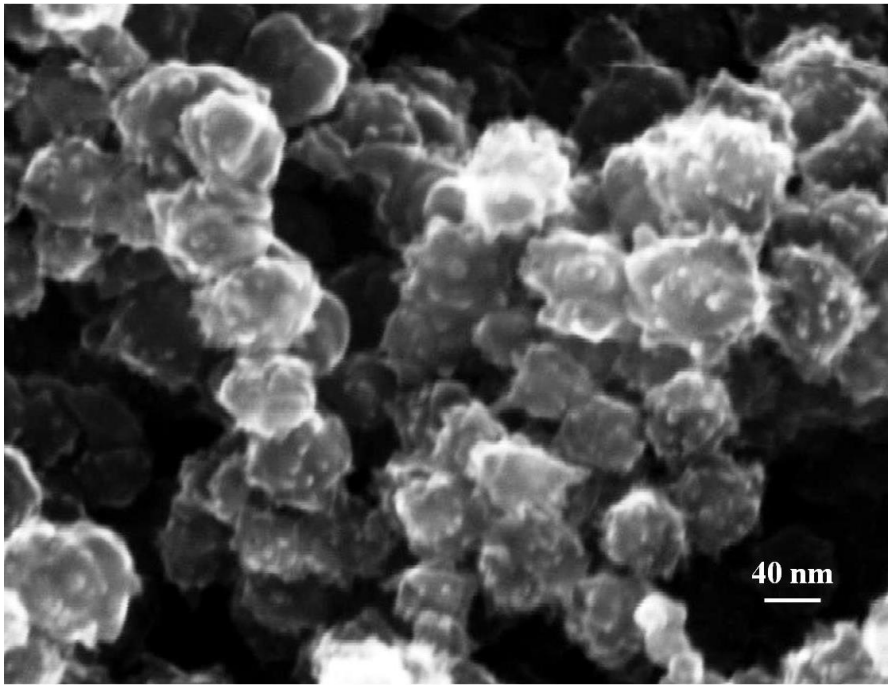

Figure 6.1: SEM (Scanning Electron Microscope) images of SWCNH nanoparticles.

The use of dispersants was necessary to stabilize the nanoparticle dispersions. After careful analysis of the average size distribution of the nanoparticles in solution along time by means of a DLS apparatus, sodium *n*-dodecyl sulphate (SDS, 99%, Alfa Aesar) was used as dispersant for the nanofluid.

The nanofluids were prepared by dispersing the nanoparticles in water by a two-step method. Different preparation methods (ultrasonic agitation, ball milling and homogenization), described in chapter 2, and different dispersants were proven. The high pressure homogenization method turned out to be the best process to improve the suspension stability and then it was used to prepare SWCNH-water nanofluid. The nanoparticles were mechanically dispersed in water at different concentrations, *i.e.* 0.01%, 0.1%, 1% by mass. Then, a high pressure homogenizer (up to 1000 bar) was employed to optimize the dispersion. For the nanofluids at concentrations of 0.1% and 1% by mass, the ratio between nanoparticles and dispersant mass was 1:1. For the lowest concentration (0.01% by mass), the ratio was 1:3.

6.2 Nanofluids stability characterization

As described in chapter 2, the DLS technique was used to determine the tendency of the particles in suspension to settle down along time. Figure 6.2 shows the particle size distribution, according to the intensity detected by the Zetasizer, for the water-SWCNH nanofluids, just after preparation and after 18 days. The nanofluids formed by water, SDS and SWCNH are very stable even after several days. The measured nanoparticle average diameter was around 140 nm, 188 nm and 120 nm for the 0.01%, 0.1% and 1% mass concentrations, respectively. The ζ potential of nanofluids was also measured by Zetasizer Nano and in Table 6.1 the values are shown. All the measured nanofluids show a ζ potential higher than |30| mV.

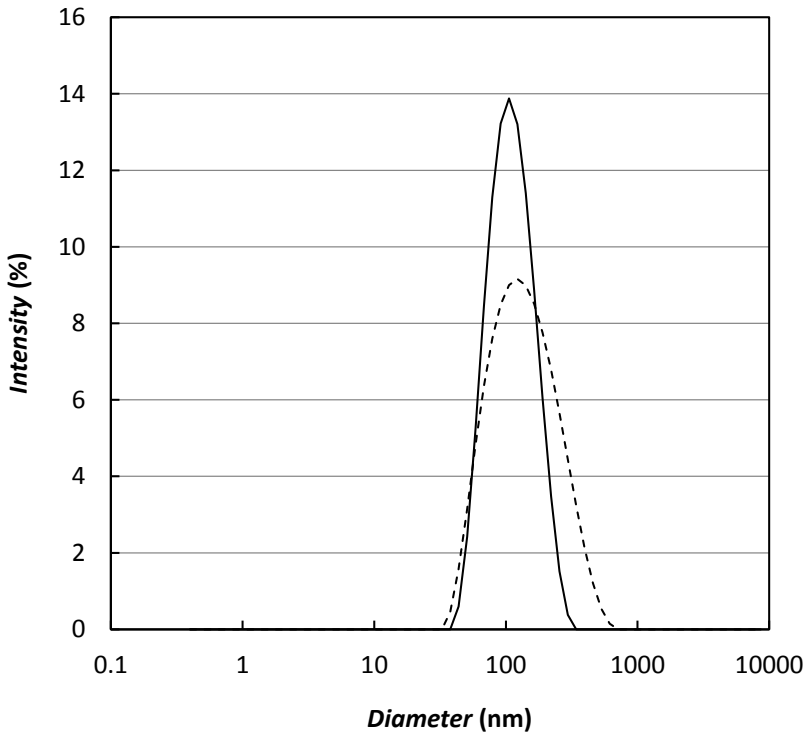

Figure 6.2: Particle diameter size distribution, according to the intensity, for the water-SWCNH nanofluids (with dispersants), (─) just after preparation and (- - -) after 18 days.

Table 6.1: ζ potential for SWCNH nanofluids with dispersants.

nanofluid	ζ potential (|mV|)
SWCNH 1 wt%, SDS 1 wt%	56
SWCNH 0.1 wt%, SDS 0.1 wt%	57
SWCNH 0.01 wt%, SDS 0.03 wt%	50

6.3 Dynamic Viscosity

The dynamic viscosity data were measured at ambient pressure and in a temperature range between 10°C and 80°C. All the measurements were performed at constant temperature and variable shear rate, starting from 200 1/s to 1600 1/s and vice versa, at constant step of about 150 1/s (except for temperatures higher than 60°C, at which faster measurements had to be performed, due to water evaporation). A conditioning step of 10 seconds was carried out and a pre-shear rate at 200 1/s was applied before the measurements to remove any possible fluid "memory", due to the sample preparation, storage and loading. Each experimental point is the average of three values of viscosity, sampled under constant shear rate.

The investigated fluids, apart from bidistilled water, were:

- water + SDS at 0.03%, 0.1% and 1% by mass;
- water + SWCNH at 0.01%, 0.1%, 1% by mass + SDS at 0.03%, 0.1% and 1% by mass, respectively.

In Figure 6.3, viscosity data of the measured fluids at 10°C are represented.

As shown in the figure, base fluids formed by water and SDS, both at the 0.03% and 0.1% by mass, have viscosities very similar to water. SDS shows its influence at concentration of 1% by mass, with a viscosity enhancement of about 7%. Even viscosities of nanofluids with SWCNH at 0.01% and 0.1% are similar or lower than those of water. On the contrary, the viscosity of water-SDS-SWCNH at 1% nanofluid increases of about 13%.

Table 6.2 summarizes the viscosity measurements for all the SWCNH-nanofluids at the different compositions at constant shear rate (about 800 1/s). It should be noted that measurements at 80°C are difficult to perform, since water begins to vaporize and nanoparticles begin to aggregate.

In Figure 6.4, the trend of the shear stress as a function of the shear rate is shown, at each composition, at 10°C, evidencing a Newtonian behaviour of the nanofluids.

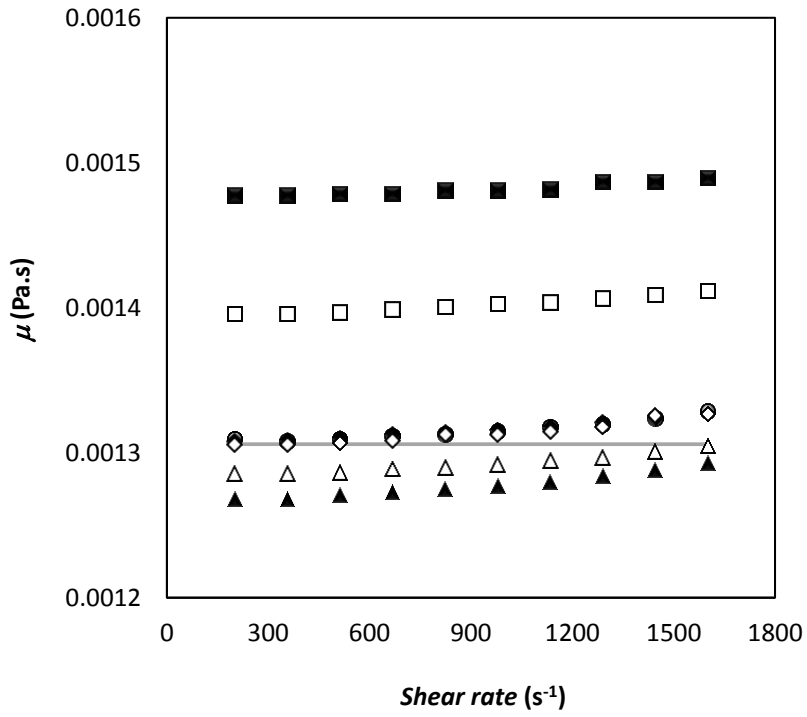

Figure 6.3: Dynamic viscosity at 10°C of (●) water, water and SDS at (Δ) 0.03%, (◊) 0.1% and (□) 1% in mass, (▲) water-0.03% SDS and 0.01% SWCNH, (♦) water-0.1% SDS and 0.1% SWCNH and (■) water-1% SDS and 1% SWCNH; (—) water calculated by Refprop 9.0 [4].

Table 6.2: Experimental viscosity data for water-based nanofluids with at constant shear rate (about 800 1/s).

***T* (°C)**	**SWCNH 0.01 wt% (mPa·s)**	**SWCNH 0.1 wt% (mPa·s)**	**SWCNH 1 wt% (mPa·s)**
10	1.29	1.31	1.48
20	1.04	1.00	1.19
30	0.80	0.76	0.92
40	0.65	0.64	0.76
50	0.55	0.55	0.65
60	0.47	0.49	0.53
70	0.41	0.40	0.46
80	0.36	0.32	0.43

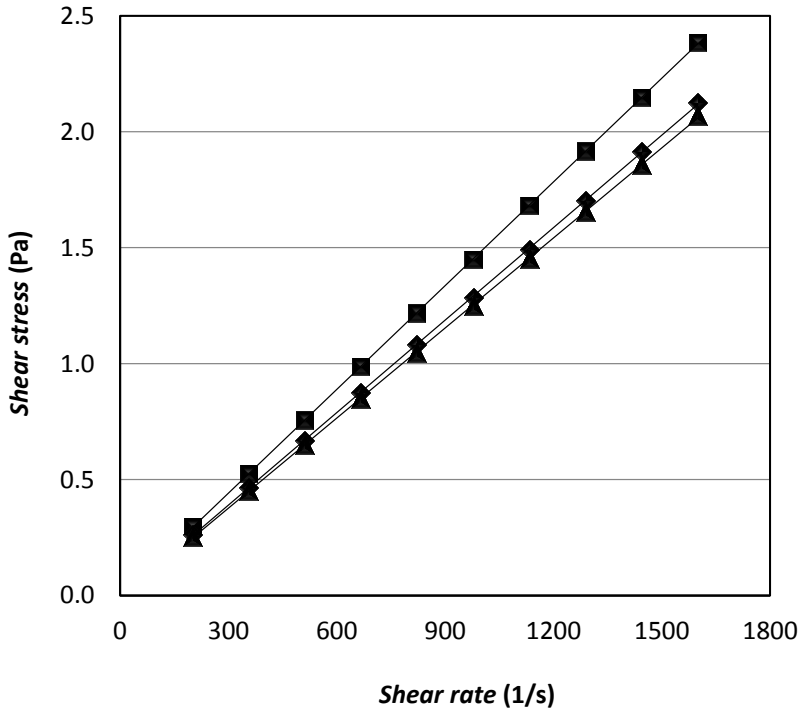

Figure 6.4: Shear stress as a function of shear rate for water-SWCNH-SDS nanofluid at 10°C. (▲) 0.01% SWCNH, (♦) 0.1% SWCNH and (■) 1% SWCNH.

6.4 Comparison with published literature

Up today, no literature data are available for the same nanofluids here considered, *i.e.* fluids formed by the same nanoparticles, base fluids, dispersants, at the same compositions and with the same preparation methods.

In literature, several theoretical models have been proposed to correlate viscosity data of nanofluids and few of them were applied to these experimental data. Considered models are Einstein model (equation 3.3), Brinkman model (equation 3.4) and Batchelor model (equation 3.5), described in paragraph 3.1.1.

As shown in Figure 6.5, equations 3.3, 3.4 and 3.5 of paragraph 3.1.1 are able to estimate nanofluids viscosity for the lowest compositions, but overestimate the suspensions at 1% wt. These results are in contrast with literature, *e.g.* [5], where these equations underestimated nanofluids viscosity for concentrations higher than 1% vol. It could be due to different employed preparation methods, dispersants and nanoparticle dimensions.

Recent studies suggested correlations between the nanofluids high viscosity and the nanoparticles aggregation [6, 7-9]. Different models have been proposed taking into account this phenomenon, as the Krieger–Dougherty equation [5]

$$\mu_{nf} = \mu_f \left(1 - \frac{\varphi_a}{\varphi_m}\right)^{-[\eta]\varphi_m} \tag{6.1}$$

where φ_m is the maximum concentration at which nanofluid can flow, φ_a the effective aggregates volume fraction (and here it is considered as φ) and $[\eta]$ is the intrinsic viscosity (for non-interacting, rigid spherical particles, 2.5).

Afterwards, Chen *et al*. [6] assumed that the aggregates density change with the radial position and then it is not uniform in the nanofluid, by means of the equation

$$\varphi_a = \varphi \left(\frac{a_a}{a}\right)^{3-D} \tag{6.2}$$

where, a_a and a are the aggregates and prime nanoparticles radii, respectively. D is the fractal index, that is 1.8 for nanoparticles [7-9]. So, equation 6.1 becomes

$$\mu_{nf} = \mu_f \left(1 - \frac{\varphi}{\varphi_m}\left(\frac{a_a}{a}\right)^{1.2}\right)^{-[\eta]\varphi_m} \tag{6.3}$$

Then, a simplified equation was proposed [10] as

$$\mu_{nf} = \mu_f \left(1 - \frac{\varphi}{\varphi_m}\right)^{-2} \tag{6.4}$$

In order to apply equations 6.1 to 6.4, φ_m should be calculated. Although the present experimental data are only at three different concentrations, restricting the validity range of the models, φ_m was calculated, basing on [11], on all the experimental data, being 6.85% for SWCNH nanofluids.

The correlation results are added in Figure 6.5. It is evident that also equations 6.1, 6.3 and 6.4 can estimate nanofluids viscosity only for the lowest compositions, overestimating the suspensions at 1% wt.

Nevertheless, the applicability of theoretical models to nanofluids is a still unsolved problem. Here, a simple equation, with similar form to equaton 3.5, is proposed to correlate these experimental data

$$\mu_{nf} = \mu_f \left(1 + a\phi + b\phi^2\right) \tag{6.5}$$

For the same base fluid and nanoparticle, this equation was regressed on the viscosity data at different temperatures (taken into account by means of the base fluid viscosity at that

temperature) and nanofluid concentrations. The regressed parameters are summarized in Table 6.3. As shown in Figures 9 and 10, this equation well represents the experimental data.

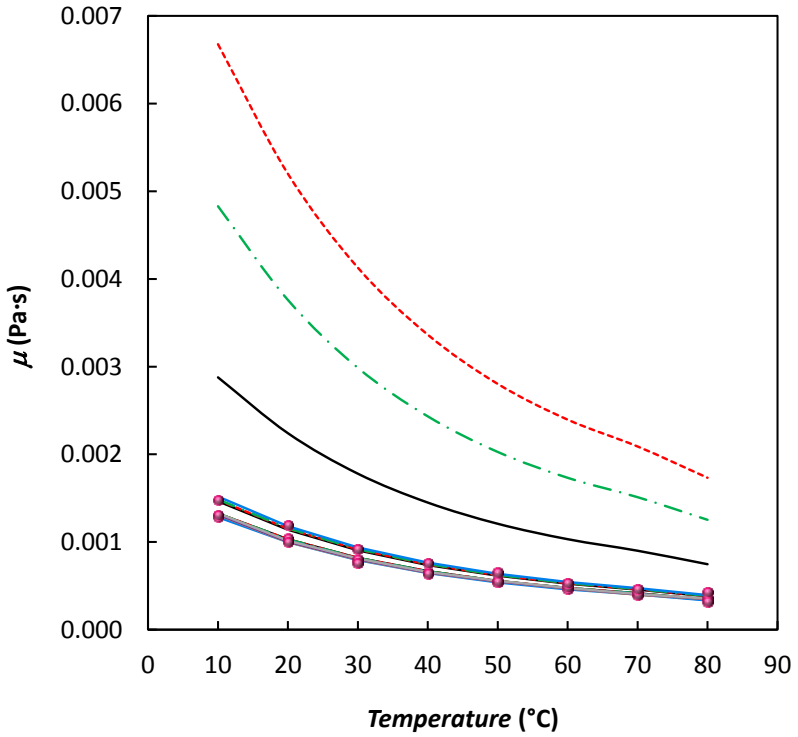

Figure 6.5: Viscosity as a function of temperature for water-SWCNH-SDS nanofluid. (●) experimental data; (—) Einstein equation (3.3); (– –) Brinkman (3.4); (—·—) Batchelor equation (3.5); (—) equation (6.1), (—) equation (6.3), (—) equation (6.4), (—) equation (6.5).

Table 6.3: Regressed parameters of equation 6.5.

nanofluid	***a***	***b***
water - SWCNH	-0.50437	1.74486

6.5 Thermal conductivity

The increasing in dynamic viscosity for water-SWCNH nanofluid at 1 wt%, makes it unsuitable for heat transfer applications. Therefore, the thermal conductivity was measured only for the nanofluid at 0.1 wt%. The results, shown in Figure 6.6 and in Table 6.4, indicate that the thermal conductivity is very similar to that of water. The reason is probably the

presence of SDS, which nullifies the increasing of thermal conductivity due to SWCNH. On the other hand, SDS is necessary to ensure the stability of the nanofluid. Other dispersants were tested, but neither of these turned out to be suitable to avoid the nanoparticles aggregation.

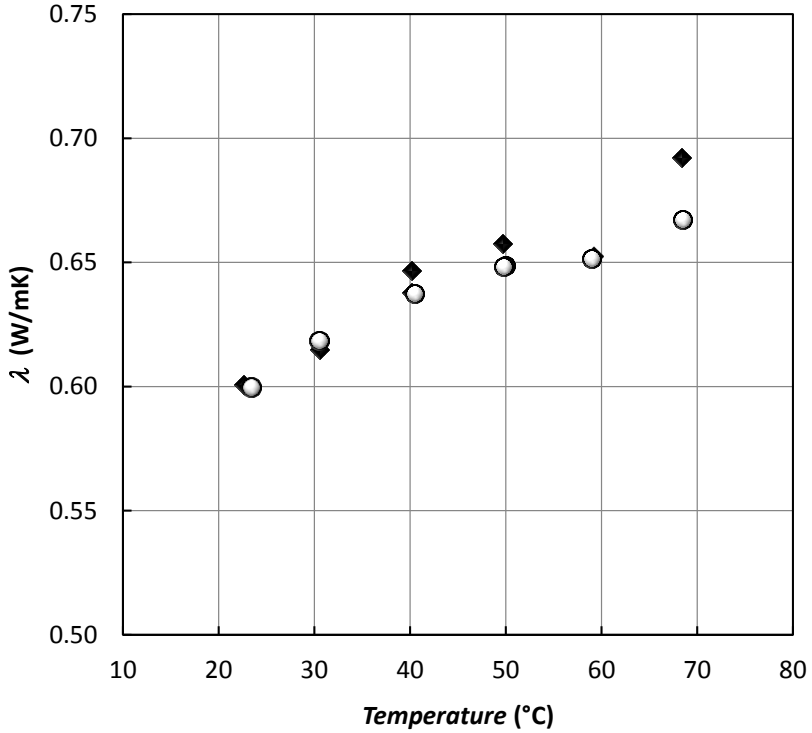

Figure 6.6: Thermal conductivity of water (○) and SWCNH in water, 0.1 wt% (♦).

Table 6.4: 2: Experimental conductivity data for SWCNH in water at 0.1 wt% and deviation % on respect to measured water ($\Delta\lambda$). $\Delta\lambda(\%) = (\lambda_{nf}-\lambda_{water})/\lambda_{water}\cdot 100$.

***T* (°C)**	**λ (W/mK)**	**$\Delta\lambda$ (%)**
22.6	0.601	-0.39
30.5	0.615	-0.23
40.2	0.638	1.09
40.2	0.647	2.50
49.7	0.658	2.25
59.2	0.653	-0.17
68.4	0.692	4.58

6.6 Conclusions

The knowledge of viscosity is important for its influence on both the heat transfer and the energy required to pump the nanofluid in the circuits where they are used as secondary fluids.

Nanofluids based on water and SWCNH, with the addition of SDS as dispersant, showed a Newtonian behaviour at each composition. Negligible variations on the viscosity of the nanofluids in relation to water are observed at nanoparticles concentrations up to 0.1% in mass fraction. On the contrary, a significant increase is measured for nanoparticles concentration of 1 wt%. Part of this increment is due to the addition of the dispersants.

Few theoretical models were applied to regress the experimental data, but they were found able to represent only nanofluids with nanoparticle concentrations lower than 1% wt. Then, a new correlation was proposed to represent the experimental data for the SWCNH/water nanofluids.

Thermal conductivity was measured for the nanofluid at 0.1 wt% and the nanofluid behaviour was very similar to that of water, probably due to the presence of SDS.

References

[1] M. Yudasaka, S. Iijima, V. H. Crespi, "Carbon Nanotubes", *Topics in Applied Physics*. Jorio A, Dresselhaus G, Dresselhaus MS, editor. Vol. 111. Berlin/Heidelberg: Springer; Single-wall carbon nanohorns and nanocones; 605–629 (2008).

[2] S.U.S. Choi, Z. G. Zhang, W. Yu, F. E. Lockwood, E. A. Grulke, "Anomalous Thermal Conductivity Enhancement in Nanotube Suspensions", *Applied Physics Letters*, 79, 2252-2254 (2001**)**.

[3] J. Miyawaki, M. Yudasaka, T. Azami, Y. Kubo, S. Iijima, "Toxicity of single-walled carbon nanohorns", *ACS Nano*, 2, 213–226 (2008).

[4] E.W. Lemmon, M.L. Huber, M.O. McLinden, NIST Standard Reference Database 23, Reference Fluid Thermodynamic and Transport Properties (REFPROP), version 9.0; National Institute of Standards and Technology (2010).

[5] I.M. Krieger, T.-J. Dougherty, "A mechanism for non-Newtonian flow in suspension of rigid spheres", *Transaction of the Society of Rheology,* 3,137–152 (1959).

[6] H. Chen, Y. Ding, Y. He, C. Tan, "Rheological behaviour of ethylene glycol based titania nanofluids", *Chemical Physics Letters*, 444, 333–337 (2007).

[7] B.X. Wang, L.P. Zhou, X.P. Peng, "A fractal model for predicting the effective thermal conductivity of liquid with suspension of nanoparticles", *International Journal of Heat and Mass Transfer*, 46, 2665–2672 (2003).

[8] C.W. Nan, R. Birringer, D.R. Clarke, and H. Gleiter, "Effective thermal conductivity of particulate composites with interfacial thermal resistance", *Journal of Applied Physics*, 81, 10, 6692-6699 (1997).

[9] R. Prasher, P.E. Phelan, P. Bhattacharya, "Effect of aggregation kinetics on the thermal conductivity of nanoscale colloidal solutions (nanofluid)", *Nano Letters*, 6, 1529–1534 (2006).

[10] T. Kitano, T. Kataoka, T. Shirota, "An empirical equation of the relative viscosity of polymer melts filled with various inorganic fillers", *Rheologica Acta*, 20, 207–209 (1981).

[11] D.M. Liu, "Heat Transfer Enhancement of Nanofluids", *Journal of Materials Science*, 35, 5503–5507 (2000).

Chapter 7

Water based SiO_2 nanofluid characterization

In literature, measurements of thermal properties for water-based nanofluids are frequently not coherent, probably due to different methods of nanofluids preparation and insufficient information on the nanoparticles characteristics. To evaluate the reasons for these discrepancies, within an International Nanofluid Property Benchmark Exercise (INPBE), thermal conductivity of identical samples of stable colloidal dispersions of nanoparticles was studied at ambient temperature by over 30 organizations worldwide, using a variety of experimental approaches [1]. The authors concluded that thermal conductivity data obtained by using different experimental techniques could be different. They provide information about the experimental approaches and observed that thermal conductivity differences tend to disappear when the data are normalized to the measured thermal conductivity of the base-fluid. Moreover, classic effective medium theory for well-dispersed particles by Maxwell (equation 3.14) and recently generalized theory by Nan *et al.* [2] were found to be in good agreement with the experimental data, suggesting that no anomalous enhancement of thermal conductivity was achieved in the nanofluids tested in this exercise.

Nevertheless, it is worth noting the measurements were performed only at ambient temperature, not taking into account the influence of temperature on the possible thermal conductivity enhancement.

Considering oxide nanoparticles can be of particular interest for industrial application because of their low cost, high stability and easy production, here the same nanofluid belonging to set 3 in [1] was considered for a series of measurements with the following aims:

- to check the accuracy of the thermal conductivity apparatus used in this work by comparing our results with those of INPBE;
- to extend the temperature range of the measurements and to consider various nanoparticles concentrations, to check the validity of classical theory also at temperatures different from ambient;

- to measure viscosity as a function of temperature to evaluate the viscosity enhancement.

7.1 Nanofluid preparation

The nanofluid is formed by silica nanoparticles of spherical shape monodispersed in de-ionized water. It was supplied by Grace & Co. (Ludox TM-50) at a nanoparticles nominal concentration of 50% by mass (49.0-51.0%). The real concentration was evaluated by measuring the density of the nanofluid at 20°C by means of a glass vibrating tube densimeter (Anton Paar DMA 602), assuming a linear dependence of density from the volumetric fraction of nanoparticles and a density of 2200 kg/m^3 for SiO_2. The actual SiO_2 mass fraction resulted to be 54%.

Bidistilled water (CARLO ERBA, Bidistilled water, CAS Nr 7732-18-5) was added to the commercial nanofluid to obtain the other three nanofluid compositions: 1 wt%, 5 wt% and 27 wt%. Each fluid obtained in this way was further sonicated in order to completely disperse the nanoparticles in the water.

7.2 Nanofluids stability characterization

The nanoparticles size declared by the supplier was 22 nm. Using the DLS technique, the mean particle diameter, measured 3 times for each sample, was around 30 nm for the 1 wt% solution, 25 nm for 5 wt% and 20 nm for 27 wt%, showing a slight dependence of size on nanoparticles concentration. The forth fluid (54 wt%) was not measured since this concentration is too high, giving problems of multiple scattering. The measured diameters were basically constant for more than 20 days after preparation at all the concentrations, demonstrating the strong stability of the various nanofluids. The mean particle diameters are represented in Figure 7.1.

Water-SiO_2 nanofluids ζ potential was in the range between -35 mV and -45 mV for all the nanoparticles concentrations, corresponding to strong repulsive interactions and reduced tendency to form aggregates, then confirming the stability of the nanofluids.

The pH of each nanofluid was almost independent from nanoparticles concentration, ranging from 9.1 at 54 wt% to 9.9 at 1 wt%.

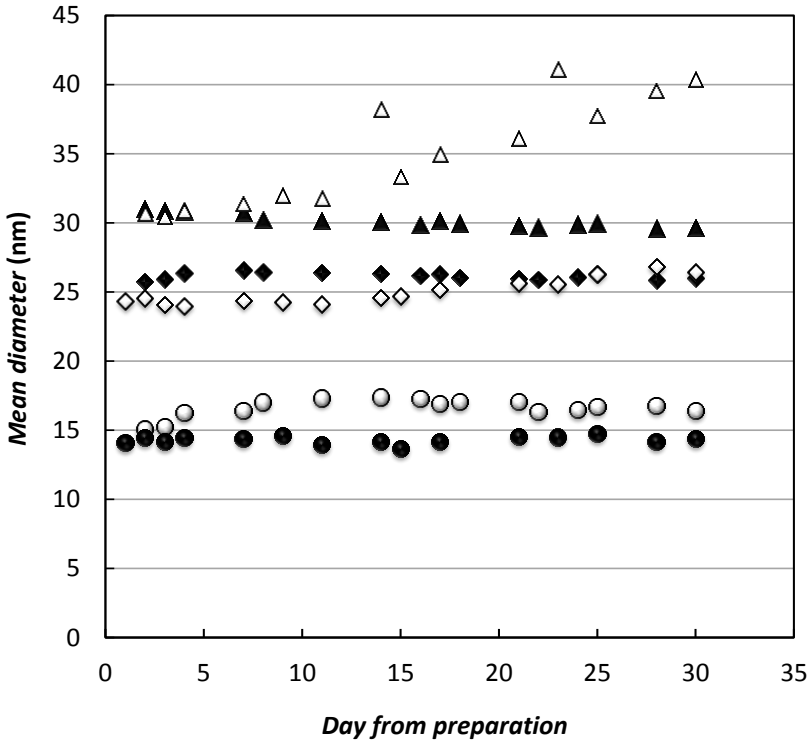

Figure 7.1: Nanoparticles mean diameter in relation to the time elapsed from the day of preparation in water-based nanofluids containing SiO_2 at 1 wt% (Δ) static and (▲) stirred samples, 5 wt% (◊) static and (♦) stirred samples, 27 wt% (○) static and (•) stirred samples.

7.3 Thermal conductivity

Thermal conductivity of all selected water-SiO_2 nanofluids was measured at ambient pressure as a function of temperature in the range between 10°C and 70°C, with steps of 10°C, for all the selected nanoparticles concentrations, in order to evaluate the enhancement with respect to pure water.

Figure 7.2 shows nanofluids thermal conductivity as a function of temperature, while Figure 7.3 presents the ratio between the thermal conductivity of nanofluids and that of water (enhancement). First, it should be noted that the thermal conductivity, measured at 20°C and 54 wt% (0.728 W/mK), is in good agreement (the deviation is 0.1%) with that measured at the same conditions by [1] (0.729 W/mK). Thermal conductivity increases almost linearly with temperature at concentrations higher than 1% wt. During the measurements, some instability is observed at temperatures higher than 50°C, probably due to the evaporation of the sample.

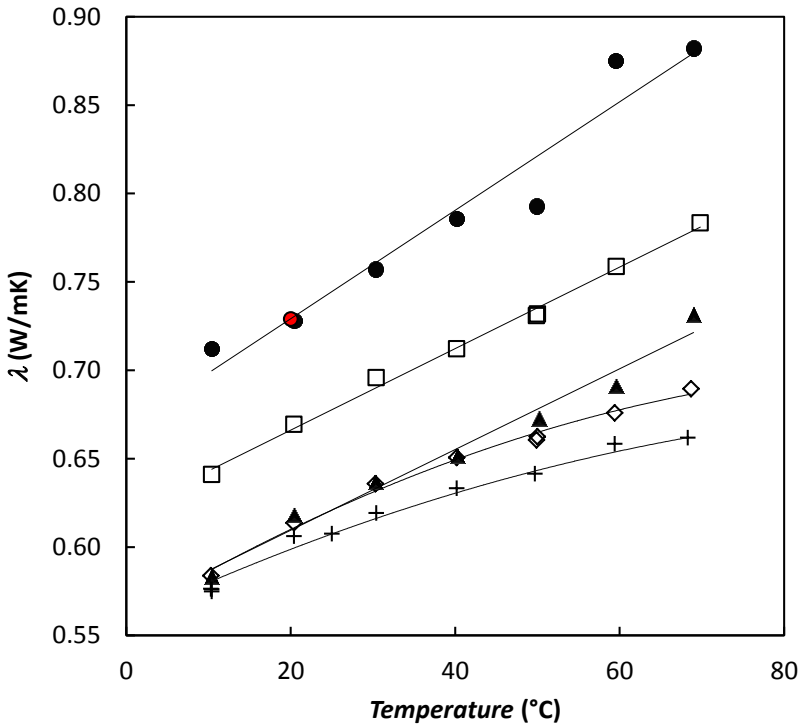

Figure 7.2: Thermal conductivity of water-SiO_2 nanofluids as a function of temperature. Nanofluid at 1 wt% (◊), 5 wt% (▲), 27 wt% (□), 54 wt% (●),Buongiorno *at al*. [1] (●), experimental water (+).

For this reason, in Figure 7.3 the enhancement is represented only up to 50°C. The enhancement is strongly dependent on concentrations, even if it is less than proportional to concentration (*e.g.*: enhancement below 27% for 54 wt% nanofluid at any temperature). Moreover, it is less sensitive to temperature than thermal conductivity, with an increase of only few percent between 10°C and 50°C at all concentrations.

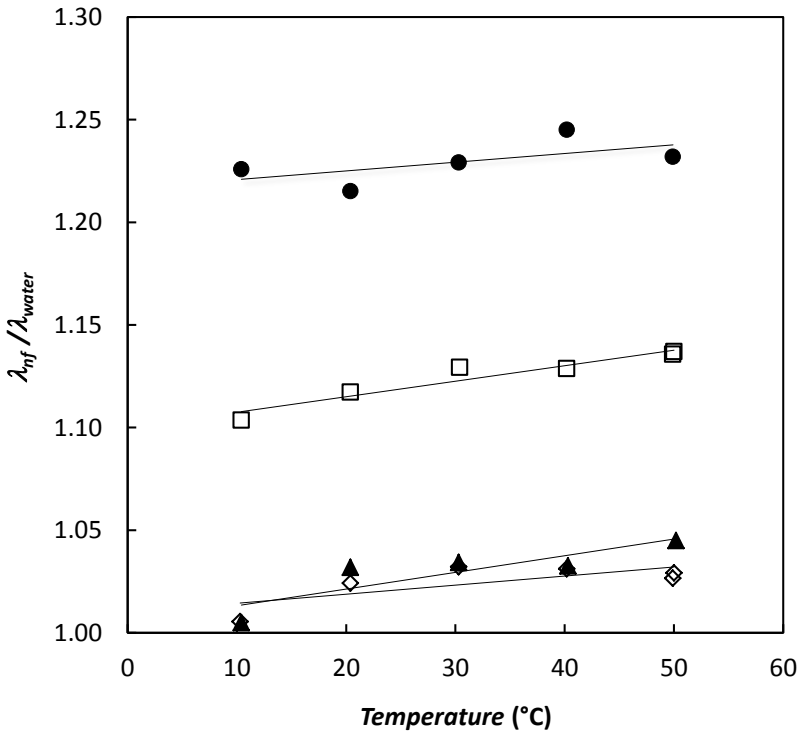

Figure 7.3: Thermal conductivity ratio between water-SiO_2 nanofluids and water as a function of temperature. Nanofluid at 1 wt% (◊), 5 wt% (▲), 27 wt% (□), 54 wt%(●).

7.4 Dynamic Viscosity

Dynamic viscosity data of pure water and water-based nanofluids were measured from 10°C to 70°C by increments of 20°C per step. At concentrations between 1 wt% to 27 wt%, the ratio between shear stress and shear rate was constant in the measurements shear rate range at all the temperatures, highlighting a Newtonian behaviour of the nanofluids. Figure 7.4 shows that viscosity values, taken at a constant shear rate of 550 (1/s), decrease with lower declination at increasing temperatures.

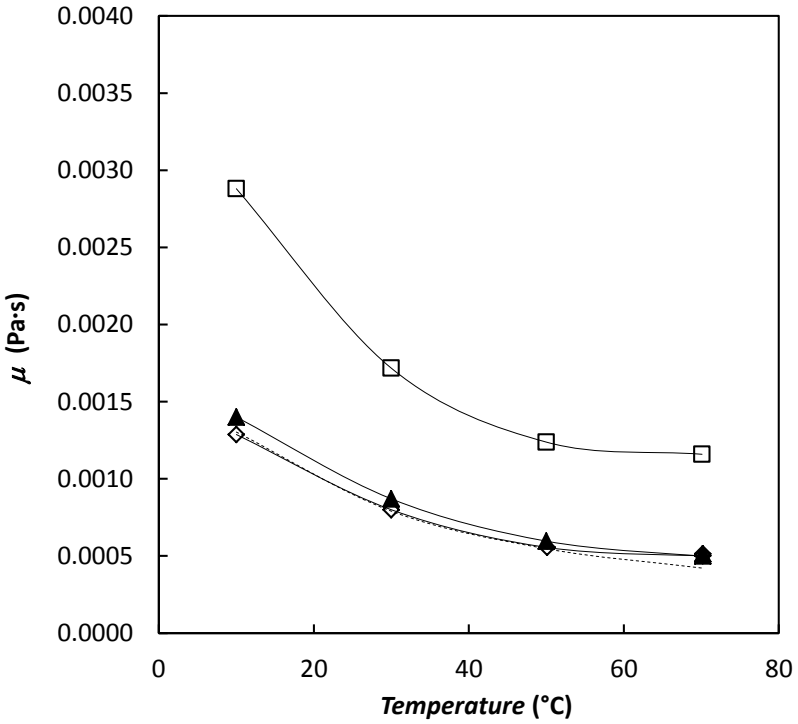

Figure 7.4: Viscosity of water-SiO_2 nanofluids as a function of temperature. Nanofluid at 1 wt% (◊), 5 wt% (▲), 27 wt% (□), water (----).

Viscosity at concentrations below 5 wt% is practically the same as that of water. This can be seen even better in Figure 7.5, were the ratio between nanofluids viscosity and water viscosity is reported. At given concentration, the viscosity ratio is practically constant with temperature, except at 70°C, at which the ratio is increased, probably due to some aggregation phenomena. Viscosity for the 27 wt% nanofluid is more than twice the viscosity of water.

Nanofluid with 54 wt% SiO_2 nanoparticles showed a non-Newtonian behaviour and a viscosity one order of magnitude higher than that at other concentrations. Moreover, the viscosity increased with temperature at temperatures higher than 50°C. This behaviour is probably due to strong aggregation of nanoparticles. The viscosity behaviour at this concentration was not included in the figures for to the particular high values.

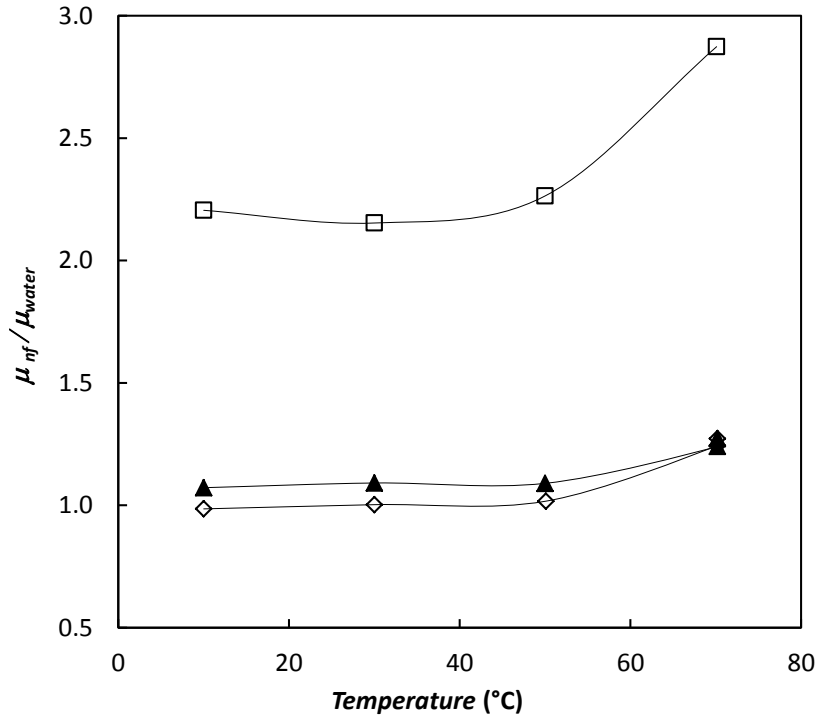

Figure 7.5: Viscosity ratio between water-SiO_2 nanofluids and water as a function of temperature. Nanofluid at 1 wt% (◊), 5 wt% (▲), 27 wt% (□).

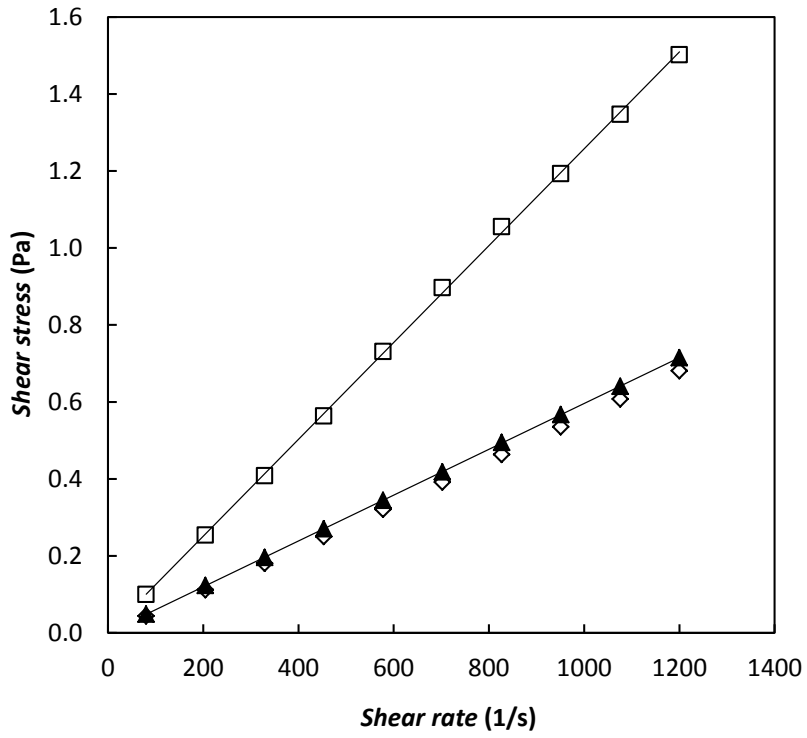

Figure 7.6: Shear stress as a function of shear rate for water-SiO_2 nanofluids. Nanofluid at 1 wt% (◊), 5 wt% (▲), 27 wt% (□).

7.5 Comparison with published literature

As discussed in the paragraph 7.3, the thermal conductivity measured at 20°C and 54 wt% is compatible, within the experimental accuracy, with that measured at the same conditions by [1]. Other literature papers, which consider the nanofluid SiO_2 in water, examine the possible technical applications and do not measure the thermophysical properties. For example, in [3] water-based SiO_2 nanofluid was used in a loop thermosyphon and in [4] SiO_2 nanoparticles suspension in water was used in a car radiator.

To make a comparison with literature models, density of SiO_2 is assumed 2200 kg/m^3 as reported in [1] and the volume fraction here considered are 0.0046, 0.0234, 0.1439 and 0.3479.

Thermal conductivity data were compared with equation 3.15. Hamilton and Crosser model overestimates the thermal conductivity results at the highest volume fractions. In fact, the deviations of the equation 3.15 from experimental data are -1.5% at 1 wt%, 2.3% at 5 wt%, 29.8% at 27 wt% and 97.2 at 54 wt%.

Dynamic viscosity data were compared with equation 3.5. Batchelor model is in good agreement with the experimental data for the nanofluids at 1 wt%, and 5 wt% and for temperature from 10°C to 50°C. The model overestimates experimental data of 22.3% at 1 wt% and 16.5% at 5 wt%, at 70°C. For nanofluid at 27 wt%, the model overestimates experimental data from 44.1% to 92.0%.

In [6] heat transfer of SiO_2 in water nanofluid was studied in horizontal tubes founding an increasing from 10% to 60% compared to pure water coefficient.

7.6 Conclusions

Viscosity and thermal conductivity for nanofluids formed by water and SiO_2 nanoparticles with concentration from 1% to 54% by mass were measured in the range of temperatures between 10°C and 70°C. The thermal conductivity, at ambient temperature for the nanofluid at 54 wt%, was compared with the benchmark study [1] result, finding a good agreement. Thermal conductivity clearly enhances with reference to water, but only at the higher concentrations with a weak dependence on temperature. At the same time, viscosity increases even more significantly and, for this reason, water-based nanofluids with silica nanoparticles should not be suitable for thermal applications.

References

[1] J. Buongiorno, D. Venerus, N. Prabhat, T. McKrell, J. Townsend, R. Christianson, Y. Tolmachev, P. Keblinski, L. Hu, J. Alvarado, I. Bang, S. Bishnoi, M. Bonetti, F. Botz, A. Cecere, Y. Chang, G. Chen, H. Chen, S. Chung, M. Chyu, S. Das, R. Di Paola, Y. Ding, F. Dubois, G. Dzido, J. Eapen, W. Escher, D. Funfschilling, Q. Galand, J. Gao, P. Gharagozloo, K. Goodson, J. Gutierrez, H. Hong, M. Horton, K. Hwang, C. Iorio, S. Jang, A. Jarzebski, Y. Jiang, L. Jin, S. Kabelac, A. Kamath, M. Kedzierski, L. Kieng, C. Kim, J. Kim, S. Kim, S. Lee, K. Leong, I. Manna, B. Michel, R. Ni, H. Patel, J. Philip, D. Poulikakos, C. Reynaud, R. Savino, P. Singh, P. Song, T. Sundararajan, E. Timofeeva, T. Tritcak, A. Turanov, S. Van Vaerenbergh, D. Wen, S. Witharana, C. Yang, W. Yeh, X. Zhao, S. Zhou, "A benchmark study on the thermal conductivity of nanofluids", *Journal of Applied Physics*, 106, 094312 (2009).

[2] C. W. Nan, R. Birringer, D. R. Clarke, and H. Gleiter, "Effective thermal conductivity of particulate composites with interfacial thermal resistance", *Journal of Applied Physics*, 81, 10, 6692-6699 (1997).

[3] Y.J Chen, P.Y. Wang, Z.H. Liu, "Application of water-based SiO_2 functionalized nanofluid in a loop thermosyphon", *International Journal of Heat and Mass Transfer*, 56, 59-68 (2013).

[4] A.M. Hussein, R.A. Bakar, K. Kadirgama, "Study of forced convection nanofluid heat transfer in the automotive cooling system", *Case Studies in Thermal Engineering*, 2, 50–61(2014).

[5] A. A. R. Darzi, M. Farhadi, K. Sedighi, R. Shafaghat, K. Zabihi, "Experimental investigation of turbulent heat transfer and flow characteristics of SiO_2/water nanofluid within helically corrugated tubes", *International Communications in Heat and Mass Transfer*, 39, 1425–1434 (2012).

[6] S. Ferrouillat, A. Bontemps, J.P. Ribeiro, J.A. Gruss, O. Soriano, "Hydraulic and heat transfer study of SiO_2/water nanofluids in horizontal tubes with imposed wall temperature boundary conditions", *International Journal of Heat and Fluid Flow*, 32, 424-439 (2011).

Chapter 8

Water based Fe_2O_3 nanofluid characterization

The purpose of this chapter is to investigate thermal conductivity and dynamic viscosity of water-based nanofluids containing iron oxide (Fe_2O_3) in concentrations ranging between 5 and 20% in mass. Oxide nanoparticles are easier to obtain and less expensive than other nanoparticles, as metals and carbon nanotubes. Amongst them, Fe_2O_3 is already used to produce stable and commercially available water nanofluids. In this investigation, the effect of temperature and nanoparticles concentration on thermal conductivity and dynamic viscosity of Fe_2O_3 water-based nanofluids is studied.

Experimental results will be compared with some literature models and an experimental correlation for nanofluids viscosity will be proposed.

8.1 Nanofluid preparation

The studied nanofluid is formed by hematite (Fe_2O_3) nanoparticles, monodispersed in de-ionized water. It was supplied by Sigma Aldrich at a nanoparticles nominal concentration of 20% by mass.

Bidistilled water (Carlo Erba, CAS Nr 7732-18-5) was added to the commercial nanofluid to obtain the other two nanofluid compositions: 5 wt% and 10 wt%.

These two compositions were prepared starting from the original nanofluid, sonicated for one hour by means of an ultrasonic bath (Bransonic, Ultrasonic cleaner Branson 2210, output power 90 W) and adding bidistilled water in a weighed amount, measured by an analytical balance (Gibertini E42S 240 g FS), with an uncertainty of 0.002 g. Each fluid obtained in this way was further sonicated for one hour, in order to improve the dispersion of nanoparticles in the water.

No dispersant was added to the fluid.

8.2 Nanofluids stability characterization

As described in chapter 2.5, DLS technique was used to check the actual average dimension of the nanoparticles in solution and the ζ potential was measured to analyse the stability of the nanofluids. The mean particle diameter was around 67 nm and it did not change with the particle concentration. In Figure 8.1, the particle size distribution detected by the Zetasizer is represented. A further particle size measurement was performed after almost three months and the same average diameter was found. This indicates that no aggregation occurs in few months.

Fe_2O_3-water nanofluid ζ potential was around +56 mV for the 5 wt% solution, +57 mV for the 10 wt% solution, +49 mV for the 20 wt% solution. Since a value of ζ potential out of the range between 30 mV and -30 mV indicates high charged surface and hence a strong electrical repulsion among the particles, all the nanofluids seem to be very stable.

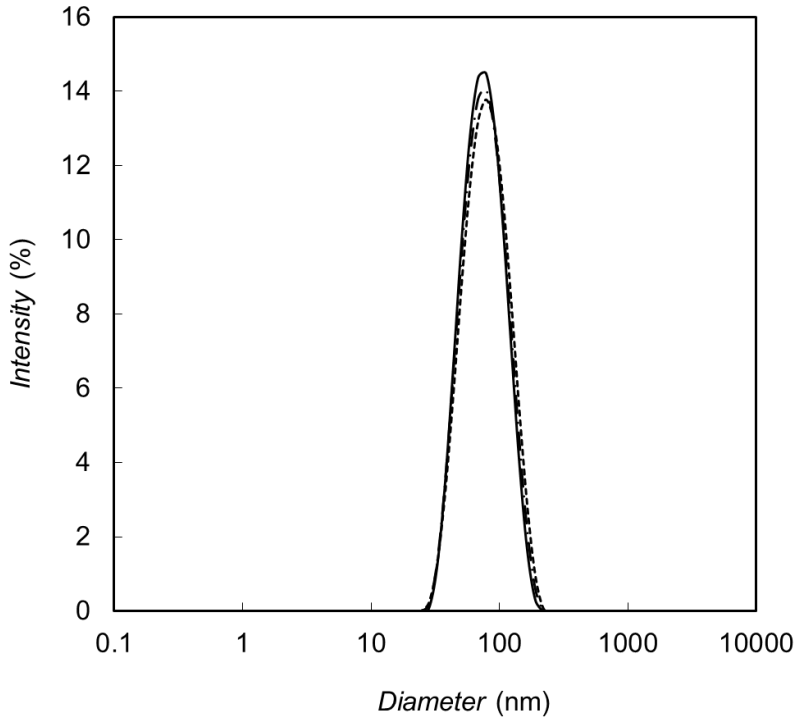

Figure 8.1: Nanoparticles size distribution for water containing 5 wt% (− · −), 10 wt% (---), 20 wt% (—) Fe_2O_3.

The pH of each nanofluid was measured with a pH meter as described in chapter 2.5. The measured values were 3.45 for the 5 wt% solution, 3.33 for 10 wt% and 3.34 for 20 wt% at 26°C. As described in [1], the isoelectric point for water-hematite nanofluid is observed at

pH 6.1. Then the measured pH values of these solutions are far from this point, as further confirmation, together to the ζ potential (always positive and higher than 30 mV), of the nanofluids stability.

8.3 Thermal conductivity

Thermal conductivity measurements were performed in the temperature range between 10°C and 70°C, with steps of 20°C, at ambient pressure. Figure 8.2 presents nanofluids thermal conductivity as a function of mass fraction and temperature. Figure 8.3 shows an almost linear enhancement with temperature at all the concentrations examined up to 50°C. In the figure, error bars relating to the declared instrument uncertainty (5%) are added. Some instability is observed at temperature of 70°C, probably due to the introduction of convective motions in the liquid or aggregation of the nanoparticles, but these phenomena cannot be evaluated during the conductivity tests. Table 8.1 presents the experimental data and the ratio between the thermal conductivity of the nanofluids and water at the same temperature.

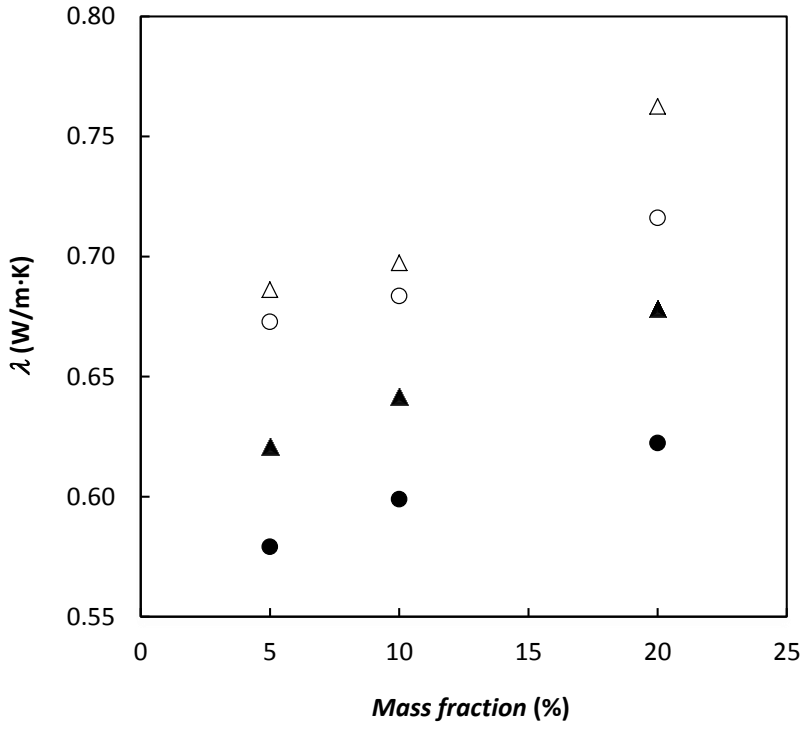

Figure 8.2: Experimental thermal conductivity of water-Fe_2O_3 nanofluid, (●) 10°C, (▲) 30°C, (○) 50°C, (Δ) 70°C, as a function of mass fraction.

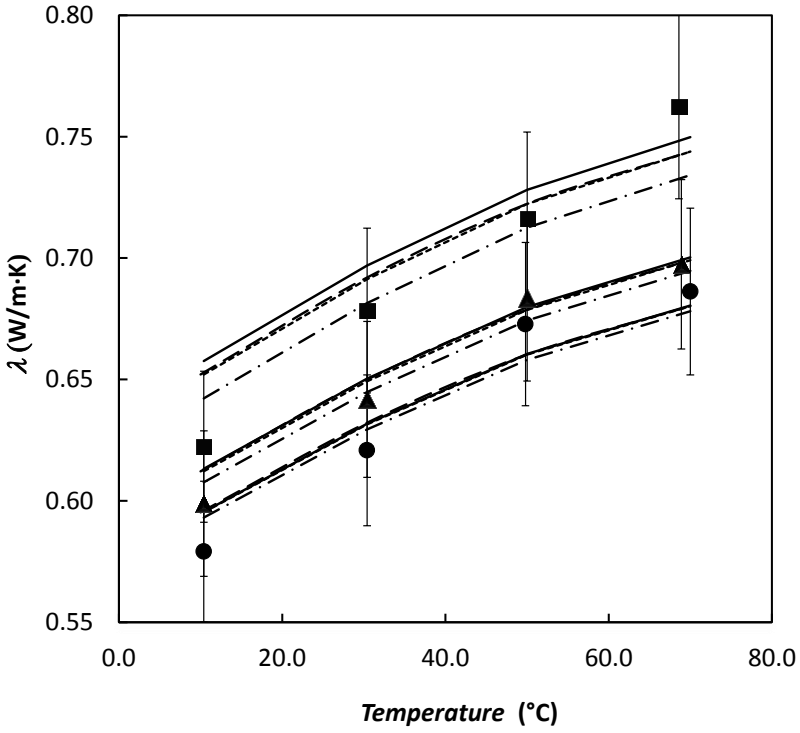

Figure 8.3: Experimental thermal conductivity of water-Fe_2O_3 nanofluid, (●) 5 wt%, (▲) 10 wt%, (■) 20 wt%, as a function of temperature. Comparison with Maxwell model (3.15) (─ ─), Bruggeman model (3.16) (─), Lu and Lin model (3.17) (– · –), Xuan model (3.18) (---). Error bars correspond to 5% uncertainty.

Table 8.1: Experimental thermal conductivity data and thermal conductivity ratio for Fe_2O_3 water-based nanofluids

Mass fraction	5 wt%		10 wt%		20 wt%	
Vol. fraction	0.99 vol%		2.08 vol%		4.55 vol%	
***T* (°C)**	λ_{exp} **(W/m·K)**	$\lambda_{exp}/\lambda_{water}$	λ_{exp} **(W/m·K)**	$\lambda_{exp}/\lambda_{water}$	λ_{exp} **(W/m·K)**	$\lambda_{exp}/\lambda_{water}$
10.4	0.5791	1.00	0.5989	1.03	0.6223	1.07
30.4	0.6208	1.01	0.6418	1.04	0.6784	1.10
50.0	0.6728	1.05	0.6835	1.06	0.7161	1.11
70.0	0.6862	1.03	0.6974	1.05	0.7625	1.15

8.4 Dynamic viscosity

Dynamic viscosity measurements were performed at 5 wt%, 10 wt% and 20 wt% in the temperature range between 10°C and 70°C, with steps of 20°C.

Figure 8.4 shows the flow curves at 10°C for water and all nanofluids. The same trend was found at all the measured temperatures. In Table 8.2, the experimental data are reported at shear rate around 800 1/s. Under the imposed conditions, the nanofluids appeared to have a Newtonian behaviour, as it can be deduced by Figure 8.5, where shear stress is represented as a function of shear rate for the measurements at 30°C. All isotherms are linear and converge to the origin of the diagram.

Figure 8.6 shows the trend of viscosity as a function of nanoparticles concentration at all temperatures. Viscosity improves in an exponential way at each temperature, reaching a maximum value of 0.00309 Pa·s at 20 wt% and 10°C. The enhancement on respect to pure water was 21%, 47% and 136% at 5 wt%, 10 wt% and 20 wt%, respectively. Viscosity decreases if temperature increases, with the same trend for all the concentrations.

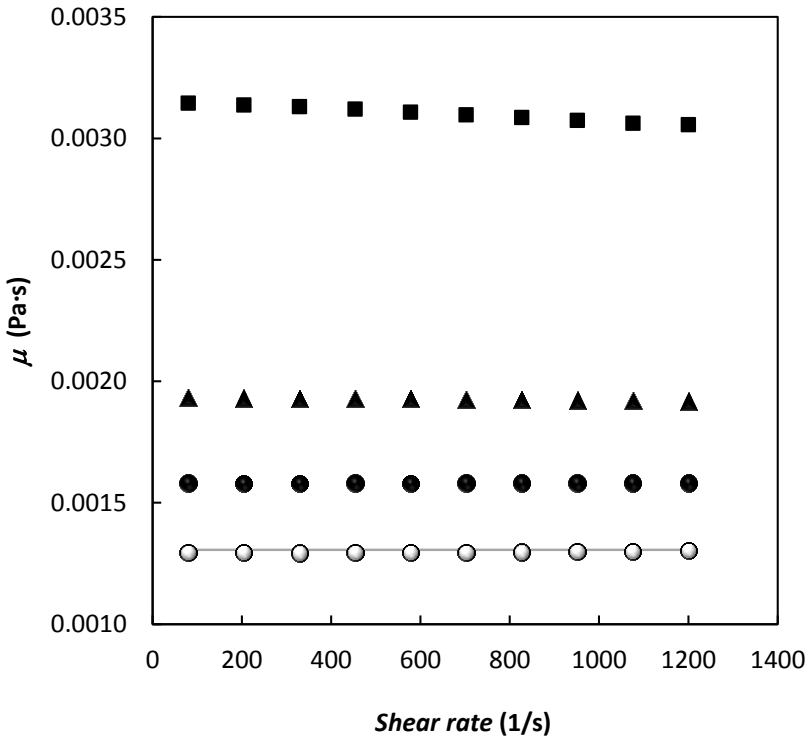

Figure 8.4: Dynamic viscosity of Fe_2O_3 at 10°C. (○) water, (●) 5 wt%, (▲) 10 wt%, (■) 20 wt% compared to (─) Refprop 9.0 [2].

Table 8.2: Experimental viscosity data at constant shear rate (about 800 1/s) and viscosity ratio for Fe_2O_3 water-based nanofluids.

Mass fraction	5 wt%		10 wt%		20 wt%	
Vol. fraction	0.99 vol%		2.08 vol%		4.55 vol%	
***T* (°C)**	μ_{exp} **(Pa s)**	μ_{exp}/μ_{water}	μ_{exp} **(Pa s)**	μ_{exp}/μ_{water}	μ_{exp} **(Pa s)**	μ_{exp}/μ_{water}
10	0.00158	1.21	0.00192	1.47	0.00309	2.36
30	0.00099	1.24	0.0012	1.51	0.00199	2.49
50	0.00066	1.21	0.00081	1.49	0.00129	2.36
70	0.00053	1.32	0.00067	1.65	0.0011	2.72

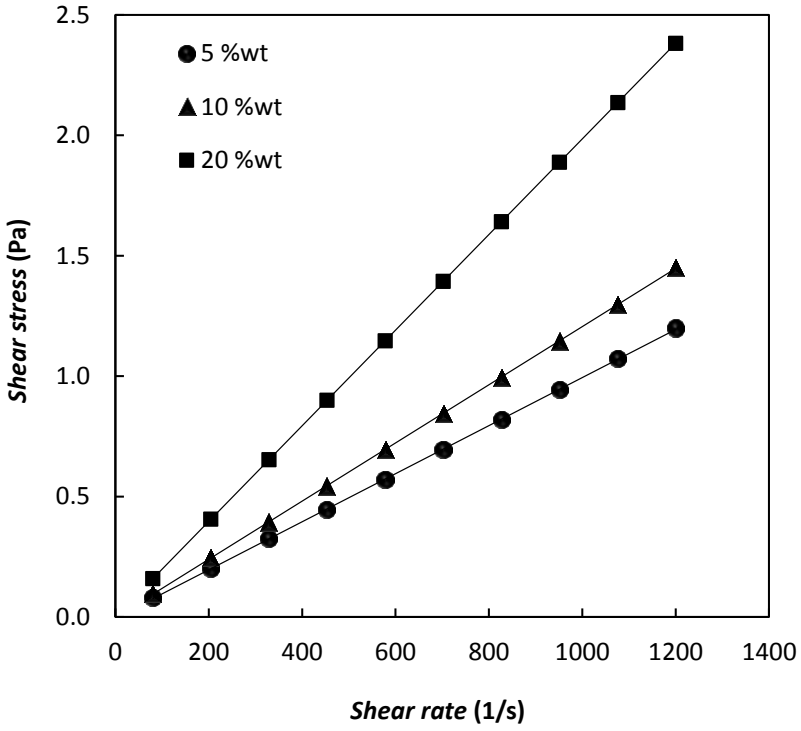

Figure 8.5:Shear stress as a function of shear rate for water-Fe_2O_3 nanofluid at 30°C. (●) 5 wt%, (▲) 10 wt%, (■) 20 wt%.

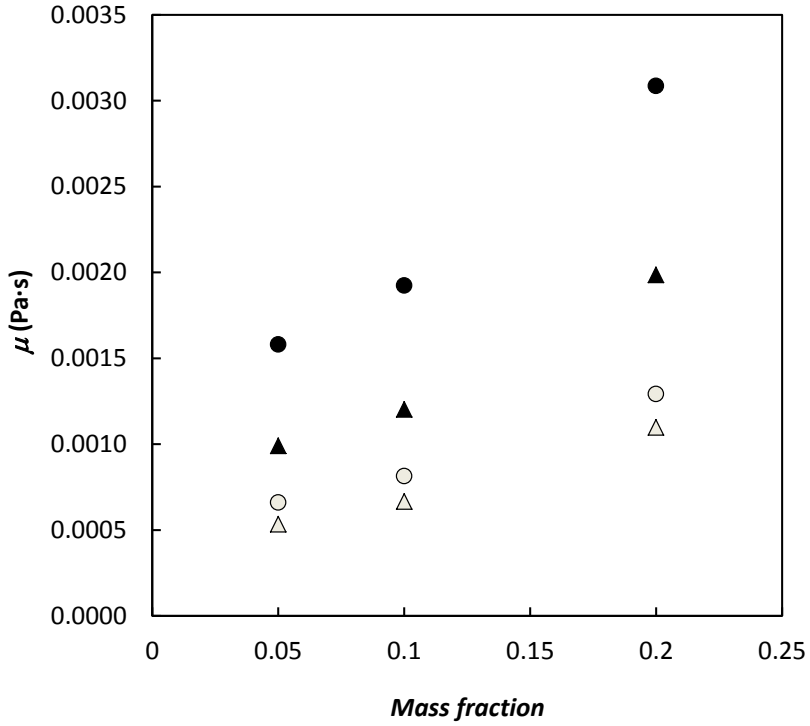

Figure 8.6: Dynamic viscosity on mass fraction of water-Fe_2O_3 nanofluid at (●) 10°C, (▲) 30°C, (○) 50°C, (Δ) 70°C.

8.5 Comparison with literature

In literature, a study on dynamic viscosity of hematite dispersed in water is [3], in which Phuoc and Massoudi observed the rheological properties of Fe_2O_3 water-based nanofluids in concentrations between 1 and 4 % in mass. They found a non-Newtonian behaviour, but their results cannot be compared with results here presented, because their concentrations are lower and they always used polymer dispersants, which strongly affect rheological behaviour. Another study on the rheological properties of Fe_2O_3 nanofluids is [4], in which the base-fluid is ethylene glycol. Other studies consider the applications of ferro-nanofluids on a micro-transformer [5], or the electrical and magnetic properties of ferro-nanofluid on transformers [6] or magnetic nanofluids [7] based on Fe_3O_4 nanoparticle, but no other studies on thermal conductivity or dynamic viscosity of Fe_2O_3 water-based nanofluids have been found. Hence, only a comparison with literature model was done.

8.5.1 Thermal conductivity

In Figure 8.3 measured thermal conductivity results are compared with classical effective thermal conductivity model (equation 3.15). Thermal conductivity of the added solid

particles is 15.42 W/m·K [8]. At the lower temperature, the model overestimates the experimental results, but, starting from temperatures around 50°C, theoretical and experimental results are in quite good agreement.

In literature, several models have been proposed. Amongst these, few models have been chosen for comparison, Bruggeman model (3.16), Lu and Lin model (3.17) and Xuan *et al*. model (3.18), described in chapter 3.2.1.

All these models were added to Figure 8.3, together with the experimental uncertainties. Their behaviour is very similar. They overestimate thermal conductivity values at temperature lower than 50°C, while they underestimate at higher temperature for all the nanofluids, although the data are always within the experimental uncertainties.

8.5.2 Dynamic viscosity

In literature, several theoretical models have been proposed to predict the viscosity of a particle suspension. They are discussed in chapter 3.1.1. In particular Einstein model (3.3), Brinkman model (3.4), and Batchelor model (3.5).

Moreover, Krieger-Dougherty equation (6.1) and equation 6.4 were considered. In order to apply equations 6.1 and 6.4, φ_m should be calculated. Basing on [9], the maximum solid concentration can be estimated by

$$\varphi_m = \frac{1-\beta}{\alpha} \tag{8.1}$$

where α and β are calculated by the following equation [10]

$$\mu_{nf} = \mu_f \left(1-\alpha\varphi-\beta\right)^{-2} \tag{8.2}$$

Basing on the experimental data α = 0.07298 and β = 0.03402 , then φ_m becomes 13.24.

A comparison between experimental data and equations is shown in Figure 8.7. Equations 3.4 and 3.5 overlap equation 6.1.

All these equations underestimated nanofluids viscosity, confirming their incapability to model this property for nanofluids.

Here, a simple equation, with similar form to equation 3.5, is proposed to correlate the experimental data

$$\mu_{nf} = \mu_f \left(1+a\varphi+b\varphi^2\right) \tag{8.3}$$

This equation was regressed basing on all experimental data for nanofluids and water viscosity calculated by [2] at the same temperatures. The regressed parameters are *a*=18.64 and *b*=248.30. As shown in Figure 8.7 this equation well represents the experimental data.

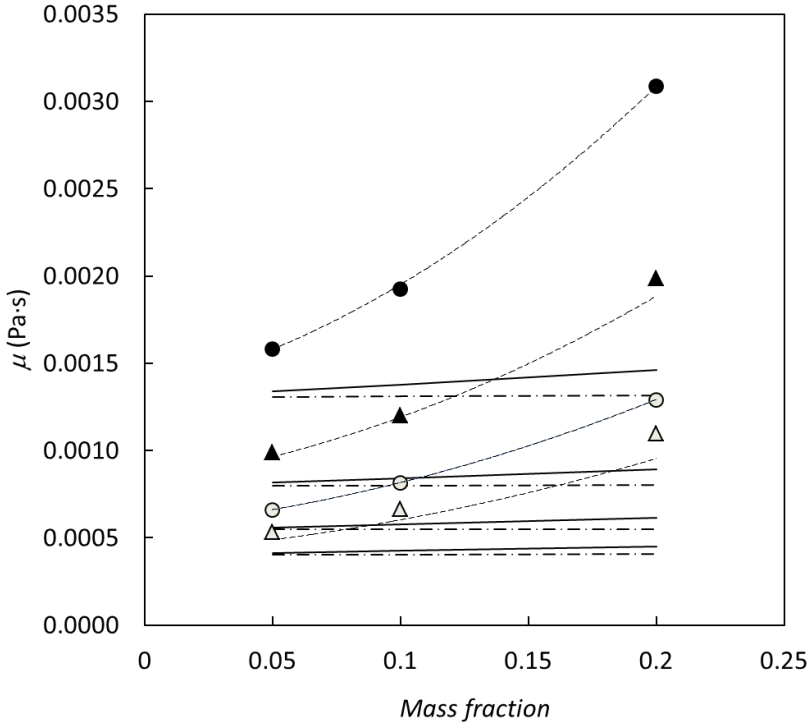

Figure 8.7: Experimental dynamic viscosity of water-Fe_2O_3 nanofluid at (●) 10°C, (▲) 30°C, (○) 50°C, (Δ) 70°C on respect to mass fraction. Comparison with theoretical models: (──) equation 6.1, (– · –) equation 6.4, (----) equation 8.3. Equations 3.4 and 3.5 overlap equation 6.1.

8.6 Conclusions

Fe_2O_3 water-based nanofluids have long time stability also at high concentration as 20 wt%. Thermal conductivity increases with mass fraction and with temperature. Thermal conductivity ratio is greater at the highest concentrations. The rheological behaviour of the nanofluids is Newtonian and the dynamic viscosity increases considerably in respect of water, mainly at mass fraction of 20%. Therefore, the increment in thermal conductivity is combined with a rising in dynamic viscosity. For this reason, Fe_2O_3 water-based nanofluid, studied in this work, is not energetically convenient for technical applications.

In order to complete the analysis on Fe_2O_3 water-based nanofluids and with the aim to obtain a useful nanofluid for heat transfer applications, other fluids (Figure 8.8), prepared with the single step method, are currently under studying. Different chemical agents have been tested as dispersants, to improve the nanoparticles stability. DLS measurements have

been done for each nanofluid, but several fluids reveal low stability, as shown in Figure 8.9. The characterization of stable fluids will be done in the next future.

Figure 8.8: Fe_2O_3 water-based nanofluids prepared using single step method and different chemical agent to improve the stability.

Figure 8.9: Sample for DLS measurements. Settling of nanoparticles is evident.

References

[1] S.U.S. Choi, "Nanofluid technology: current status and future research", Energy Technology Division, Argonne National Laboratory, Argonne.

[2] E.W. Lemmon, M.L. Huber, M.O. McLinden, NIST Standard Reference Database 23, Reference Fluid Thermodynamic and Transport Properties (REFPROP), version 9.0; National Institute of Standards and Technology (2010).

[3] T.W. Phuoc and M. Massoudi, "Experimental observations of the effects of shear rates and particle concentration on the viscosity of Fe_2O_3–deionized water nanofluids", *International Journal of Thermal Sciences*, 48, 1294-1301 (2009).

[4] M.J. Pastoriza-Gallego, L. Lugo, J.L. Legido, M.M. Piñeiro, "Rheological non-Newtonian behaviour of ethylene glycol-based Fe_2O_3 nanofluids", *Nanoscale Research Letters*, 6, 1, 560 (2011).

[5] T.H. Tsai, L.S. Kuo, P.H. Chen, D.S Lee, C.T. Yang, "Applications of ferro-nanofluid on a micro-transformer", *Sensors*, 10, 9, 8161-8172 (2010).

[6] T.H. Tsai, P.H. Chen, D.S. Lee, C.T. Yang, "Investigation of electrical and magnetic properties of ferro-nanofluid on transformers", Nanoscale Research Letters, 6, 264 (2011).

[7] I. Nkurikiyimfura, Y. Wanga, Z. Pan, "Heat transfer enhancement by magnetic nanofluids - A review", *Renewable and Sustainable Energy Reviews*, 21, 548–561 (2013).

[8] C. Clauser and E. Huenges, Rock Physics and Phase Relations, A Handbook of Physical Constants, edited by T. J. Ahrens (American Geophysical Union), Washington, D.C. (1995).

[9] T. Kitano, T. Karaoka and T. Shirota, "An empirical equation of the relative viscosity of polymer melts filled with various inorganic fillers", *Rheologica Acta*, 20, 207-209 (1981).

[10] D.M. Liu, "Particle packing and rheological property of highly-concentrated ceramic suspensions: ϕ_m determination and viscosity prediction", *Journal of Materials Science*, 35, 5503-5507 (2000).

Chapter 9

Water based ZnO nanofluid characterization

In this chapter the stability of zinc oxide (ZnO)-water nanofluid is discussed. The thermal conductivity and the dynamic viscosity of the nanofluid at 1, 5, 10 wt% have been measured. The local heat transfer coefficient for the 5 wt% and 10 wt% nanofluids has been measured.

9.1 Nanofluid preparation

The studied nanofluid is formed by ZnO nanoparticles dispersed in water. It was supplied by Sigma-Aldrich at nanoparticles concentration of 50% by mass. In the suspension, 3-aminopropyltriethoxysilane was present as dispersant at 2 wt%.

Bidistilled water (Carlo Erba, CAS Nr 7732-18-5) was added to the commercial nanofluid to obtain other three compositions: 1 wt%, 5 wt%, 10 wt%, *i.e*. 0.18 vol%, 0.93 vol% and 1.95 vol%. Each nanofluid was obtained starting from the fluid at 50 wt% after one hour sonication and adding bidistilled water in a weighted amount, measured by an analytical balance (Gibertini E42S 240 g FS), with an uncertainty of 0.0002 g. Each composition was further sonicated in order to completely disperse the nanoparticles in the water.

9.2 Nanofluids stability characterization

The stability characterization was carried on using the DLS technique. Mean dimension was measured at 25 °C with a scattering angle of 173°.

In order to verify the dependency of the diameter size from the concentration of the solution, each nanofluid was sonicated and the nanoparticle size was measured three times. The mean values of the diameters were 63 nm at 1 wt%, 59 nm at 5 wt% and 59 nm at 10 wt%.

Figure 9.1 shows the particle size distribution, according to the intensity detected by the Zetasizer, for the water-ZnO nanofluids at these compositions. The absence of particle micrometer-sized aggregates and the mean particle dimension constancy confirm the good stability of the obtained dispersions.

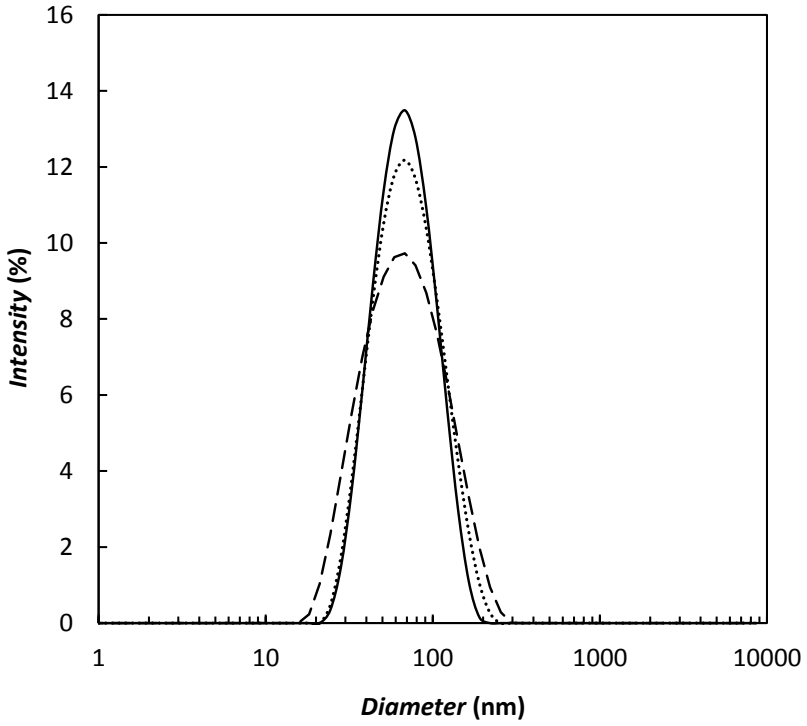

Figure 9.1: Particle diameter size distribution, according to the intensity, for the water-ZnO nanofluids at (···) 1%, (—) 5%, (– –) 10%.

As described in chapter 2, the stability of suspension was verified along time. The variations along time of the ZnO nanoparticle mean diameters are shown in Figure 9.2. The behaviour is very similar for each composition. In the case of static solutions the mean size slightly decreased to around 40 nm after 32 days, indicating a partial precipitation. However, after sonication for one hour, a mean particle size centred around 60 nm was always recovered, suggesting the absence of further aggregation phenomena.

This result is interesting because it indicates the fluid at the concentrations here analysed can be used in devices where they are frequently or continuously stirred, *e.g.* in plants with forced circulation.

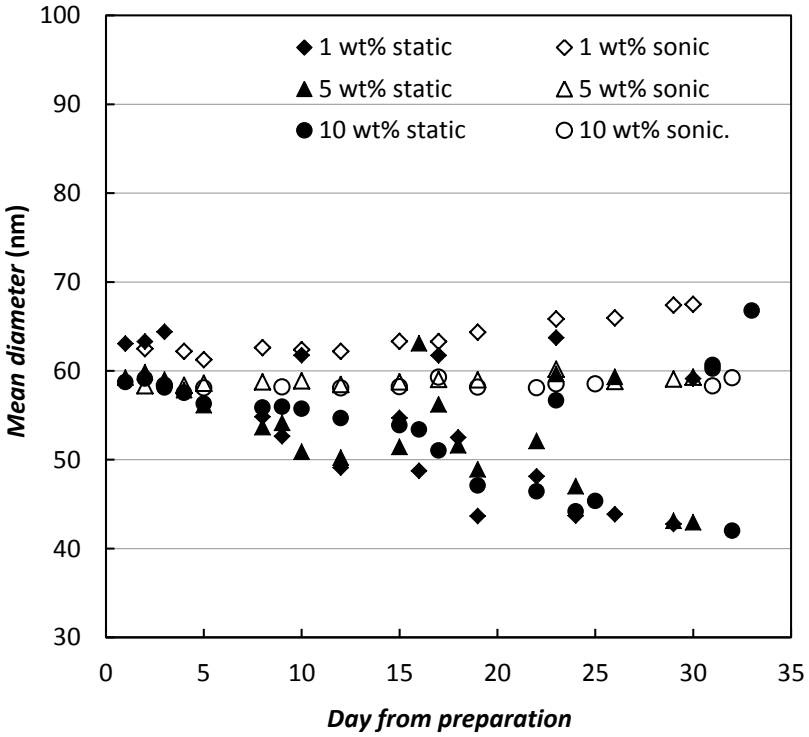

Figure 9.2: The variation along time of the ZnO nanoparticle mean diameters. (♦) 1 wt%, (▲) 5 wt%, (●) 10 wt%. Empty symbols stay for stirred samples, full symbols for static samples.

ZnO-water nanofluid Zeta potential was around +48 mV for the 1 wt% solution, +44 mV for the 5 wt% solution and +47 mV for the 10 wt% solution, therefore all the nanofluids proved to be stable.

The pH were 7.5 for 1 wt% solution, 7.3 for 5 wt% and 7.3 for 10 wt% at 23°C.

9.3 Thermal conductivity

The thermal conductivity data of ZnO-water nanofluids, measured from 10 to 70°C, are summarized in Table 9.1. Figure 9.3 shows the ratio ($\lambda_{nf}/\lambda_{water}$) between the thermal conductivities of the nanofluid and water, Refprop 9.0 [1]. The thermal conductivity ratio increases with temperature and with the mass concentration. Nanofluids at 5 wt% and 10 wt% show the higher enhancements of 12% and 15% at 70°C, while the suspension at 1 wt% shows a water-like behaviour.

Table 9.1: Thermal conductivity data for water and ZnO-water nanofluids.

$$\Delta\lambda\% = 100 \cdot \frac{\left(\lambda_{nf} - \lambda_{water}\right)}{\lambda_{water}}$$

T (°C)	λ_{nf} (W/m·K)	λ_{water} [1] (W/m·K)	$\Delta\lambda\%$
		water	
10.7	0.5803	0.5814	-0.19
23.4	0.5997	0.6044	-0.78
30.5	0.6186	0.6163	0.37
40.5	0.6374	0.6313	0.97
50.0	0.6486	0.6436	0.78
49.8	0.6482	0.6434	0.75
59.0	0.6516	0.6534	-0.28
68.5	0.6671	0.6619	0.79
		1 wt% ZnO-water	
10.8	0.5468	0.5816	-6.37
20.5	0.5670	0.6156	-2.50
30.1	0.6006	0.5994	-5.72
39.6	0.6219	0.6300	-1.30
49.4	0.6428	0.6428	-0.01
60.4	0.6801	0.6548	3.72
70.2	0.6942	0.6632	4.46
		5 wt% ZnO-water	
10.4	0.5813	0.5807	0.10
20.4	0.6087	0.5992	1.56
30.4	0.6357	0.6161	3.08
40.2	0.6607	0.6309	4.51
50.1	0.6854	0.6437	6.09
60.3	0.7203	0.6547	9.10
70.3	0.7538	0.6634	12.00
		10 wt% ZnO-water	
10.4	0.5865	0.5808	0.96
20.4	0.6219	0.5992	3.65
30.5	0.6467	0.6163	4.70
40.5	0.6842	0.6313	7.73
50.5	0.7142	0.6442	9.80
60.5	0.7455	0.6549	12.16
70.5	0.7768	0.6635	14.58

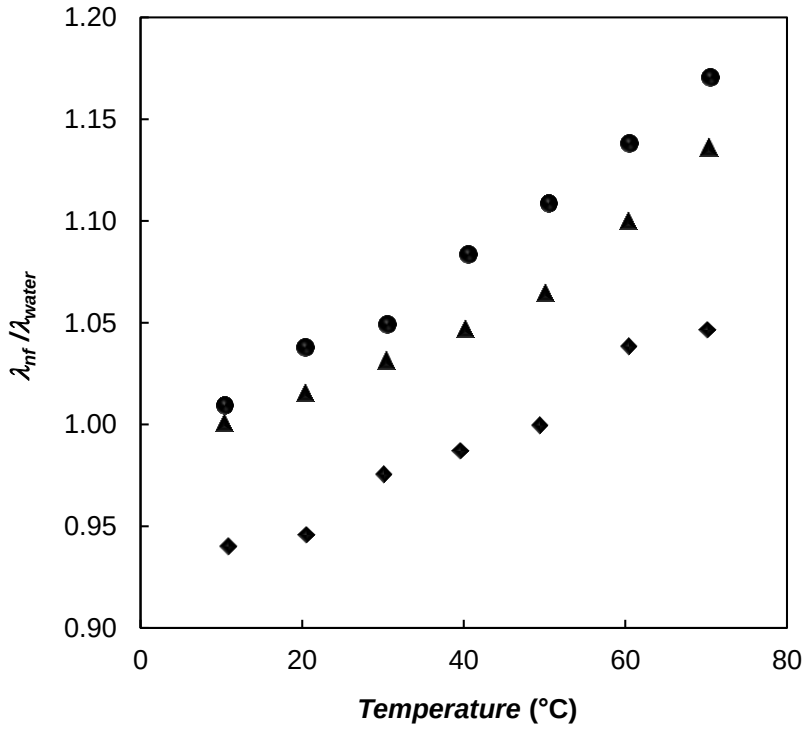

Figure 9.3: Thermal conductivity ratio ($\lambda_{nf}/\lambda_{water}$) between nanofluid and water. (♦) 1 wt%, (▲) 5 wt%, (●) 10 wt%.

9.4 Dynamic Viscosity

The dynamic viscosity for the ZnO-water nanofluid was measured at temperatures ranging between 10 and 70°C and variable shear rates between 80 and 1200 1/s, as shown in Figure 9.4 for the measurements at 10°C. In Figure 9.5 and Table 9.2, the experimental data are summarized at a constant shear rate of 827 1/s, together with the deviations compared to the base fluid, *i.e*. water, Refprop 9.0 [1]. As shown, the viscosity of the nanofluid at 1% was very similar to that of water, while a viscosity increase of about 5% was found for the nanofluid at 5 wt% and around 12% for the suspension at 10 wt%. This behaviour was almost independent with temperature.

Nanofluids have Newtonian behaviour at each studied composition. As example, Figure 9.6 represented shear stress as a function of shear rate at 10°C. For all the isotherms, the measurements are linear and converge to the origin of the diagram.

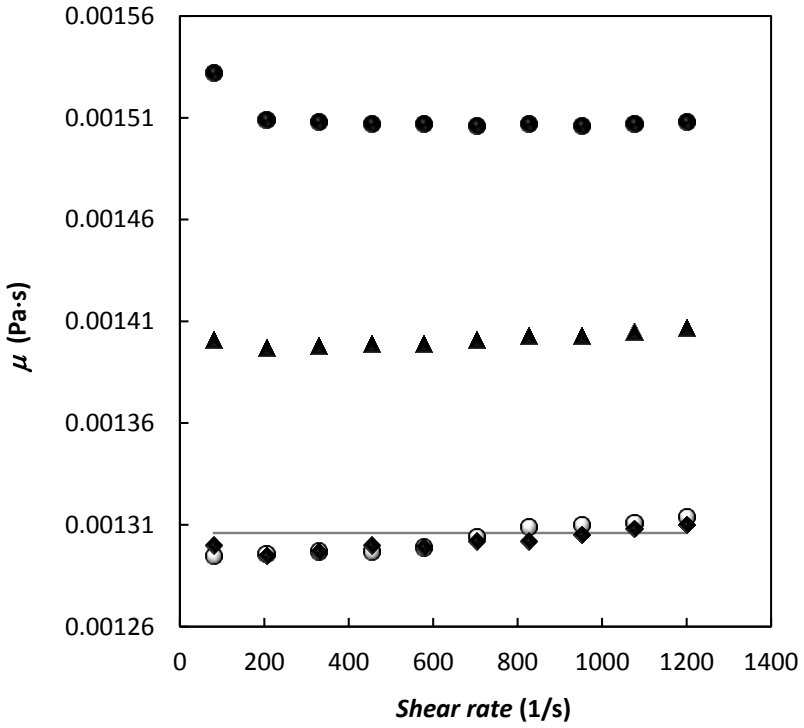

Figure 9.4: Dynamic viscosity data for water and ZnO-water nanofluids at 10°C.
(o) water, (♦) 1 wt%, (▲) 5 wt%, (●) 10 wt%, (—) Refprop 9.0 [1].

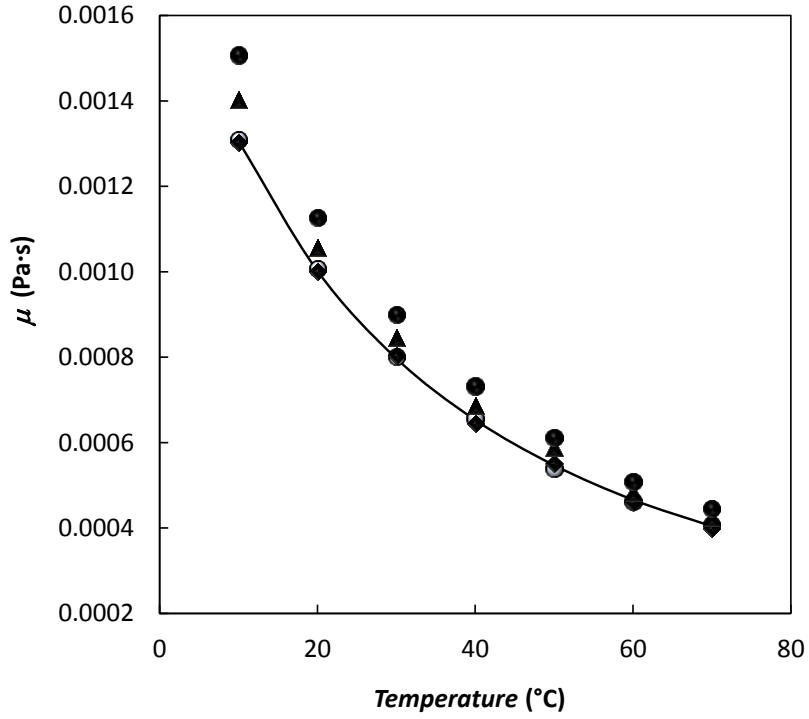

Figure 9.5: Dynamic viscosity as a function of temperature.
(o) water, (♦) 1 wt%, (▲) 5 wt%, (●) 10 wt%, (—) Refprop 9.0 [1].

Table 9.2: Dynamic viscosity data for water and ZnO-water nanofluids.

$$\Delta\mu\% = 100 \cdot \frac{\left(\mu_{nf} - \mu_{water}\right)}{\mu_{water}}$$

T (°C)	μ_{nf} (Pa·s)	μ_{water} [1] (Pa·s)	$\Delta\mu\%$
	Water		
10.0	0.001309	0.001306	0.23
20.0	0.001007	0.001002	0.50
30.0	0.000802	0.000797	0.63
40.0	0.000655	0.000653	0.31
50.0	0.000539	0.000547	-1.46
60.0	0.000461	0.000466	-1.07
70.0	0.000408	0.000404	0.99
	1 wt% ZnO-water		
10.0	0.001302	0.001306	-0.31
20.0	0.001001	0.001002	-0.10
30.0	0.000804	0.000797	0.88
40.0	0.000644	0.000653	-1.38
50.0	0.000551	0.000547	0.73
60.0	0.000460	0.000466	-1.24
70.0	0.000398	0.000404	-1.49
	5 wt% ZnO-water		
10.0	0.001403	0.001306	7.43
20.0	0.001056	0.001002	5.39
30.0	0.000846	0.000797	6.15
40.0	0.000687	0.000653	5.21
50.0	0.000588	0.000547	7.50
60.0	0.000483	0.000466	3.65
70.0	0.000425	0.000404	5.20
	10 wt% ZnO-water		
10.0	0.001507	0.001306	15.39
20.0	0.001127	0.001002	12.48
30.0	0.000900	0.000797	12.92
40.0	0.000732	0.000653	12.10
50.0	0.000611	0.000547	11.70
60.0	0.000508	0.000466	9.01
70.0	0.000445	0.000404	10.15

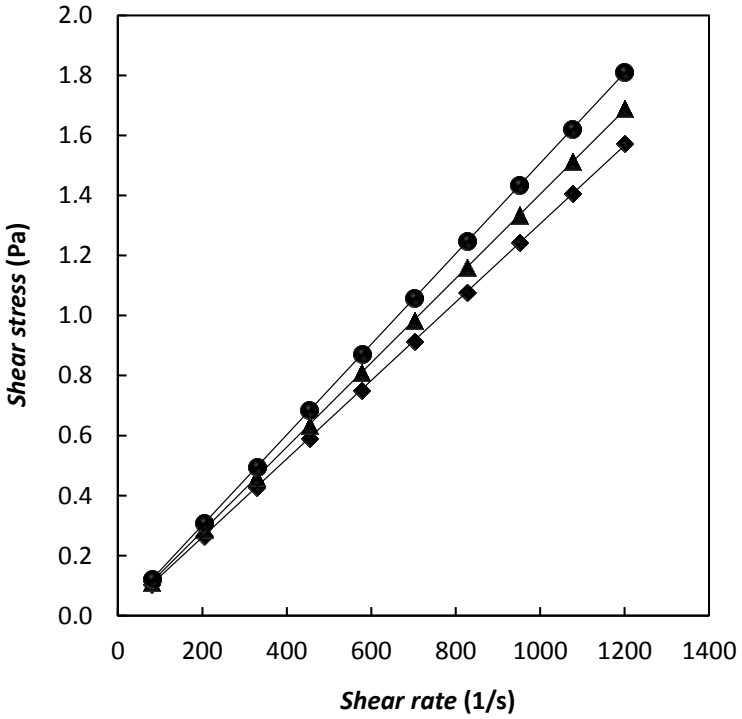

Figure 9.6: Newtonian behaviour for the ZnO-water nanofluid at 10°C. (♦) 1 wt%, (▲) 5 wt%, (●) 10 wt%.

9.5 Heat transfer coefficient

A study of the heat transfer coefficient for the nanofluids at 5 wt% and 10 wt% was performed at temperatures ranging between 19 and 40°C, in order to understand the actual thermal capability of nanofluids formed by water and ZnO.

As described in chapter 4, preliminary tests using pure water as reference fluid were made. All the measurements were performed in a heat power range from 200 to 400 W, with a thermal balance within 5%.

Starting from this analysis on water, then the nanofluids were taken under consideration. The bulk temperature profile, derived from the measurement of water-ZnO nanofluid, is shown in Figures 9.7 - 9.12 as a function of the adimensional length (distance from the inlet/inner pipe diameter). Figures 9.7 – 9.9 show temperature profiles for the nanofluid at 5 wt% and different Reynolds numbers, while Figures 9.10 – 9.12 show temperature profiles for the nanofluid at 10 wt% and different Reynolds numbers.

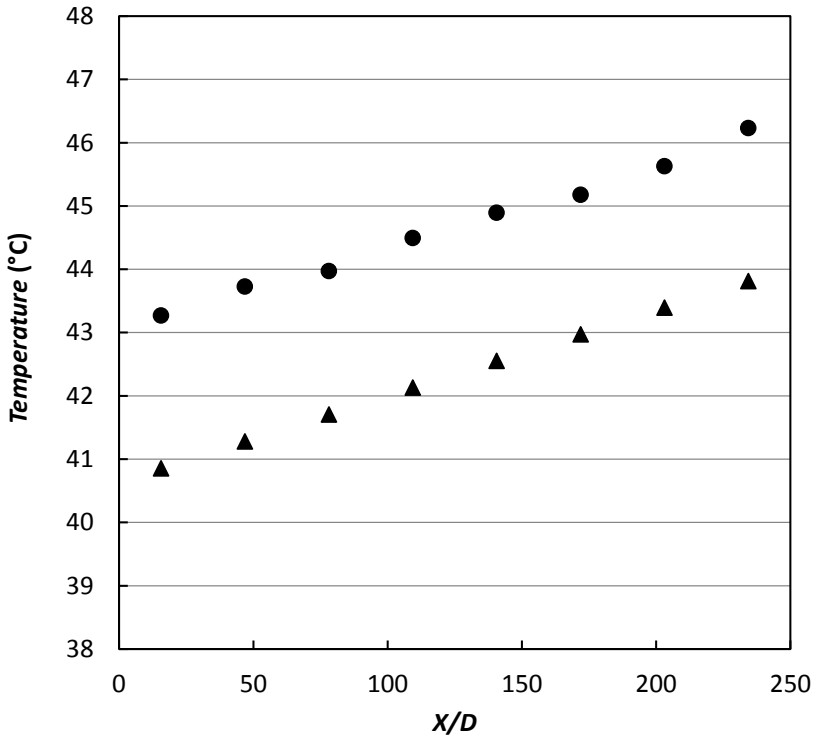

Figure 9.7: ▲ bulk and ● wall temperature profile of nanofluid at 5 wt%, as a function of the adimensional length. Re 6960, heat flux 5308 W/m^2 and mass flow rate 0.0512 kg/s.

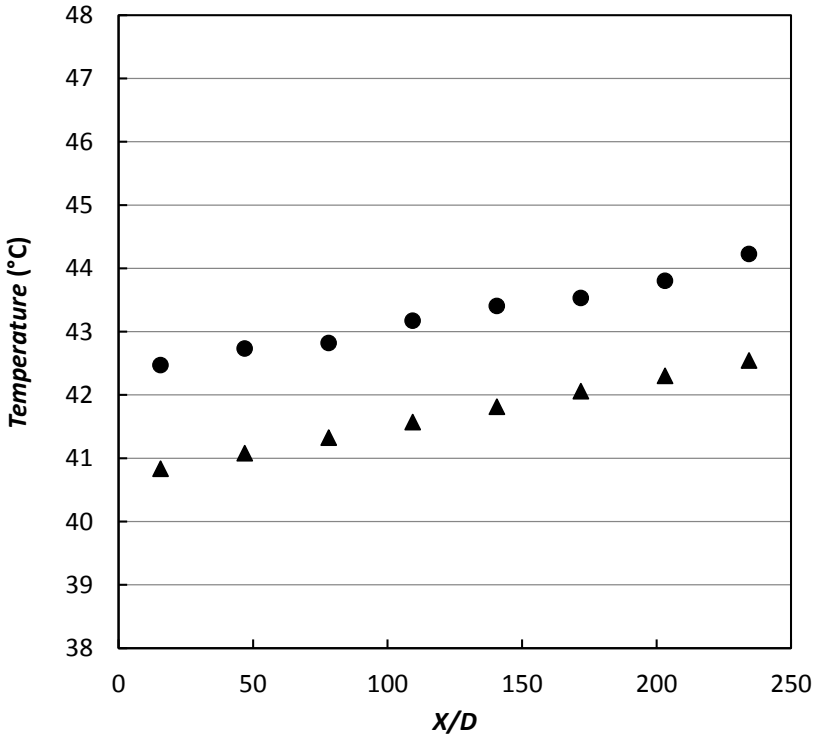

Figure 9.8: ▲ bulk and ● wall temperature profile of nanofluid at 5 wt%, as a function of the adimensional length. Re 11933, heat flux 5308 W/m^2 and mass flow rate 0.0512 kg/s.

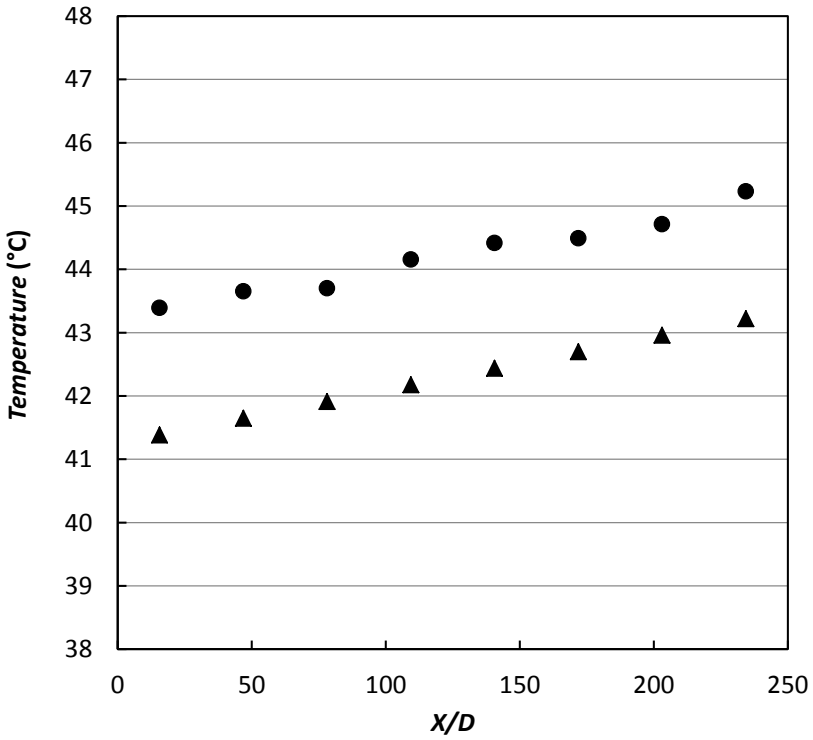

Figure 9.9: ▲ bulk and ● wall temperature profile of nanofluid at 5 wt%, as a function of the adimensional length. Re 16842, heat flux 7958 W/m^2 and mass flow rate 0.0715 kg/s.

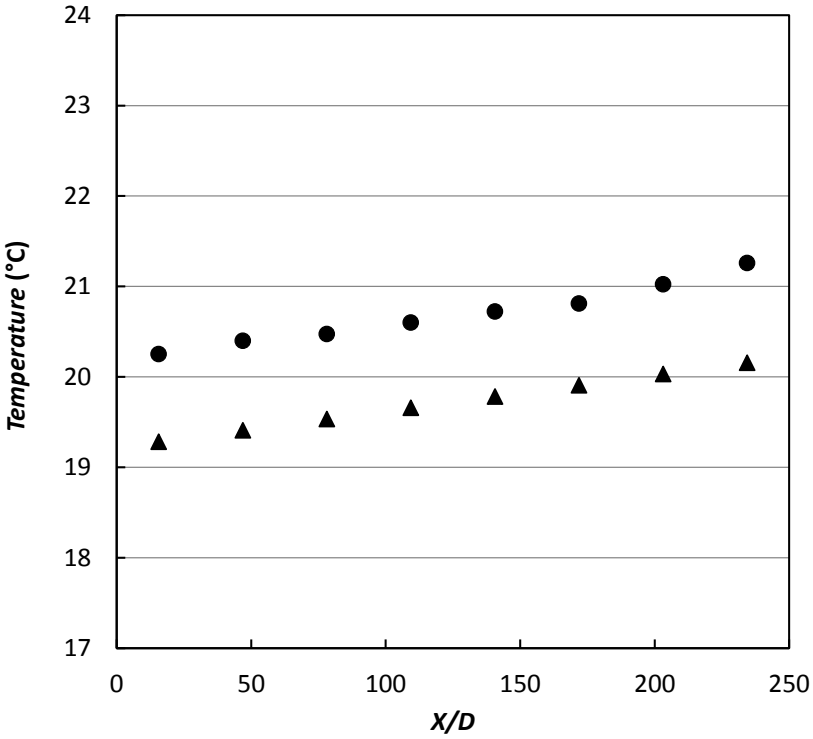

Figure 9.10: ▲ bulk and ● wall temperature profile of nanofluid at 10 wt%, as a function of the adimensional length. Re 7324, heat flux 2654 W/m^2 and mass flow rate 0.0525 kg/s.

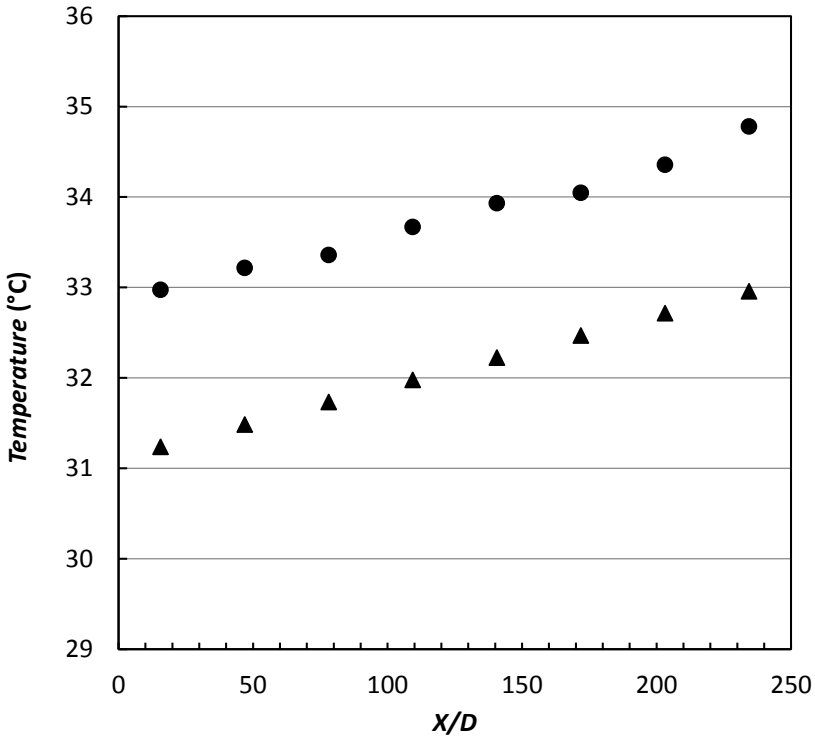

Figure 9.11: ▲ bulk and ● wall temperature profile of nanofluid at 10 wt%, as a function of the adimensional length. Re 9665, heat flux 5308 W/m^2 and mass flow rate 0.0533 kg/s.

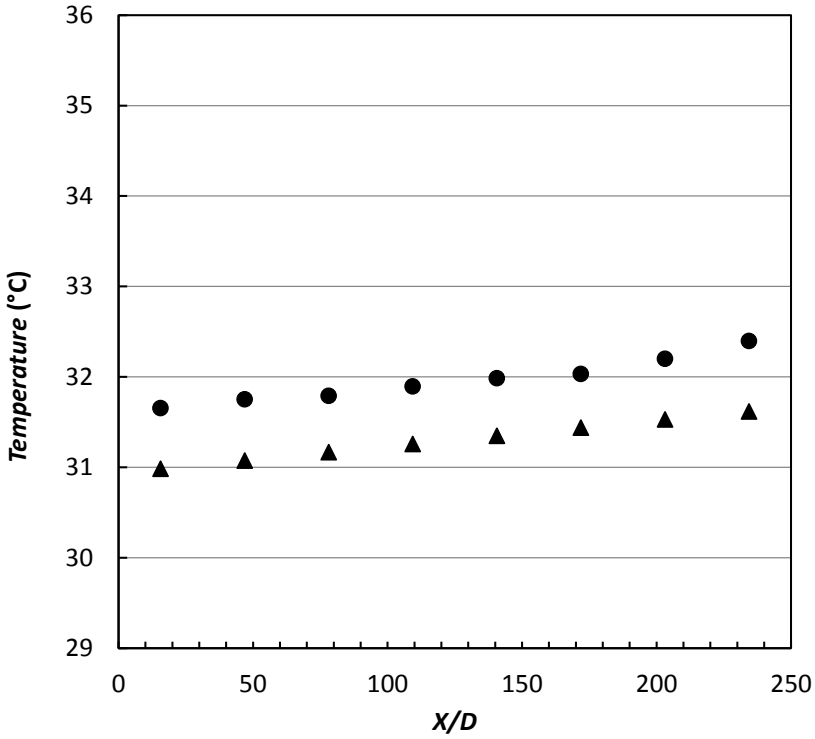

Figure 9.12: ▲ bulk and ● wall temperature profile of nanofluid at 10 wt%, as a function of the adimensional length. Re 12960, heat flux 2654 W/m^2 and mass flow rate 0.0724 kg/s.

Experimental water heat transfer coefficients were compared with nanofluid heat transfer coefficient data, obtained in the same test configuration. Figures 9.13-9.15 show the heat transfer coefficient, α, as a function of specific mass flow rate, G, for water and nanofluids at three different inlet temperatures, *i.e*. 19°C, 30°C, 40°C. Experimental data indicate that there is not an increase in heat transfer coefficient for this nanofluid at temperatures of 19°C, 30°C and 40°C, on respect to water, with even lower heat transfer coefficients, *e.g*. -7% at 30°C.

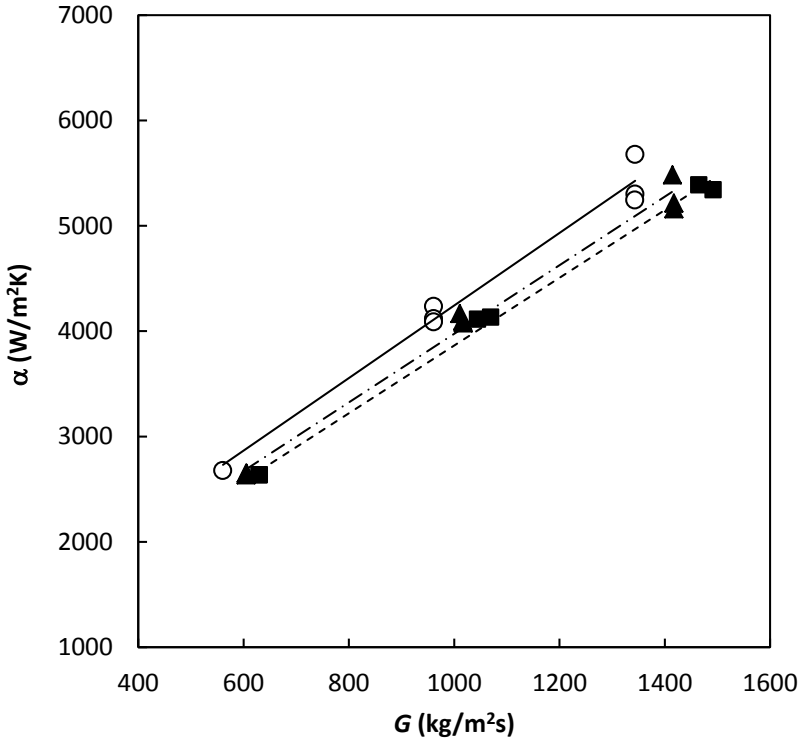

Figure 9.13: Heat transfer coefficient (α) in turbulent flow for (○, ▬) water and ZnO-water nanofluid at (▲, ▬ · ▬) 5 wt%, (■, − −) 10 wt%. T_{in} = 19°C.

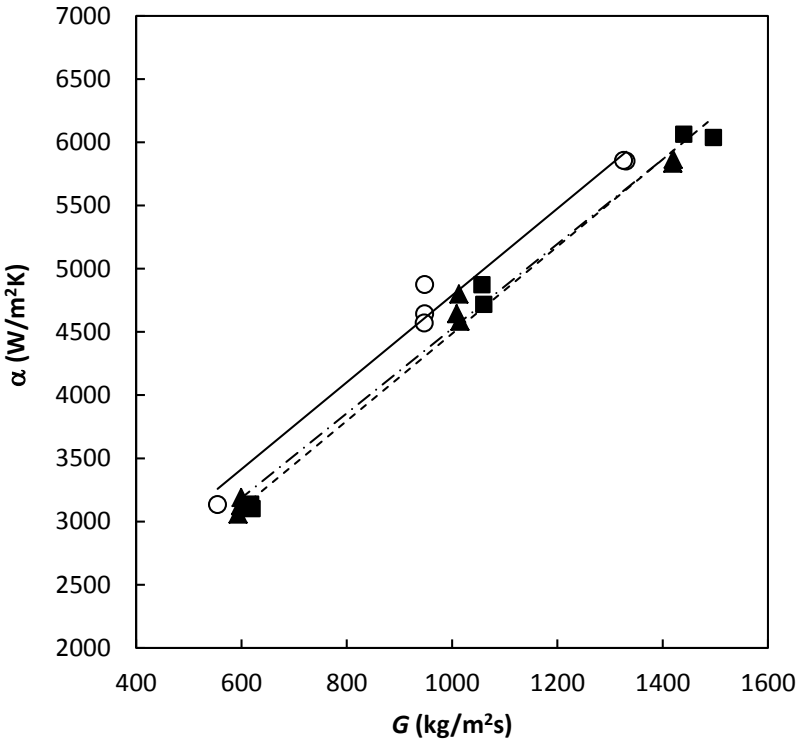

Figure 9.14: Heat transfer coefficient (α) in turbulent flow for (○, ▬) water and ZnO-water nanofluid at (▲, ▬ · ▬) 5 wt%, (■, − −) 10 wt%. T_{in} = 30°C.

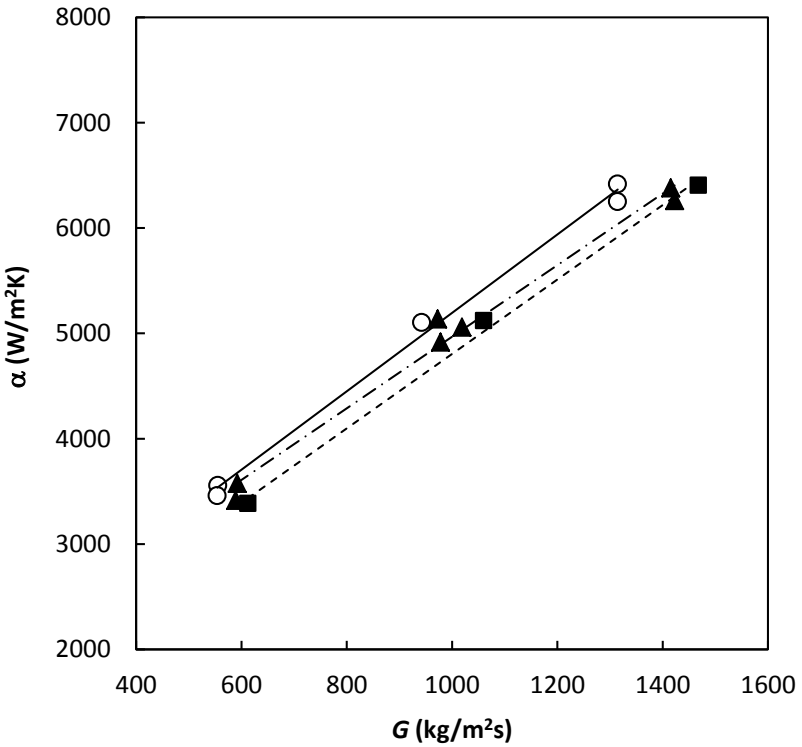

Figure 9.15: Heat transfer coefficient (α) in turbulent flow for (○, ▬) water and ZnO-water nanofluid at (▲, ▬ · ▬) 5 wt%, (■, − −) 10 wt%. T_{in} = 40°C.

9.6 Comparison with published literature

In literature, several papers present studies on ZnO nanoparticles dispersed in Ethylene Glycol [2-4] or water-ethylene glycol [5] mixtures, but only few works consider ZnO nanoparticles dispersed in pure water. Amongst them, Jalal *et al*. [6] and Zhang *et al*. [7] studies ZnO-water nanofluids as potential antibacterial agent and Singh [8] presented the ZnO nanoparticles synthesis and their electrical properties and thermal conductivity. Only two papers investigate ZnO-water nanofluid thermal conductivity or dynamic viscosity, as Ferrouillat *et al*. [9] and Suganthi and Rajan [10].

9.6.1 Thermal conductivity

Water/ZnO nanofluids with concentrations similar to those studied in this work (2.4 wt% and 5 wt%) have been measured by *Ferrouillat et al.* [9]. Unfortunately, thermal conductivity data are shown in figure, and not numerically indicated in a table, therefore only a qualitative comparison is possible. From this comparison, it can be observed that thermal conductivity of nanofluid is slightly higher than water conductivity, similar to case here studied.

9.6.2 Dynamic viscosity

Dynamic viscosity results, similar to those found in this work, were found in Suganthi and Rajan [10] and Ferrouillat *et al.* [9]. In the first paper, the relative viscosity of ZnO-water nanofluids was found to be independent on temperature. A comparison is possible for the nanofluid at 5 wt% (0.93 vol%) studied in this work and the nanofluid at 1 vol% studied in [10], from 10°C and 30°C. Experimental viscosity data, shown in a figure and not labelled, in [10] are roughtly 20% higher than those found in this work. However, these authors propose a correlation for relative viscosity, regressed, they say, on their data, for nanoparticles concentration between 0 and 1.5 vol%, which is in agreement with the data of this thesis, within 6%. From the paper [10], it is not comprehensible how experimental data and regressed equation could deviate so much.

Ferrouillat *et al.* [9] discovered a dynamic viscosity behaviour very similar to that observed in this work. A more accurate comparison is not possible, because the article does not provide the values of viscosity data.

9.6.3 Heat transfer coefficient

Ferrouillat *et al*. [9] analyse the heat transfer coefficient of two water-ZnO nanofluids (with polygonal and rod–like nanoparticles), for Re between 1000 and 10000, with fixed

wall temperature boundary conditions. Their results indicate that there is an increase in heat transfer coefficient of nanofluids compared to that of water: 8% with polygonal nanoparticles (4.4 wt%) and 3% for rod–like nanoparticles (5 wt%) at 20°C and 50°C. Therefore they found an enhancement at 5 wt% that is not found in this work.

9.7 Conclusions

ZnO-water nanofluid was found to be very stable during the analysis lasting for one month.

Thermal conductivity is similar to that of water at the lower concentration, while for nanofluids at 5 wt% and 10 wt% there are enhancements of 12% and 15% at 70°C, respectively.

The dynamic viscosity of the nanofluids at 1 wt% are very similar to water viscosity, while it increases of about 5% for the nanofluid at 5 wt% and 12% for the nanofluid at 10 wt%.

The nanofluids heat transfer coefficient at 5 wt% and 10 wt% was measured. Experimental results do not show an increase on the heat transfer coefficient for the suspensions here analysed.

It is worth noting ZnO-water nanofluids can be prepared with different technique, and properties of nanofluids mainly depend on the nanofluid preparation and on the chemical additive used to obtain a stable solution. For this reason, in order to investigate high performance nanofluid, other non-commercial ZnO-water nanofluids are currently under investigation. In particular ZnO-water at 0.5 wt%, with polyvinylpirrolidone as dispersant, is under study in CNR-ITC (Padova) laboratory.

References

[1] E. W. Lemmon, M. L. Huber, M. O. McLinden, NIST Standard Reference Database 23, Reference Fluid Thermodynamic and Transport Properties (REFPROP), version 9.0; National Institute of Standards and Technology (2010).

[2] G.J. Lee, C.K. Kim, M.K. Lee, C.K. Rhee, S. Kim, C. Kim, "Thermal conductivity enhancement of ZnO nanofluid using one-step physical method", *Thermochimica Acta*, 542, 24 (2012).

[3] M. Kole, T. K. Dey, "Effect of prolonged ultrasonication on the thermal conductivity of ZnO–ethylene glycol nanofluids", *Thermochimica Acta*, 535, 58 (2012).

[4] W. Yu, H. Xie, L. Chen, Y. Li, "Investigation of thermal conductivity and viscosity of ethylene glycol based ZnO nanofluid", *Thermochimica Acta*, 491, 92-96 (2009).

[5] M.T. Zafarani-Moattar, R. Majdan-Cegincara, "Effect of temperature on volumetric and transport properties of nanofluids containing ZnO nanoparticles poly(ethylene glycol) and water", *Journal of Chemical Thermodynamics*, 54, 55-67 (2012).

[6] R. Jalal, E. K. Goharshadia, M. Abareshi, M. Moosavic, A. Yousefi, P. Nancarro, "ZnO nanofluids: Green synthesis, characterization, and antibacterial activity", *Materials Chemistry and Physics***,** 121, 198 (2010).

[7] L. Zhang, Y. Ding, M. Povey, D. York, "ZnO nanofluids-A potential antibacterial agent", *Progress in Natural Science***,** 18, 939 (2008).

[8] A. K. Singh, "Synthesis, characterization, electrical and sensing properties of ZnO nanoparticles", *Advanced Powder Technology*, 21, 609 (2010).

[9] S. Ferrouillat, A. Bontemps, O. Poncelet, O. Soriano, "Influence of nanoparticle shape factor on convective heat transfer and energetic performance of water-based SiO_2 and ZnO nanofluids", *Applied Thermal Engineering*, 51, 839 (2013).

[10] K. S. Suganthi, K. S. Rajan, "Temperature induced changes in ZnO–water nanofluid: Zeta potential, size distribution and viscosity profiles", *International Journal of Heat and Mass Transfer*, 55, 7969 (2012).

Chapter 10

Ethylene glycol based SiC nanofluid characterization

Ethylene glycol-based (EG-based) nanofluids, containing silicon carbide (SiC) in the concentrations 0.1, 1 and 5 wt%, were characterized, in order to understand their potentiality to improve the heat transfer efficiency of the base fluid. EG can be used as a heat-transfer fluid in heating applications with maximum operating temperatures, higher than water boiling temperature.

SiC is characterized by high thermal conductivity, *i.e.* 490 W/mK [1], and it is supposed to enhance the thermal properties of EG more than other common materials, such as metal oxides.

10.1 Nanofluid preparation

EG-based nanofluids containing SiC at concentrations 0.1, 1 and 5 wt% were supplied by Nanograde Llc. An anionic dispersant (not specified by the manufacturer) was added to the suspensions at concentrations 0.008, 0.08 and 0.4 wt%, respectively.

10.2 Nanofluids stability characterization

Stability of three considered suspensions, at 0.1, 1 and 5 wt%, was studied. Declared nanoparticle size by the supplier is 10-50 nm. Actual mean particle diameter was measured every day for a period of 30 days to evaluate its stability. Two samples were analysed for each nanofluid: one static and the other one shaken before each measurement to evaluate the presence of deposited agglomerated. As shown in Figure 10.1, both static and shaken samples showed a similar and practically constant values, around 100-120 nm for all nanoparticle concentrations, along the 30 days period. Only the shaken sample at 5 wt% nanoparticle concentrations showed higher mean diameters, increasing with time, denoting progressive agglomeration and deposition of part of the nanoparticles.

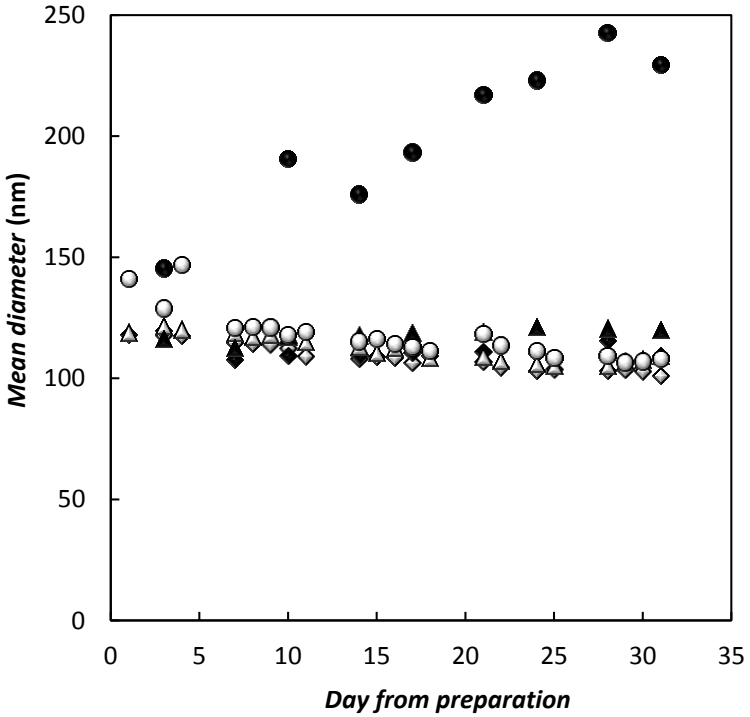

Figure 10.1: Dimensional stability analysis in 30 days. (◊) 0.1 wt%, (Δ) 1 wt%, (○) 5 wt%, static samples (empty symbols) and shaken samples (full symbols).

10.3 Thermal conductivity

The thermal conductivity data were measured, using a TPS 2500 S (Hot Disk), between 10°C and 70°C, at ambient pressure. All the measured data are summarised in Table 10.1, Figure 10.2 shows the measured thermal conductivity, whereas Figure 10.3 shows the ratio between the thermal conductivity of nanofluids and that of EG, indicating the enhancement obtained by adding nanoparticles. Pure EG thermal conductivity was calculated on the base of [2].

Thermal conductivity ratio ($\lambda_{nf}/\lambda_{EG}$) increases with temperature and concentrations. Suspensions at 0.1% and 1% do not show large differences in thermal conductivity, probably due to the presence of the dispersant, that should have thermal conductivity lower than EG. The ratio ranges from around 1.05 at 10°C to around 1.10 at 70°C. Higher enhancements, up to 21%, are shown by the nanofluid at 5%, at 70°C.

Table 10.1: Thermal conductivity data for EG-SiC nanofluids.

$\Delta\% = (\lambda_{exp}-\lambda_{EG})/\lambda_{EG}\cdot 100$

ω	T (°C)	λ_{exp} (W/mK)	λ_{EG} (W/mK) [2]	$\Delta\%$
0.1%	10.3	0.256	0.245	4.43
	30.3	0.267	0.250	6.74
	50.0	0.277	0.255	8.52
	69.0	0.284	0.260	9.16
1%	10.4	0.259	0.245	5.65
	30.3	0.271	0.250	8.32
	50.0	0.280	0.255	9.57
	69.7	0.289	0.260	11.26
5%	10.4	0.275	0.245	11.93
	30.3	0.288	0.250	15.09
	50.0	0.297	0.255	16.56
	69.8	0.315	0.260	21.07

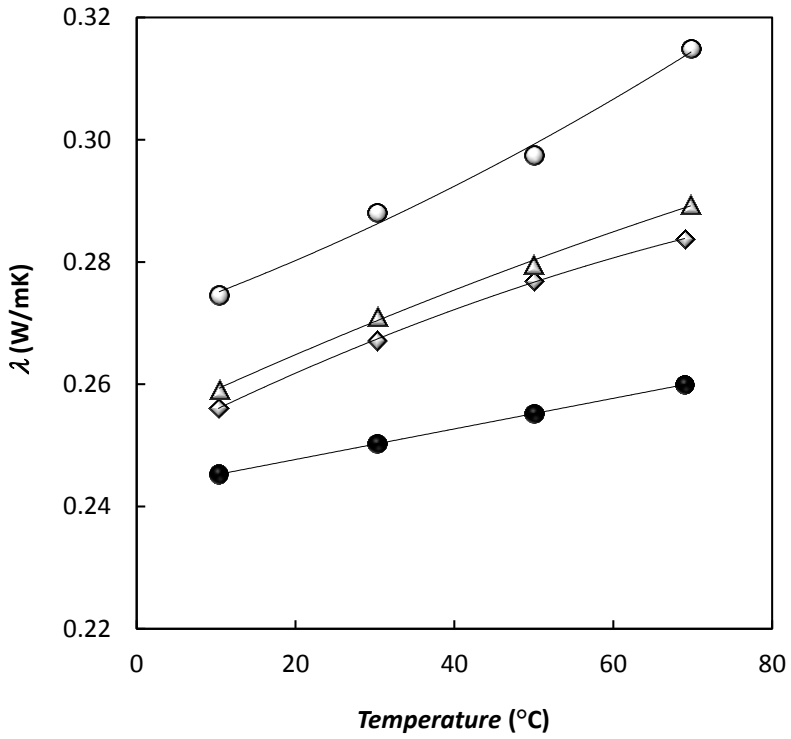

Figure 10.2: Thermal conductivity data for the EG-SiC nanofluids. (●) EG, (◊) 0.1 wt%, (Δ) 1 wt%, (○) 5 wt%.

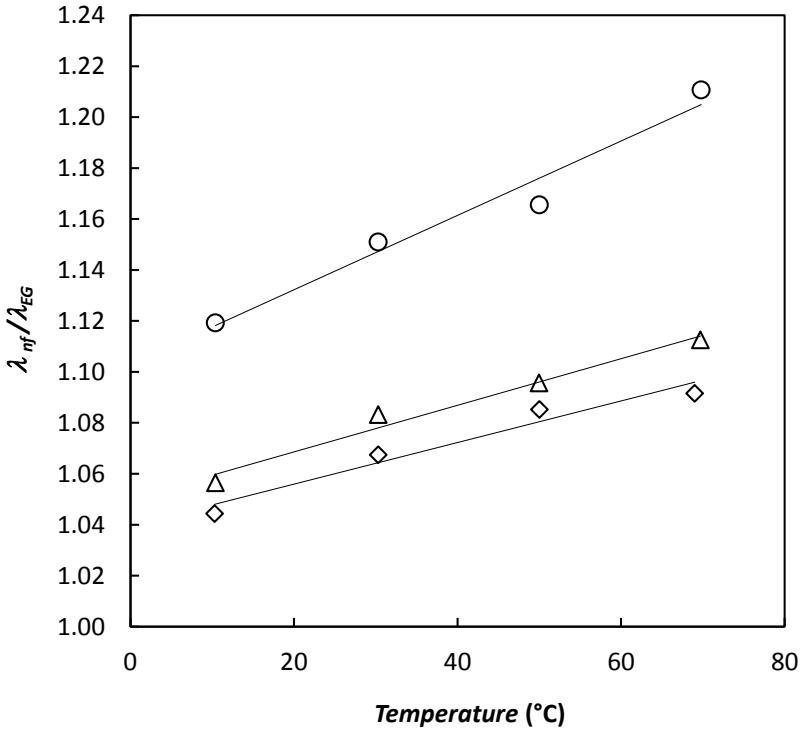

Figure 10.3: Thermal conductivity ratio for the EG-SiC nanofluids. (◊) 0.1 wt%, (Δ) 1 wt%, (○) 5 wt%.

10.4 Dynamic viscosity

The dynamic viscosity was measured at ambient pressure and in a temperature range between 10°C and 90°C by means of an AR-G2 rheometer. The experimental procedure and apparatus have been already described in chapter 3. All the data measured at shear rate 830 1/s are summarized in Table 10.2, Figure 10.4 shows the measured dynamic viscosity, whereas Figure 10.5 shows the dynamic viscosity ratio (μ_{nf}/μ_{EG}), *i.e.* the enhancement obtained by adding nanoparticles.

The dynamic viscosity of the nanofluids at 0.1 and 1 wt% is lower or similar to that of ethylene glycol. This may be due to the presence of the dispersant or to the interactions between the nanoparticles. However, the differences are of the same order of the experimental uncertainties.

For the suspension at 5 wt%, the dynamic viscosity enhancement is around 30% from 10°C to 50°C and then rapidly increases up to 70% at 90°C. This behaviour could be due to nanoparticles aggregation at elevated temperatures.

Table 10.2: Dynamic viscosity data for EG-SiC nanofluids.

$\Delta\% = (\mu_{exp}-\mu_{EG})/\mu_{EG}\cdot 100$

ω	T (°C)	μ_{exp} (Pa s)	μ_{EG} (Pa s) [2]	$\Delta\%$
	10.0	0.0330	0.0349	-5.35
	20.0	0.0209	0.0214	-2.50
	30.0	0.0136	0.0140	-3.38
	40.0	0.0093	0.0097	-4.77
0.1%	50.0	0.0066	0.0070	-5.96
	60.0	0.0051	0.0053	-3.64
	70.0	0.0038	0.0041	-5.49
	80.0	0.0031	0.0032	-2.48
	90.0	0.0024	0.0026	-6.65
	10.0	0.0343	0.0349	-1.86
	20.0	0.0218	0.0214	1.51
	30.0	0.0140	0.0140	-0.67
	40.0	0.0096	0.0097	-1.59
1%	50.0	0.0069	0.0070	-2.11
	60.0	0.0053	0.0053	0.18
	70.0	0.0039	0.0041	-3.17
	80.0	0.0033	0.0032	1.35
	90.0	0.0025	0.0026	-4.12
	10.0	0.0452	0.0349	29.51
	20.0	0.0289	0.0214	35.02
	30.0	0.0185	0.0140	31.66
	40.0	0.0129	0.0097	32.66
5%	50.0	0.0093	0.0070	32.90
	60.0	0.0074	0.0053	41.36
	70.0	0.0058	0.0041	43.14
	80.0	0.0053	0.0032	63.90
	90.0	0.0044	0.0026	69.63

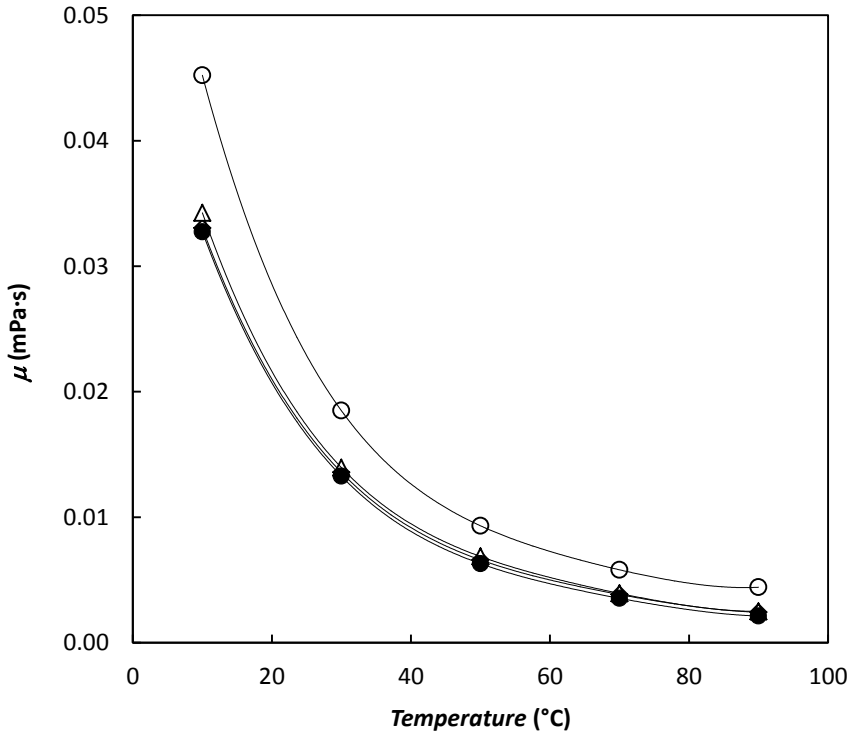

Figure 10.4: Dynamic viscosity data for the EG-SiC nanofluids. ● EG, (◊) 0.1 wt%, (Δ) 1 wt%, (○) 5 wt%.

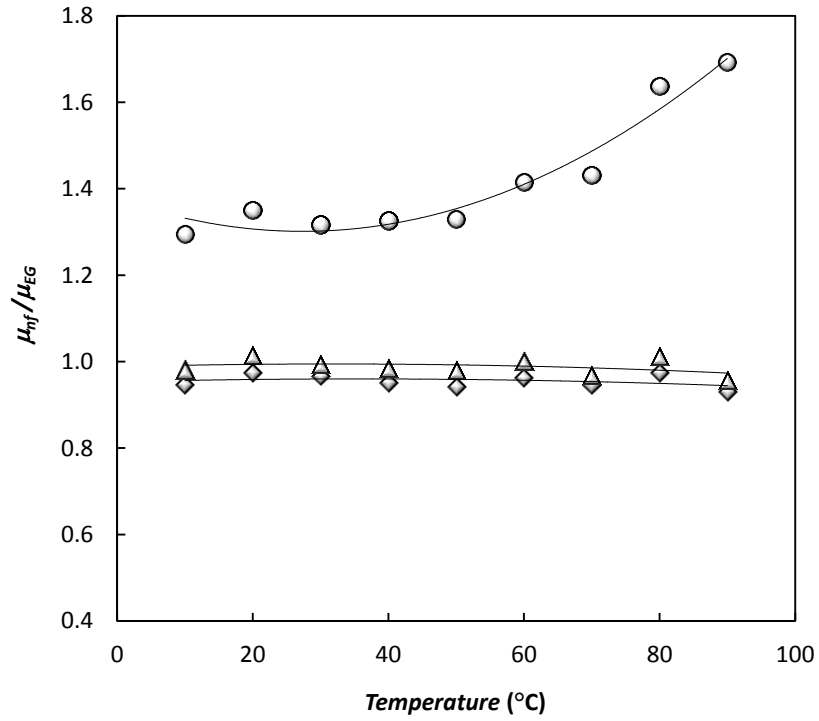

Figure 10.5: Dynamic viscosity ratio for the EG-SiC nanofluids. (◊) 0.1 wt%, (Δ) 1 wt%, (○) 5 wt%.

It should be noted that all the nanofluids at 0.1 wt% and 1 wt% show a Newtonian behaviour, as pointed out in Figure 10.6. Whereas nanofluid at 5 wt% seems to indicate shear-thinning behaviour.

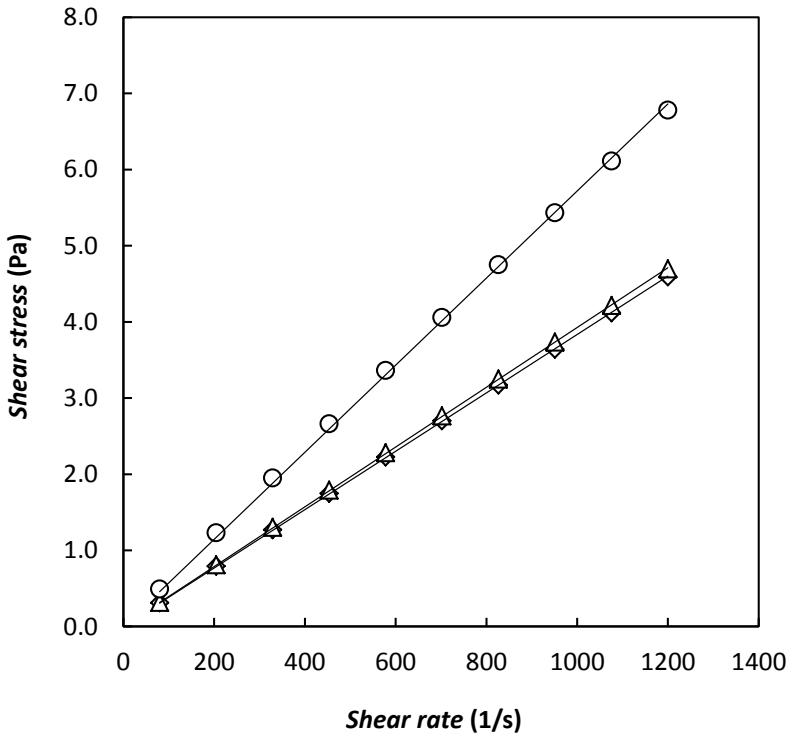

Figure 10.6: Shear stress as a function of shear rate for EG-SiC nanofluids at 70°C. (◊) 0.1 wt%, (Δ) 1 wt%, (○) 5 wt%. The same behaviour repeats for all the temperatures.

10.5 Heat transfer coefficient

The heat transfer coefficient of pure EG was previously measured in the experimental apparatus at the inlet fluid temperature of 32°C and 50°C. The temperature range is imposed by functional limits of the measuring apparatus. Laminar flow was investigated measuring the heat transfer coefficient at three flow rates from 0.0423 to 0.0782 kg/s for each temperature. Reynolds numbers ranged from 550 to 930 and from 950 to 1740, for 30°C and 50°C, respectively. Experimental thermal conductivity and dynamic viscosity data were used to calculate the convective heat transfer coefficient. Nanofluid density ρ_{nf} and nanofluid heat capacity $c_{p,nf}$ were calculated knowing SiC density and heat capacity (ρ_{SiC}, $c_{p,SiC}$) and base fluid density and heat capacity (ρ_{fluid}, $c_{p,fluid}$) at each temperature, the suspension volume fraction φ and mass fraction ω, with the correlations 3.19 and 3.20.

Heat transfer behaviour of EG-SiC nanofluids in mass concentration of 0.1 and 1% was studied at the same conditions imposed for pure EG and the results are shown in Figure 10.6 and 10.7. Nanofluid behaviour is very similar to pure EG in the entire investigated specific mass flow rate, *G*. The deviations between the experimental heat transfer coefficients of nanofluids and pure EG are lower than 0.5%. This value is lower than the experimental uncertainty on the heat transfer coefficient, and then the fluids can be considered very similar in terms of heat transfer coefficient. Therefore, nanofluids at 0.1 and 1% are not indicated to the substitution of pure glycol in heat transfer applications, at the temperatures here considered.

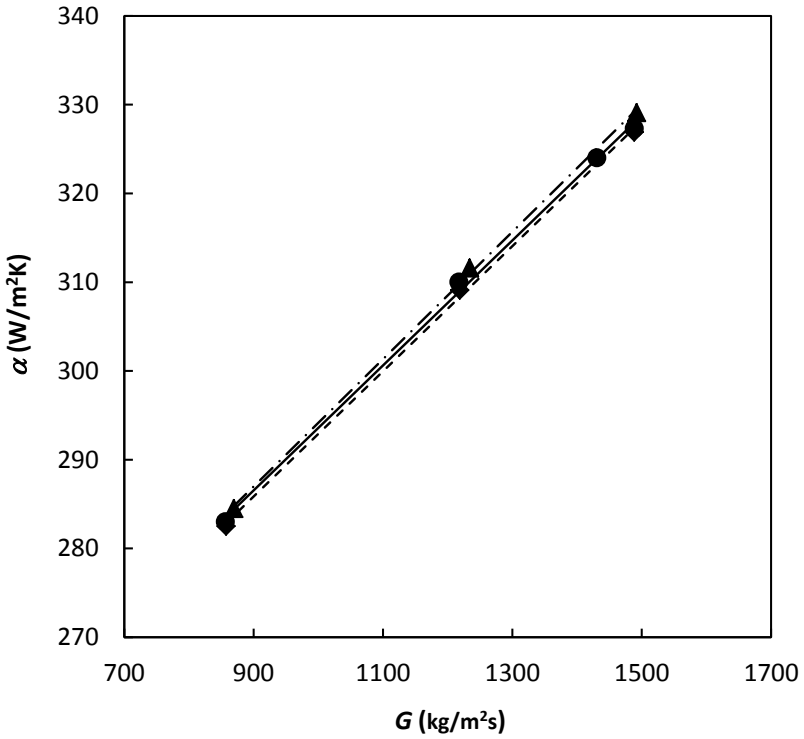

Figure 10.6: Heat transfer coefficient (α), as a function of specific mass flow rate, *G*, for EG (● ─) and EG-SiC nanofluids in mass concentration of 0.1% (♦ − −) and 1% (▲− · −), at 32°C.

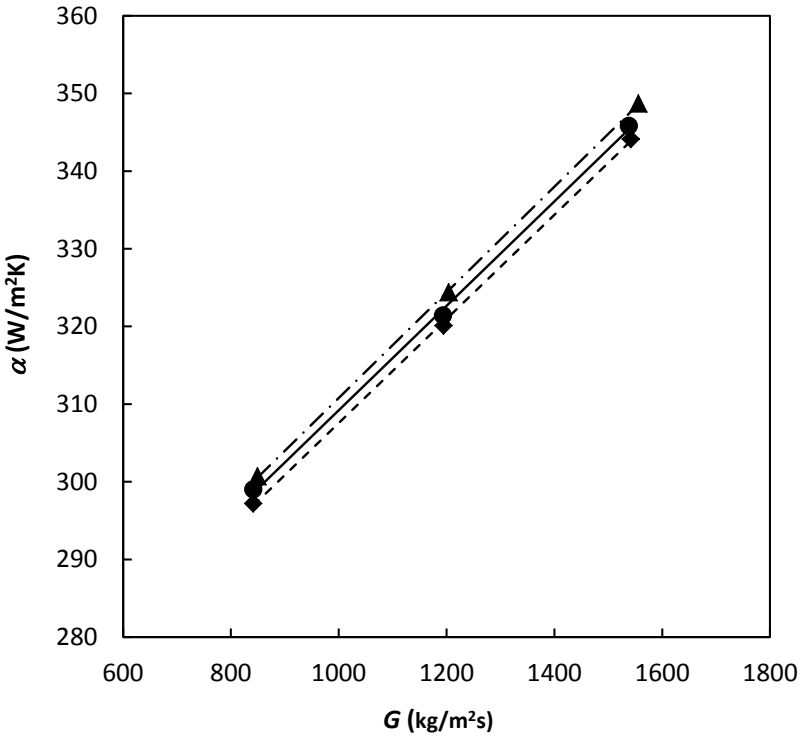

Figure 10.7: Heat transfer coefficient (α), as a function of specific mass flow rate, *G*, for EG (● ─) and EG-SiC nanofluids in mass concentration of 0.1% (♦ − −) and 1% (▲− · −), at 50°C.

10.6 Comparison with published literature

Only few data are available for thermal conductivity of EG-SiC nanofluids, while no rheological properties were found in the literature.

10.6.1 Thermal conductivity

Xie *et al.* [1] studied the thermal conductivity of two kinds of SiC nanoparticles, with average size of 26 nm and 600 nm, respectively, in water and ethylene glycol.

Considering the dimensions of the nanoparticles employed for the preparation of the nanofluids here studied, a comparison can be done only with the suspension containing the smaller particles.

In [1] thermal conductivity of suspensions with concentrations up to 4% by volume were measured only at 4°C. Considering that compositions and temperatures are different from those studied in this paper and that in [1] no data are explicitly reported, but only graphically represented in the figures, a quantitative comparison is quite difficult.

However, the suspension at roughly 2 vol% could be compared to that at 5 wt%, *i.e*. 1.82 vol%. In [1], the suspension at 2% shown an enhancement of about 7% in thermal conductivity at 4°C, that can be considered in reasonable agreement with the increase of about 12% found with the suspension at 5 wt% at 10°C.

10.6.2 Heat transfer coefficient

Heat transfer behaviour was studied for water-SiC nanofluids in turbulent flow [3, 4], but no heat transfer coefficient data were found in the literature for SiC in ethylene glycol.

10.7 Conclusions

Viscosity and thermal conductivity for nanofluids formed by ethylene glycol (EG) and SiC nanoparticles were measured at various concentrations and temperatures. The thermal conductivity enhancement is relatively high at all the concentrations and is increasing with temperature up to more than 20% for the 5 wt% nanofluid. The viscosity enhancement is negligible or negative at concentrations up to 1 wt%. Vice versa, it is quite significant for the 5 wt% nanofluid, with a strong increase at temperatures higher than 50°C, suggesting aggregation of the nanoparticles.

The results of heat transfer measurements indicate EG-SiC nanofluids here studied are not promising as heat transfer media.

References

[1] H. Xie, J. Wang, T. Xi, Y. Liu, "Thermal conductivity of suspensions containing nanosized SiC particles", *International Journal of Thermal Sciences*, 23, 571-580 (2002).

[2] M.J. Assael, E. Charitidou, S. Avgoustiniatos, W.A. Wakeham, "Absolute Measurements of the Thermal Conductivity of Mixtures of Alkene-Glycols with Water", *International Journal of Thermophysics*, 10, 1127-1140 (1989).

[3] W. Yu, D.M. France, D.S. Smith, D. Singh, E.V. Timofeeva, J.L. Routbort, "Heat transfer to a silicon carbide/water nanofluid", *International Journal of Heat and Mass Transfer*, 52, 3606-3612 (2009).

[4] A. Ijam and R. Saidur, "Nanofluid as a coolant for electronic devices (cooling of electronics devices)", *Applied Thermal Engineering*, 32, 76-82 (2012).

Chapter 11

Water based Au nanofluid characterization

This chapter investigates the stability, thermal and transport properties, and convective heat transfer coefficient of water-based nanofluids containing gold (Au) nanoparticles. Nanofluids were prepared with a one-step "eco-friendly" method. Au nanoparticles were chosen because of their high thermal conductivity. Several studies have been performed on Au nanofluids thermal conductivity and, despite some exceptions, in many works there is the evidence that thermal conductivity increases as the mass concentration rises. For this reason, in this chapter, three Au-water nanofluids with different mass concentrations were analysed.

Nanofluids can be used in numerous applications involving many industrial sectors and Au-water nanofluid seems to be an interesting promising fluid. However, in literature only one practical application using water-Au nanofluid has been found. Tsai *et al*. [1] found water-Au nanofluid useful to reduce thermal resistance in heat pipe.

11.1 Nanofluid preparation

Nanofluids studied in this chapter were prepared by ISTEC-CNR laboratories in Faenza. The one pot synthesis of metal nanoparticles involves preparation under conditions where the nanoparticles nucleate and grow, usually by the reduction of metal ions in the presence of a ligand or a chelating agent that can bind to the surface of the newly formed particle, offering stability, increased control over nanoparticle size, and modifying surface reactivity (Dahl *et al*. [2]). Particularly, the stability of nanofluids is strongly dependant by chelating agents, which are always needed in order to create a stable suspension. With the aim to ensure the best chelation effect on the high reactive surface of nanoparticles, most of the organic additives added as chelating agents for metal nanoparticles are usually introduced in a very large excess with respect to the metal. Typical ligands for metals include phosphines, thiol, amines, but the more useful in term of colloidal stability are amphiphilic surfactants and some polymers as polyvinylpyrrolidone (PVP), polyvinylacetate (PVAc),

polyvinylalcohol (PVA), polyethylenglycol (PEG), chitosan, dextrane, starch, cellulose etc. However, most of the added capping agents affect the nanofluid thermal properties toward a depletion of the performance. For this reason, in order to limit the negative effect of chelants, we chose as capping agent the sodium citrate, which, with respect to other additives, does not alter thermal properties excessively, guaranteeing the suspension stability. Moreover, the amount of citrate, added as few as possible, was exploited also as reducer, thus avoiding the introduction of other reagents, which could have a detrimental effect on the thermal properties.

The following analytic grade reagents were used to prepare the test fluids: $HAuCl_4$ solution 30 wt% (Aurobit Division) and sodium citrate tribasic dihydrate (Sigma-Aldrich). The metallic nanoparticles were prepared using an "eco-friendly procedure".

In order to prepare Au colloids, 240 ml of sodium citrate solution with concentrations of 0.3 mM, 2.4 mM, and 4.8 mM was added to a round bottom flask and the solution was heated (rate 30°C/min) at ambient pressure to a temperature of 90°C using a microwave source. At this temperature, 10 ml of $HAuCl_4$ solution at concentrations of 7.5 mM, 19.3 mM, and 38.8 mM was added to the flask and stirred for 5 min. A molar ratio for citrate/Au of three was used. After reaction, red suspensions of gold nanoparticles with a solid loading of 0.02 wt%, 0.05 wt%, and 0.1 wt% were obtained, as shown in Figure 11.1.

Figure 11.1: Red suspensions of gold nanoparticles.

The solutions were heated to the synthesis temperature under magnetic stirring in a commercial microwave oven especially designed for chemical synthesis and equipped with a reflux system (Microsynth Plus, Milestone). The reaction chamber of the system is equipped with magnetic stirring, reflux system and an optical fiber temperature controller. The microwave power is generated by two 800 W magnetrons with frequencies of 2.45 GHz. The microwave power is automatically controlled to generate the desired heating (temperature)

profile. A scanning electron microscope (SEM) image of the Au nanoparticles is reported in Figure 11.2.

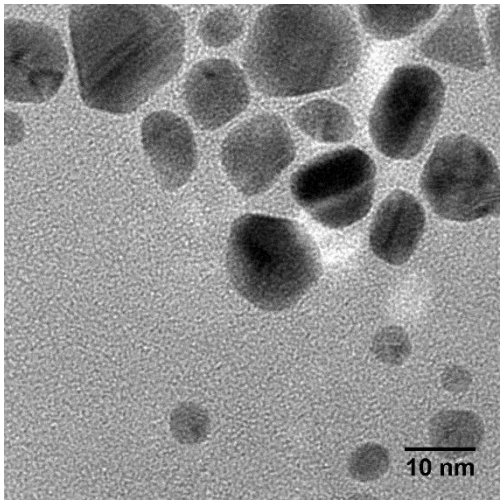

Figure 12.2: SEM image of the Au nanoparticles.

11.2 Nanofluids stability characterization

Stability of water based nanofluids containing Au in mass concentration of 0.02%, 0.05% and 0.1% was analysed. Au-water nanofluid at 0.02% has always been very stable throughout the 10 days of measurements. Nanofluid at 0.05% reveals lower stability, since nanoparticles tend to settle, although they return in suspension without forming large clusters, simply after shaking. On the contrary, nanofluid at 0.1% completely settles in 3 days after preparation and micrometric clusters are visible even to naked eye. In Figure 11.3, the difference between the nanofluid at 0.1% when just prepared and after 3 days of measurements is shown. Stability of nanofluid at 0.1% could be improved by increasing the amount of sodium citrate in solution, but this kind of synthesis is still under optimization. For this reason, nanofluid at 0.1% has not been considered for next measurements.

Figure 11.3: Nanofluid at 0.1% just prepared (on the left) and after 3 days of measurements (on the right).

11.3 Thermal conductivity

Both the nanofluids at Au compositions 0.02 and 0.05 wt% and the relative base fluids, water-sodium citrate, at 0.03 and 0.07 wt%, respectively, were measured between 10°C and 70°C, at atmospheric pressure. In Figure 12.4, all the results are summarized, while in Figure 12.5 the thermal conductivity enhancement on respect to pure water (Refprop 9.0 [3]) is presented as a function of temperature.

Thermal conductivity of base fluids water-sodium citrate is very similar to thermal conductivity of pure water for both fluids. A maximum increase up to about 5% was found rising the temperature until 70°C. Relating to nanofluids, a remarkable enhancement was found for the nanofluid at 0.02 wt%. As shown in Figure 12.5 the maximum enhancement respect to pure water is 21% at 70°C. Unexpectedly, thermal conductivity of nanofluid at 0.05 wt% is not higher than that of the base fluid and this could be due to the low stability of nanoparticles in suspension, especially at high temperature. Nanoparticles probably settled during the measurements and therefore the actual Au concentration could be lower than 0.05%.

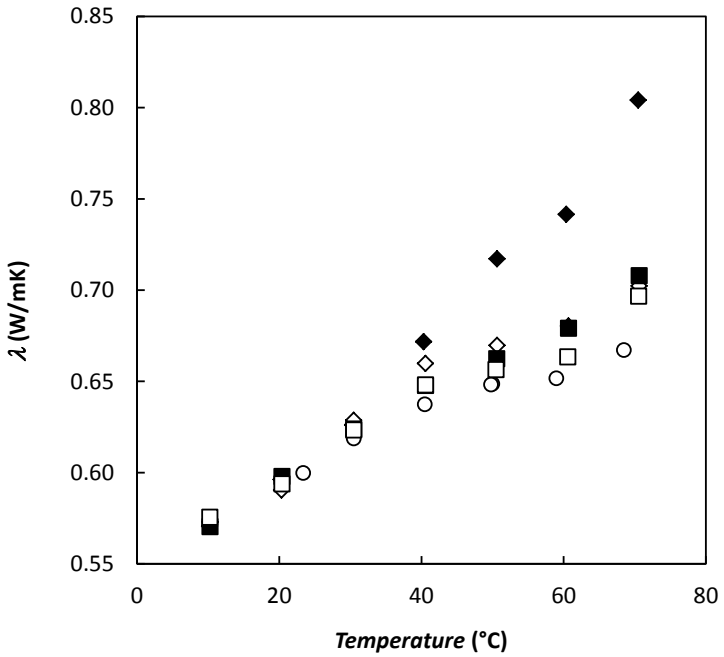

Figure 11.4: Thermal conductivity data for (○) water, Au-water at (♦) 0.02 wt%, (■) 0.05 wt% and water-sodium citrate base fluids at (◊) 0.03 wt% and (□) 0.07 wt% as a function of temperature.

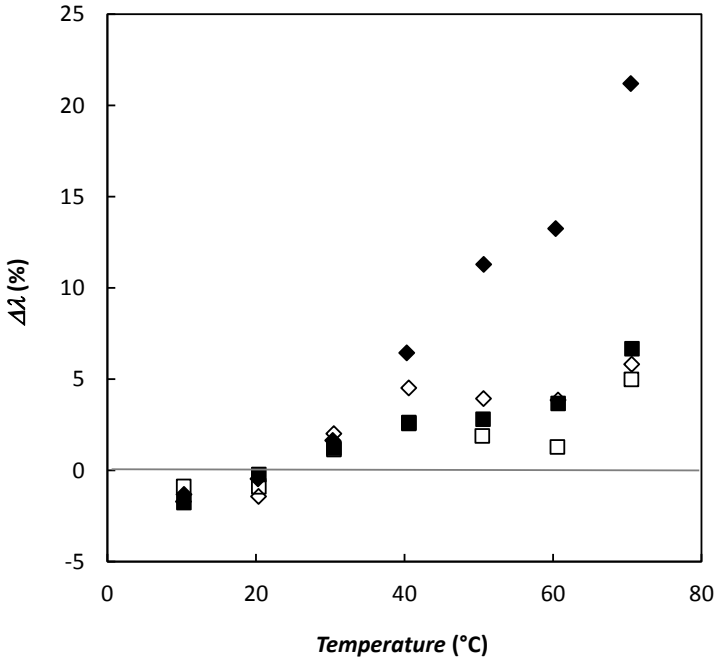

Figure 11.5: Thermal conductivity ratio for Au-water at (♦) 0.02 wt%, (■) 0.05 wt% and water-sodium citrate base fluids at (◊) 0.03 wt% and (□) 0.07 wt% as a function of temperature. $\Delta\lambda\% = 100 \cdot \dfrac{\left(\lambda_{nf} - \lambda_{water}\right)}{\lambda_{water}}$

11.4 Dynamic viscosity

Firstly, the dynamic viscosity of all the three nanofluids, at compositions of 0.02%, 0.05% and 0.1% by mass, was measured at 10°C. Nanofluid at 0.1% showed micrometric clusters visible to the naked eye, after the rheological test, as shown in Figure 11.6. For this reason, this nanofluid was neglected. Results for nanofluids at 0.02% and 0.05% are summarized in Figure 11.7. The temperature range is between 10°C and 70°C in steps of 10°C, at atmospheric pressure, and the shear rate varied from 80 1/s to 1200 1/s. No increase in viscosity, compared to pure water, was found. Considering these results, dynamic viscosity of water-sodium citrate base fluids was not measured, foreseeing it also should be similar to water.

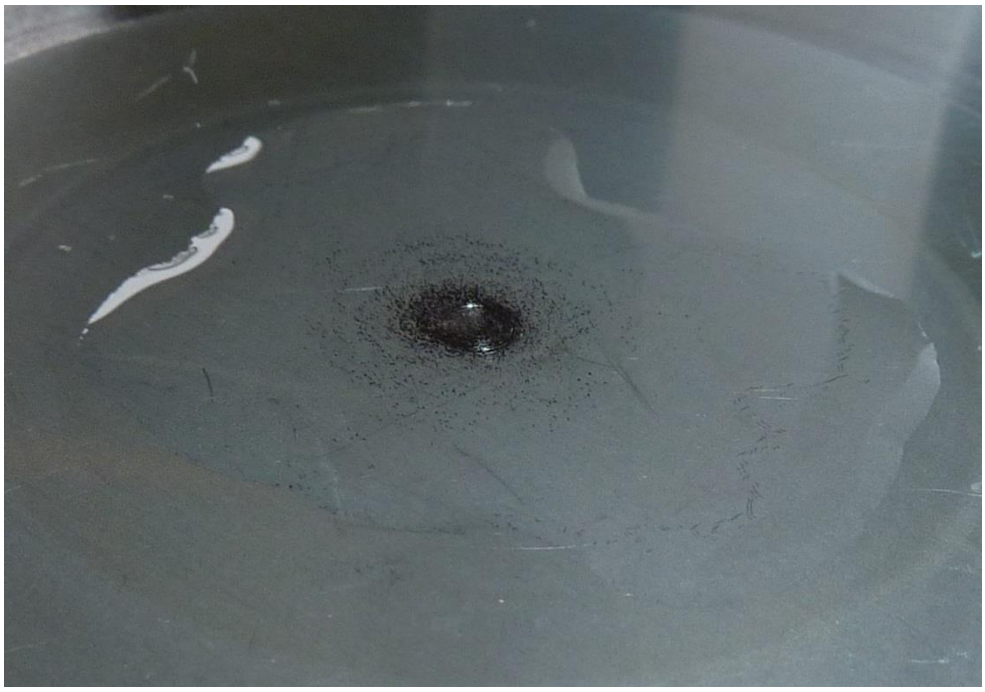

Figure 11.6: Visible clusters, after the rheological test.

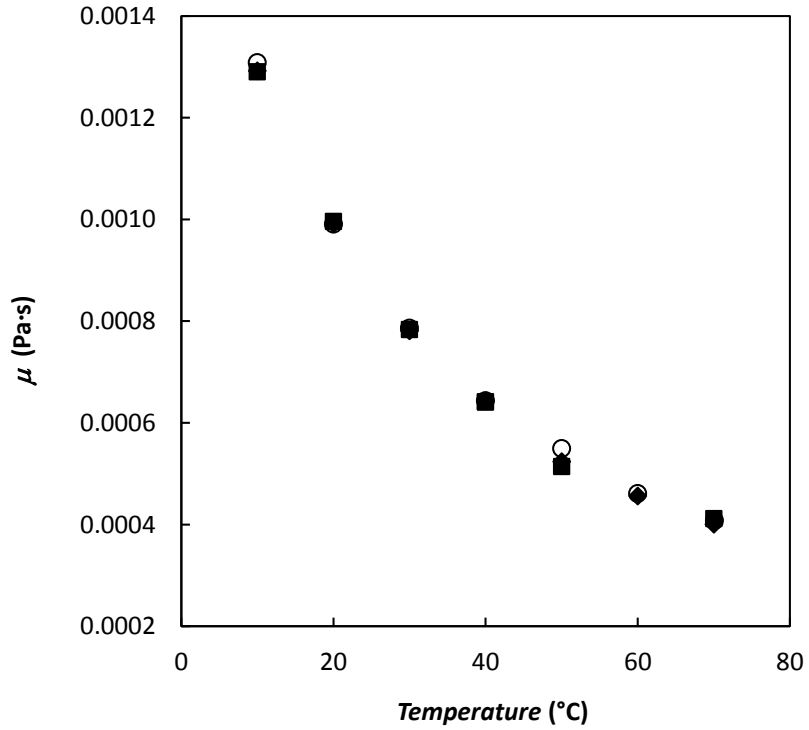

Figure 11.7: Dynamic viscosity of (○) water and Au-water at (♦) 0.02 wt%, (■) 0.05 wt% as a function of temperature.

11.5 Heat transfer coefficient

The heat transfer coefficient of the suspension at 0.02 wt% was studied at single-phase flow and at an inlet fluid temperature of 19°C and 41°C. This limited temperature range is at present imposed by functional limits of the measuring apparatus. However, it is enough to highlight the influence of temperature on the heat transfer coefficient and possibly confirm its correlation with the thermal conductivity enhancement. Considering, for this nanofluid, the strong dependence of thermal conductivity enhancements on temperature, obtaining even small heat transfer enhancements within this range of temperatures promises much higher improvements at higher temperatures. The flow rate varied in the range between 0.024 and 0.066 kg/s and Re varied from 4000 to 17000. Experimental thermal conductivity and dynamic viscosity data were used to calculate the convective heat transfer coefficient. Nanofluid density ρ and nanofluid heat capacity c_p were calculated knowing Au density and heat capacity and water density and heat capacity at each temperature, the suspension volume fraction (φ) and the mass fraction (ω). Volume fraction was determined knowing

mass fraction, and nanoparticles and water density. Mass fractions of 0.02%, 0.05% and 0.1% correspond to 0.0010%, 0.0026% and 0.0052% volume fractions, respectively.

The nanofluid at 0.02% was considered for the analysis. All the measurements were performed at heat power range from 200 to 600 W, always obtaining a thermal balance within 3.6%. Figures 12.8 and 12.9 show the heat transfer coefficient, α, as a function of specific mass flow rate, G, for water and the nanofluid at inlet temperature T_{in} of 19°C and 41°C. An enhancement of the heat transfer coefficient has been found, depending on G. It is 5-6% at G 600 kg/m^2·s and diminishes increasing G, to 3%.

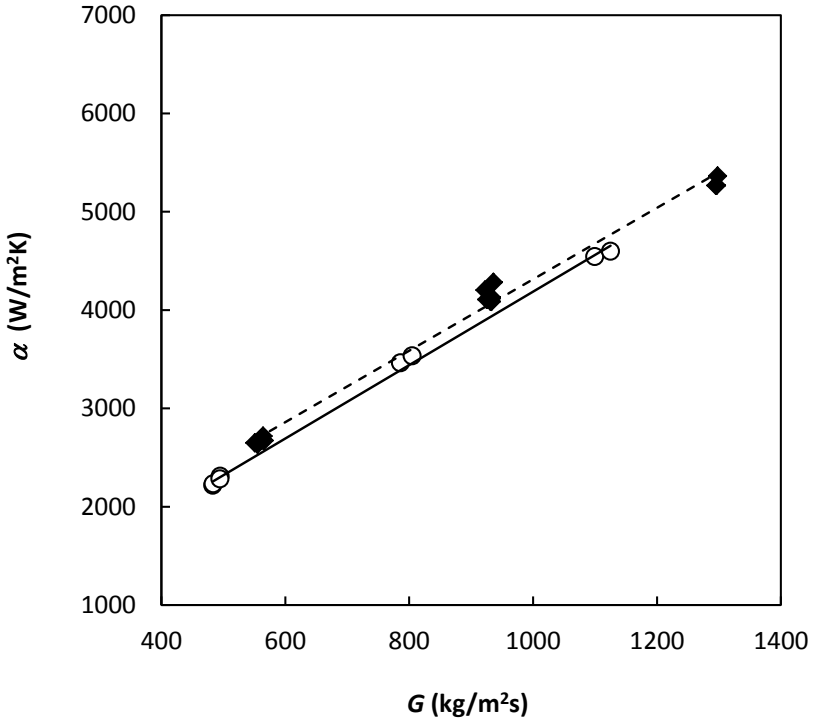

Figure 11.8: Heat transfer coefficient (α) in turbulent flow for water (○, ─) and Au-water at 0.02 wt% (♦, - -). Fluid inlet temperature is 19°C.

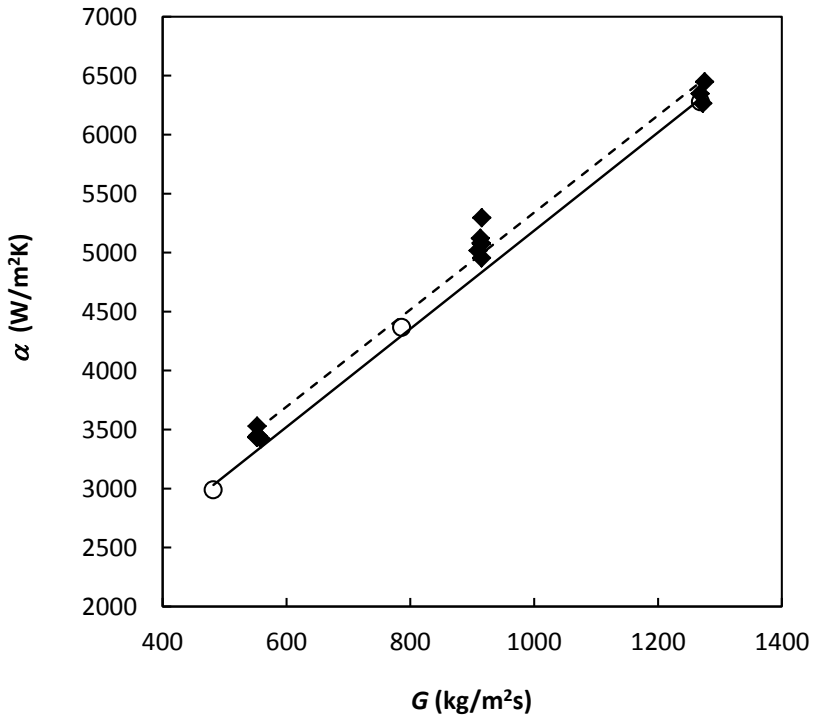

Figure 11.9: Heat transfer coefficient (α) in turbulent flow for water (○, ─) and Au-water at 0.02 wt% (♦, - -). Fluid inlet temperature is 41°C.

11.6 Comparison with published literature

Only few data are available for thermal conductivity of Au-water nanofluids, while no rheological properties were found in the literature.

11.6.1 Thermal conductivity

Several studies have been performed on Au nanofluids thermal conductivity. Amongst them, for 0.00026 volume percent of gold nanoparticles, Patel *et al*. [4] found thermal conductivity enhancement between 5% and 21% on respect to water, while Paul *et al*. [5] a maximum of 48% increment, showing a discrepancy between the literature data. Moreover, in Kim *et al*. [6], an enhancement in terms of thermal conductivity of about 9.3±5.4% was found for Au composition of 0.018 vol%.

11.6.2 Dynamic viscosity

In literature, no viscosity data was found for a comparison with this work. However, as revealed by this investigation, viscosity of nanofluids is very influenced not only by the nanoparticles mass fraction, but also by their stability, shape and size.

11.6.3 Heat transfer coefficient

In literature, no heat transfer data was found for a comparison with this work.

11.7 Conclusions

Stability, dynamic viscosity, thermal conductivity and heat transfer coefficients for nanofluids formed by water and Au nanoparticles were studied at 0.02 wt%, 0.05 wt% and 0.1 wt% at various temperatures.

The thermal conductivity of the nanofluid at 0.02 wt% showed significant enhancement (up to 20 %) compared to water. The nanofluid at 0.1 wt% was completely unstable and also the nanofluid at 0.05 wt% was too unstable during the measurement.

The dynamic viscosity of the nanofluids was found to be very similar to water, thus not penalizing flow performance.

The heat transfer coefficients of the nanofluid at 0.02 wt% showed an enhancement, compared with pure water, up to approximately 5-6% in the temperature range between 19°C and 41°C. This result is-promising and it will be interesting, for future works, to optimize a chemical synthesis able to produce nanofluids with higher nanoparticles concentration. In fact, increasing the amount of nanoparticles, thermophysical properties could be improved and nanofluids could result promising for many industrial applications.

References

[1] C.Y. Tsai, H.T. Chien, P.P Ding, B. Chan, T.Y. Luh, P.H. Chen, "Effect of structural character of gold nanoparticles in nanofluid on heat pipe thermal performance", *Materials Letters*, 58, 1461-1465 (2004).

[2] J.A. Dahl, B.L.S. Maddux, J.E. Hutchison, "Toward Greener Nanosynthesis", *Chemical Reviews*, 107, 6, 2228-2269 (2007).

[3] E.W. Lemmon, M.L. Huber, M.O. McLinden, NIST Standard Reference Database 23, Reference Fluid Thermodynamic and Transport Properties (REFPROP), version 9.0; National Institute of Standards and Technology (2010).

[4] H.E. Patel, S.K. Das, T. Sundararajan, A.S. Nair, B. George, T. Pradeep, "Thermal conductivities of naked and monolayer protected metal nanoparticle based nanofluids: Manifestation of anomalous enhancement and chemical effects", *Applied Physics Letters*, 83, 14, 2931-2933 (2003).

[5] G. Paul, T. Pal, I. Manna, "Thermophysical property measurement of nano-gold dispersed water based nanofluids prepared by chemical precipitation technique", *Journal of Colloid and Interface Science*, 349, 434–437 (2010).

[6] H.J. Kim, I.C. Bang, J. Onoe, "Characteristic stability of bare Au-water nanofluids fabricated by pulsed laser ablation in liquids", *Optics and Lasers in Engineering*, 47, 532–538 (2009).

Chapter 12

Nanofluids with Ag nanoparticles characterization

This chapter investigates stability, thermal and transport properties, and convective heat transfer coefficient of nanofluids containing silver (Ag) nanoparticles. The base-fluids are water and a mixture water-ethylene glycol (water-EG) at a mass fraction (70:30). Mixtures of water and ethylene glycol, despite they have very poor thermal properties, are commonly used heat transfer fluids in applications of air conditioning, refrigeration and heating. This nanofluid was studied with the idea of enhance water-EG heat transfer properties in order to improve the efficiency of heat transferred or reduce the size of the heat exchangers.

12.1 Nanofluid preparation

Nanofluids studied in this chapter were prepared by IENI-CNR laboratories in Padova, developing a particular procedure, involving a one-step synthesis of nanoparticles, followed by the precipitation of nanoparticles and by their re-dispersion in the base-fluid. The one-step technique was used in order to obtain re-dispersible silver nanopowders containing a controlled amount of Polyvinylpyrrolidone (PVP) as capping polymer. Besides providing a pure nanofluid, this technique also provides the possibility of producing fluids containing different amounts of nanoparticles, although keeping almost constant the morphological properties of the particles and controlling the aggregation states. Deionized water (Millipore, Billerica MA, USA, 18.2MΩ) was used as solvent and base fluid, $AgNO_3$ (purity >99 %, provided by Sigma-Aldrich), as a metal precursor, PVP provided by Sigma-Aldrich, as surfactant polymers, D-Fructose (99 % provided by Alfa-Aesar) as a reducing agent and NaOH (anhydrous pellets provided by Carlo Erba), as a catalyst of the metal salt reducing reaction, were used in the synthesis of water soluble silver nanoparticles. The one-step technique used for the reduction of $AgNO_3$, using fructose as reducing agent and PVP as surfactant polymer, allowed easily producing primary nanofluids at concentrations as high as 0.1 vol% (1.1 wt%) Ag in water. The nanopowder was obtained by controlled precipitation.

This purpose was achieved by diluting the suspensions with acetone that, acting as anti-solvent, destabilizes the colloid causing the precipitation of particles. At the same time, being the PVP poorly soluble in acetone, it is possible to tailor the amount of polymer that precipitates along with the particles by changing the volume ratio between acetone and the suspensions. Suitable amounts of each nanopowder were used for the production of re-dispersions in deionized water and in the mixture water-ethylene glycol.

Two different nanofluids were analysed. The first one is formed by 2.6 wt% of Ag nanoparticles in water and the second one by 2.5 wt% Ag nanoparticles in a mixture water-ethylene glycol at a mass fraction (70:30).

Only for thermal conductivity measurements, a commercial nanofluid Ag-water 0.0027 wt% (Sigma Aldrich), was tested.

12.2 Nanofluids stability characterization

Several methods of preparation and synthesis conditions were tested in order to obtain a stable Ag nanofluid, as indicated in Table 12.1. The most stable solution, not included in the table, was the one at 2.6 wt% Ag and 6 wt% PVP. The mean nanoparticles diameter was measured for 30 days and in Figure 12.1 the results of the dimensional analysis are presented. It is evident that the size of nanoparticles in suspension does not change significantly from the day of preparation to one month after preparation. However, there are two main peaks at about 8 and 80 nm.

As evidence of the stability of the nanofluid, the ζ potential was measured. The resulting value is -28 mV. The pH was found to be 6.9.

Also the stability of nanofluid composed by Ag nanoparticles (2.5 wt%) in water-ethylene glycol (70:30) was analysed for 30 days. In Figure 12.2, the size of the nanoparticles of the same fluid newly prepared and after 30 days of preparation is presented. The three peaks indicate the size of about 6, 50, and 5000 nm that are time constant. ζ potential measurement (-41 mV) confirms the stability of the nanofluid.

Table 12.1: Synthesis informations and parameters.

Genaral Informations				***Synthesis parameters***			
ID	***Synthesis***	***Base-fluid***	***Wt% Ag***	***Precursor***	***Synthesis temperature* (°C)**	***Wt % reducing agent***	***Wt% surfactant***
1	One-step	Water	0.1	$AgNO_3$	25	0.09 ($NaBH_4$)	0.2
2	One-step	Water	0.1	$AgNO_3$	25	0.045 ($NaBH_4$)	0.2
3	One-step	EG	0.1	$AgNO_3$	170	EG	1 (PVP)
4	One-step	EG	0.1	$AgNO_3$	180	EG	1 (PVP)
5	One-step	EG	0.1	$AgNO_3$	190	EG	1 (PVP)
6	One-step	Water	1	$AgNO_3$	75	3.3 (Fructose)	6
7	Two-step (sonication)	EG	0.1	Ag from sample 6	25	-	~0.013
8	Two-step (sonication)	EG	1	Ag from sample 6	25	-	~0.13
9	Two-step (sonication)	EG	2.5	Ag from sample 6	25	-	~0.325
10	Two-step (sonication)	EG	2.5	Ag from sample 6	25	-	~0.275
11	Two-step (sonication)	EG	2.5	Ag from sample 6	25	-	~0.3
12	Two-step (sonication)	EG	2.5	Ag from sample 6	25	-	~0.25
13	Two-step (sonication)	EG	4	Ag from sample 6	25	-	~0.4
14	Two-step (sonication)	EG	0.8	Ag from sample 6	25	-	~0.09
15	Two-step (sonication)	Water	3.5	Ag from sample 6	25	-	~0.63
16	Two-step (stirring at 55 °C)	Water	5	Ag from sample 6	55	-	~0.5
17	Two-step (ID 15 diluition)	Water	1	Ag from sample 6	25	-	~0.1
18	Two-step (ID 15 diluition)	Water	0.5	Ag from sample 6	25	-	~0.05
19	Two-step (stirring at 55 °C)	Water	10	Ag from sample 6	55	-	~1

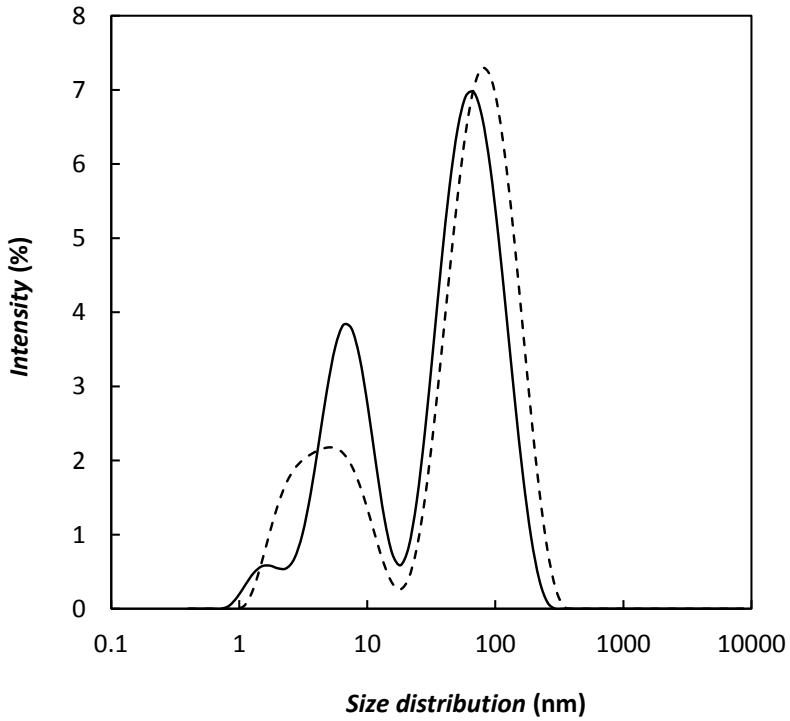

Figure 12.1: Size distribution of Ag nanoparticles in water (2.6 wt%). Continuous line shows the data to the day of the preparation, dashed line shows the data after 30 days.

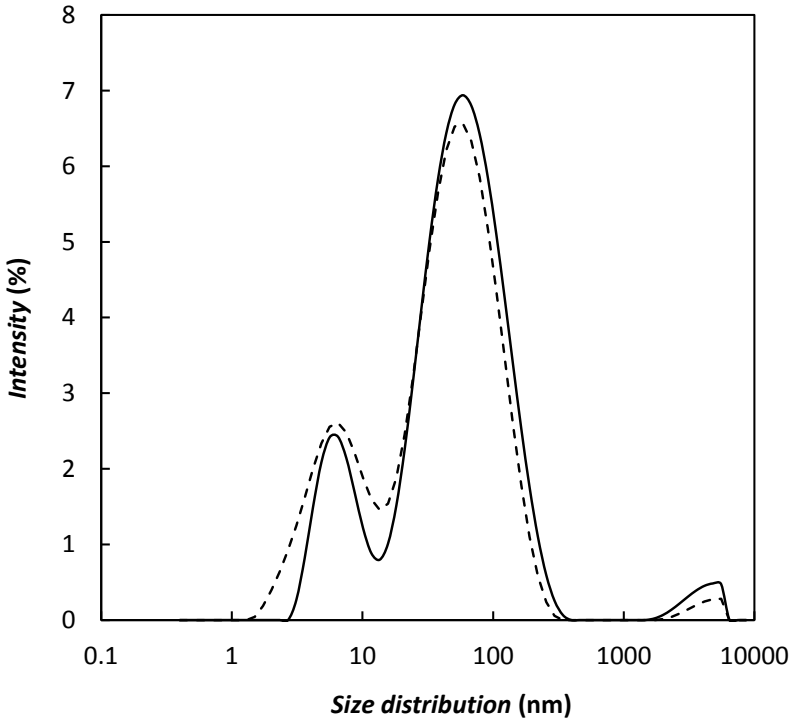

Figure 12.2: Size of Ag nanoparticles (2.5 wt%) in water-ethylene glycol (70:30). Continuous line shows the data to the day of the preparation, dashed line shows the data after 30 days.

12.3 Thermal conductivity

Thermal conductivity of water-Ag, water-EG and water-EG-Ag nanofluids was measured from 10°C to 70°C with the hot disk technique. Moreover, a commercial fluid (Ag in water at 0.0027 wt%) was tested, for comparison.

12.3.1 Water-Ag nanofluid

In Figure 12.3 the results for water-Ag nanofluid at 2.6 wt% and 0.0027 wt% are shown. It is important to note that nanofluid with order of magnitude different nanoparticles concentration reveal the same conductivity behaviour. The conductivity increases with temperature, being lower than that of water at 10°C, growing up, at 70°C, to 6.5% for nanofluid at 2.6 wt% and 12.8% for nanofluid at 0.0027 wt%. This is an interesting result highlighting the strong influence of a dispersant or of a method of preparation on the nanofluid properties. In particular, it is worth noting how the presence of PVP, fundamental for the stability, deeply penalizes the thermal properties of the nanofluid. On the contrary, in the commercial fluid, sodium citrate was used as stabilizer. It did not influence thermal properties of fluid, but only low concentrations were reachable.

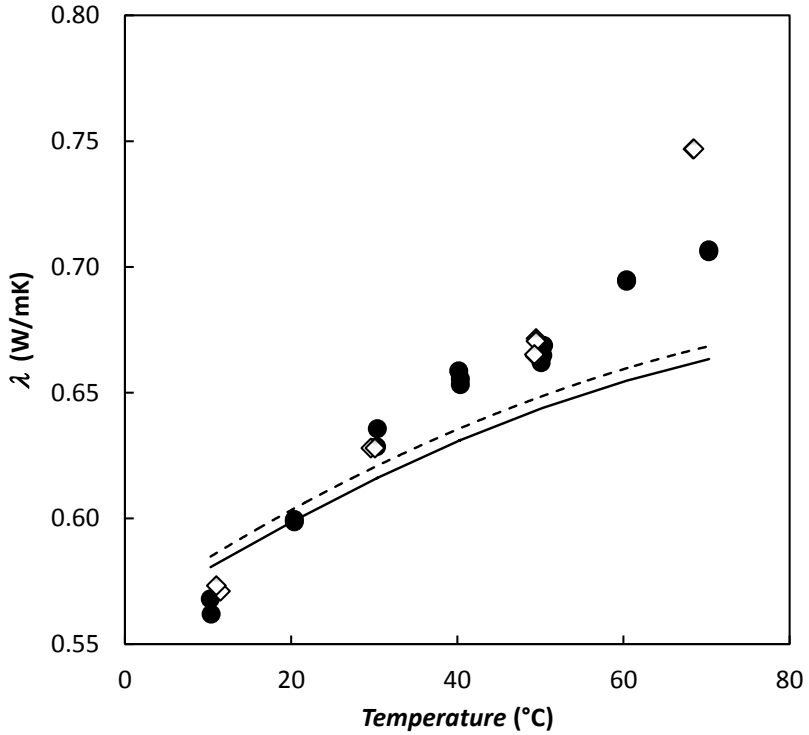

Figure 12.3: Thermal conductivity of water-based nanofluid with 2.6 wt% Ag (●) and 0.0027 wt% Ag (◊). Continuous line indicates thermal conductivity of water [1], dashed line indicates equation 3.15.

12.3.2 Water-EG nanofluid with Ag nanoparticles

In the literature, few data are available relating the thermophysical properties of ethylene glycol and its mixtures with water. For this reason, base-fluid composed of water and ethylene glycol at 70 wt% and 30 wt%, respectively, was analysed. The results are summarized in Figure 12.4 and compared with literature data [2]. The deviations between the experimental data and literature data are always lower than 5%. Then the nanofluid water-EG (70:30) nanofluid with Ag nanoparticles in mass concentration 2.5% was measured and in Figure 12.4 thermal conductivity data are shown. The enhancement of the nanofluid thermal conductivity and the measured base-fluid water-EG is always approximately 1%, therefore noticeable improvements of the thermal conductivity were not seen on respect to the base-fluid.

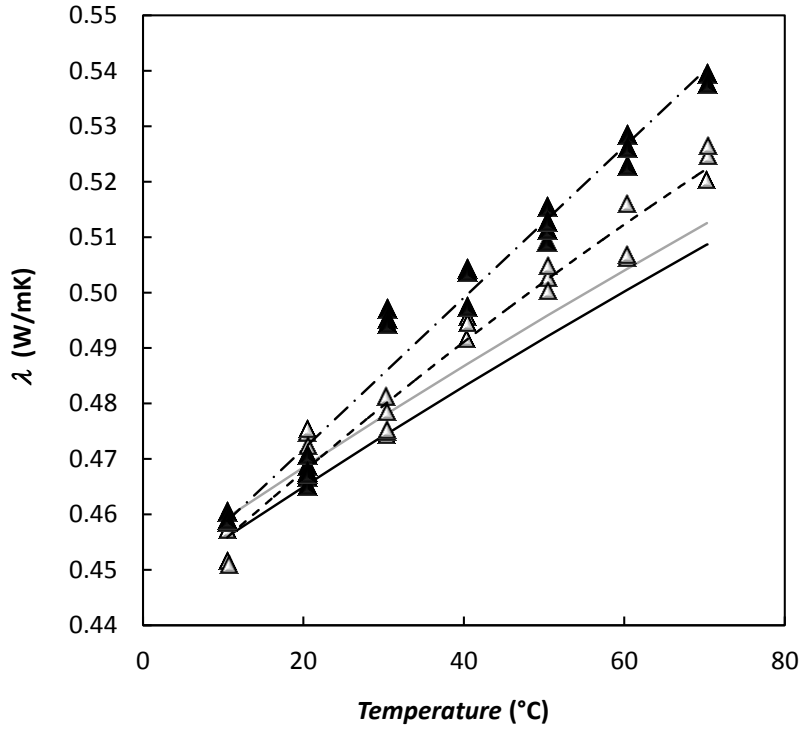

Figure 12.4: Thermal conductivity of water-EG (70:30) (Δ, - - -) and water-EG (70:30) with Ag at 2.5 wt% (▲, − · −).Continuous line indicates literature data [2] for water-EG (70:30), (—) indicates equation 3.15.

12.4 Dynamic viscosity

Dynamic viscosity was measured with a rotational rheometer in a temperature range from 10°C to 70°C.

12.4.1 Water-Ag nanofluid

Figure 12.5 illustrates the results of the measurement on water-Ag anofluid at 2.6 wt%. It is evident that the viscosity of the nanofluid is very similar to that of water, the base-fluid. The fluid has Newtonian behavior, as shown in Figure 12.6.

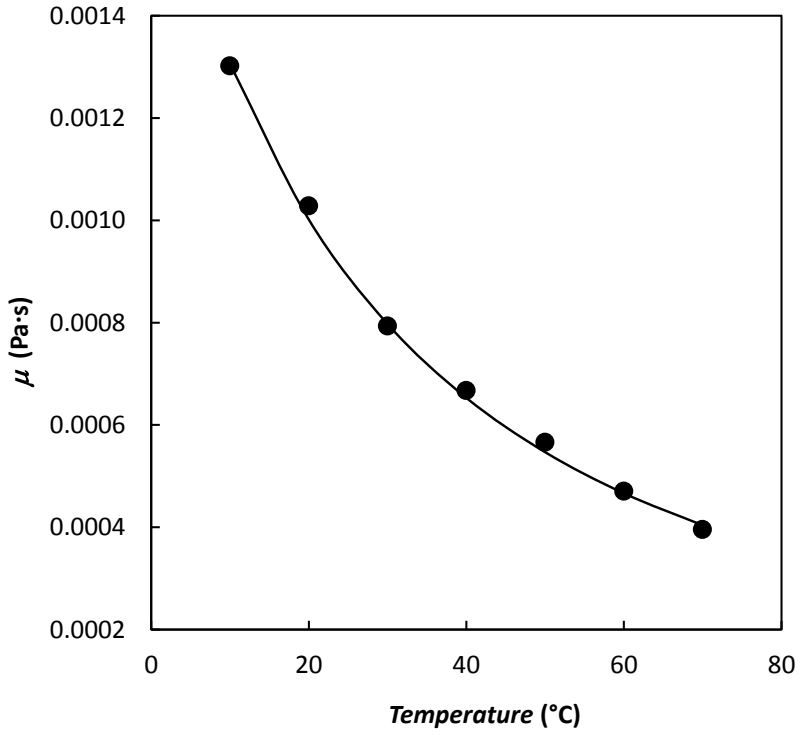

Figure 12.5: Dynamic viscosity of water-based nanofluid with 2.6 wt% Ag (●). Continuous line indicates dynamic viscosity of water [1].

12.4.2 Water-EG nanofluid with Ag nanoparticles

Since in the literature only few data are available concerning the thermophysical properties of glycol and its mixtures with water, also dynamic viscosity of the mixture of water and ethylene glycol at 70 wt% and 30 wt%, respectively, was measured. Deviations between experimental data and literature data [2] are always lower than 2.5%. Then water-EG (70:30) nanofluid with Ag nanoparticles in mass concentration 2.5% was measured and in Figure 12.7 the results are shown. The viscosity of the nanofluid and the base-fluid are very similar and the nanofluid shows a Newtonian behaviour, as shown in Figure 12.8.

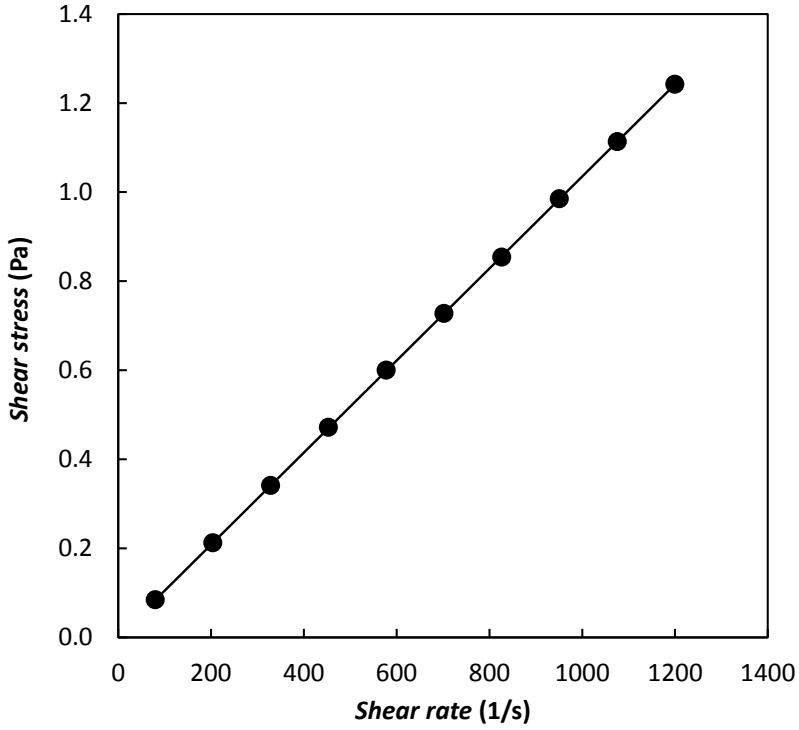

Figure 12.6: Newtonian behaviour of water-based nanofluid with 2.6 wt% Ag (●) at 20°C.

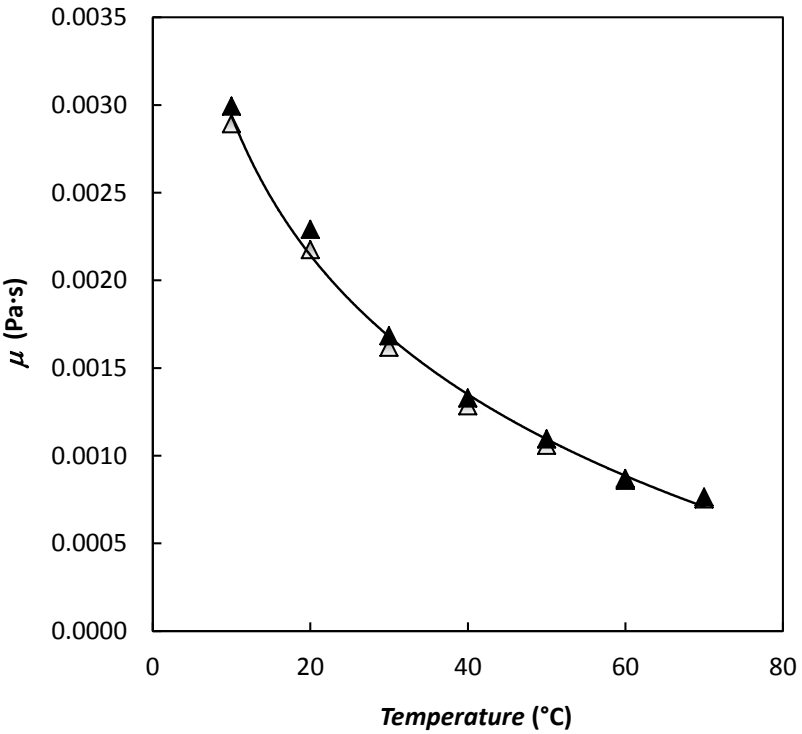

Figure 12.7: Dynamic viscosity of water-EG (70:30) (Δ) and water-EG (70:30) with Ag at 2.5 wt% (▲). Continuous line indicates literature data [2] for water-EG (70:30).

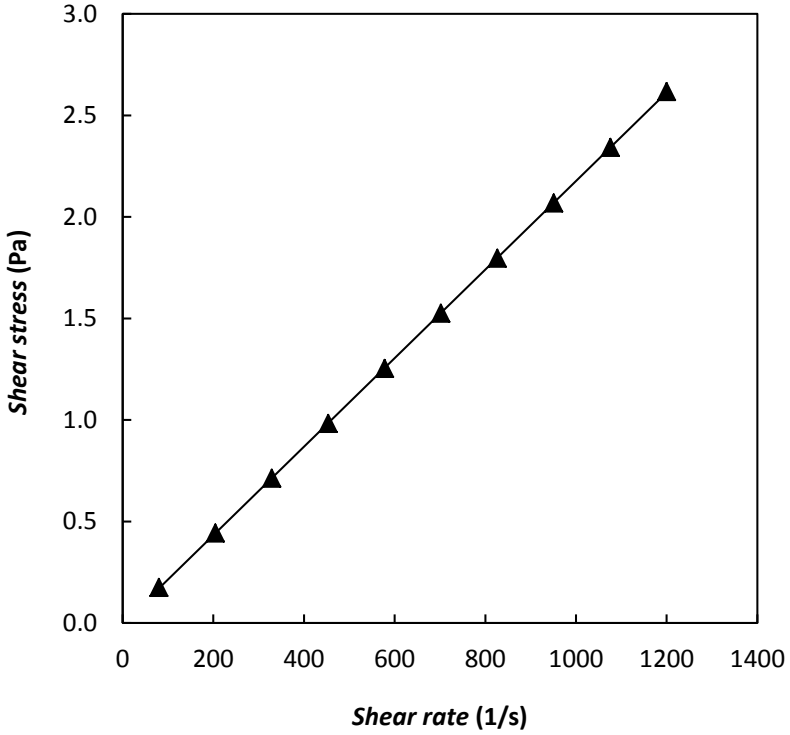

Figure 12.8: Newtonian behaviour of water-EG (70:30) nanofluid with 2.5 wt% Ag (▲), at 20°C.

12.5 Heat transfer coefficient

Heat exchange coefficient measurements were performed imposing powers from 200 W to 600 W and temperatures of the inlet fluid from 19°C to 40°C. For each condition of power and inlet temperature, the measurements were performed at variable flow rates (and thus Reynolds numbers).

12.5.1 Water-Ag nanofluid

Results on water-based nanofluid with Ag 2.6 wt% are shown in Figures 12.9, 12.10 and 12.11. Heat transfer coefficient (α) is represented as a function of specific mass flow rate, *G*. Experimental data indicate that there is not an increase in heat transfer coefficient for this nanofluid at temperatures of 19°C, 31°C and 41°C, on respect to water, with even lower heat transfer coefficients, *e.g.* -6% at 19°C.

This result is probably due to the presence of PVP, the polymer used as chemical additive to obtain a stable nanofluid, which thermal properties are worse than those of pure water, as indicated in [3].

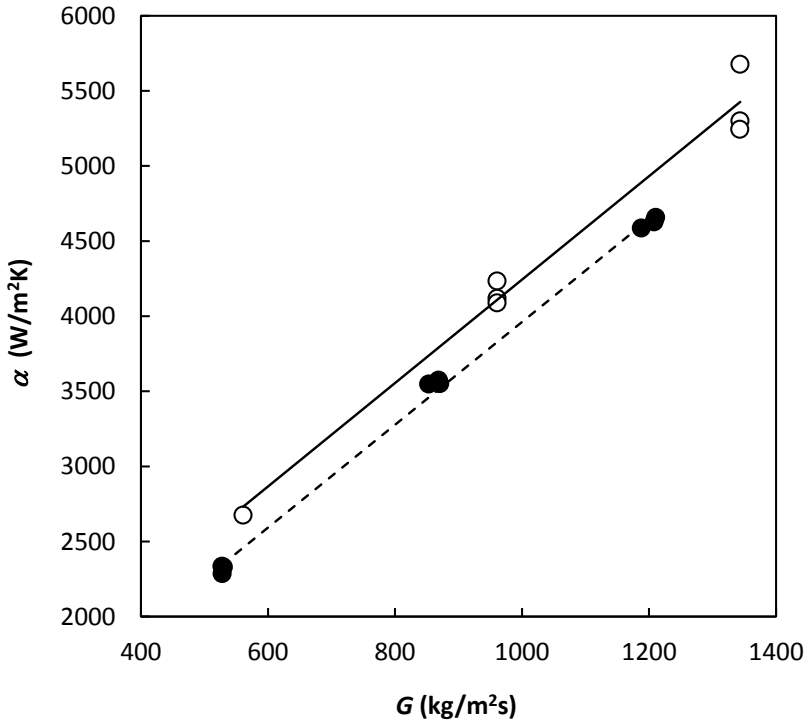

Figure 12.9: Heat transfer coefficient (α) as a function of specific mass flow rate. Water (○, ─) and water-based nanofluid with 2.6 wt% Ag (●, - -), at 19°C.

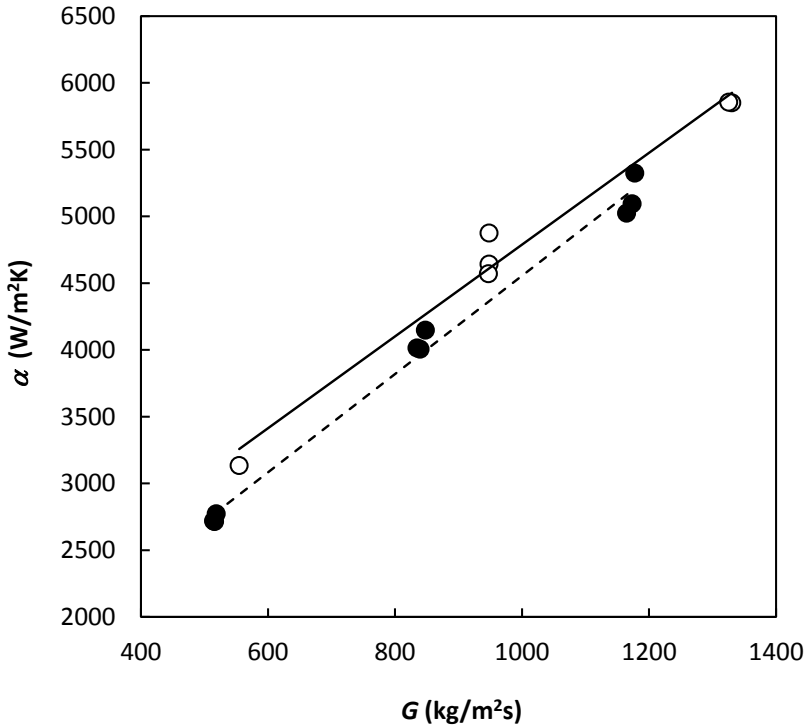

Figure 12.10: Heat transfer coefficient (α) as a function of specific mass flow rate. Water (○, ─) and water-based nanofluid with 2.6 wt% Ag (●, - -), at 31°C.

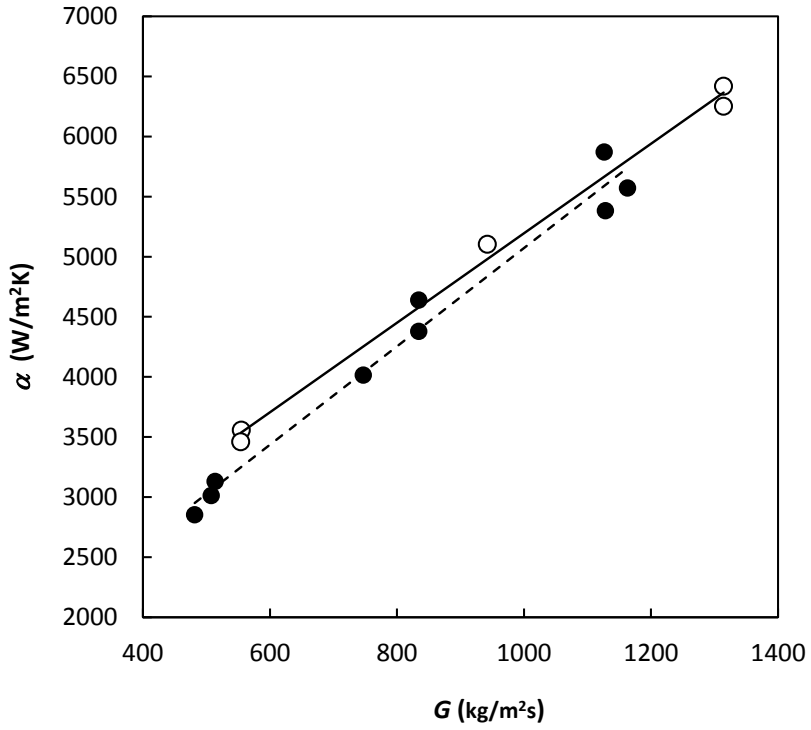

Figure 12.11: Heat transfer coefficient (α) as a function of specific mass flow rate. Water (○, ─) and water-based nanofluid with 2.6 wt% Ag (●, - -), at 41°C.

12.5.2 Water-EG nanofluid with Ag nanoparticles

In Figures 12.12, 12.13 and 12.14, convective heat transfer coefficient results, for water-EG (70:30) and water-EG (70:30) nanofluid with 2.5 wt% Ag, are shown. Inlet fluid temperatures are 19°C, 31°C and 41°C.

Also for this nanofluid, no increase in heat transfer coefficient, on respect to the base-fluid, was found.

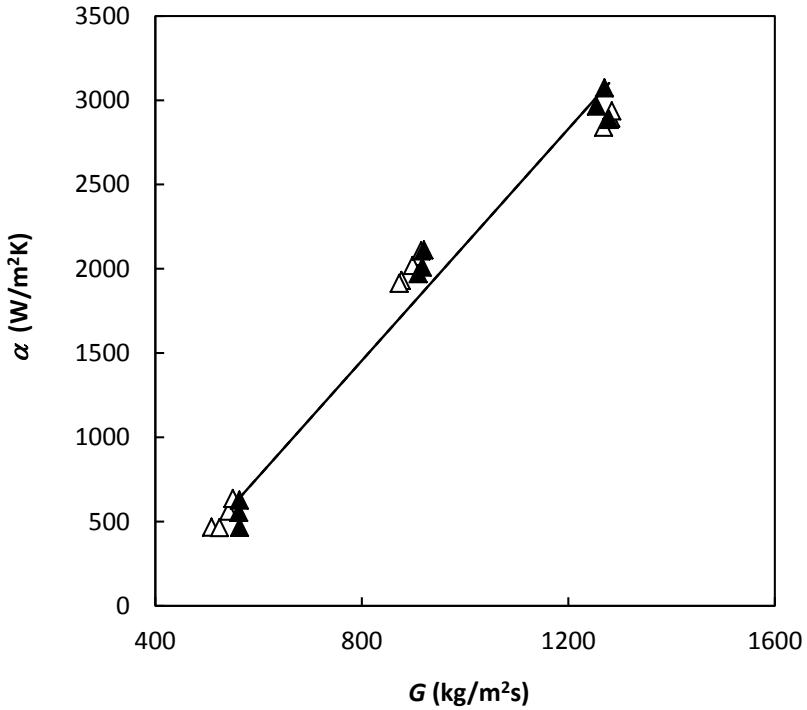

Figure 12.12: Heat transfer coefficient (α) as a function of specific mass flow rate. Water-EG (70:30) (Δ, ─) and water-EG (70:30) nanofluid with 2.5 wt% Ag (▲, - -), at 19°C.

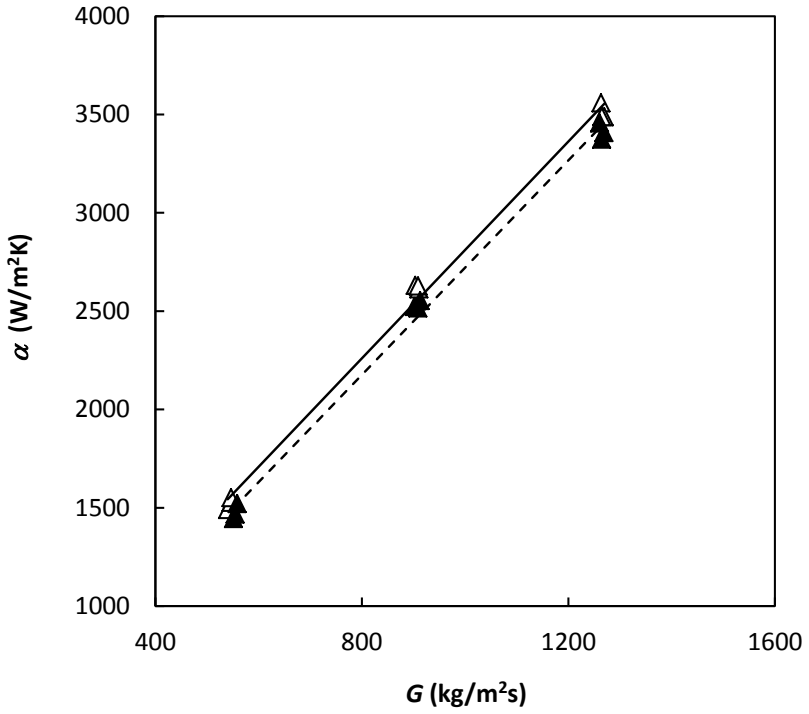

Figures 12.13: Heat transfer coefficient (α) as a function of specific mass flow rate. Water-EG (70:30) ((Δ, ─) and water-EG (70:30) nanofluid with 2.5 wt% Ag (▲, - -), at 31°C.

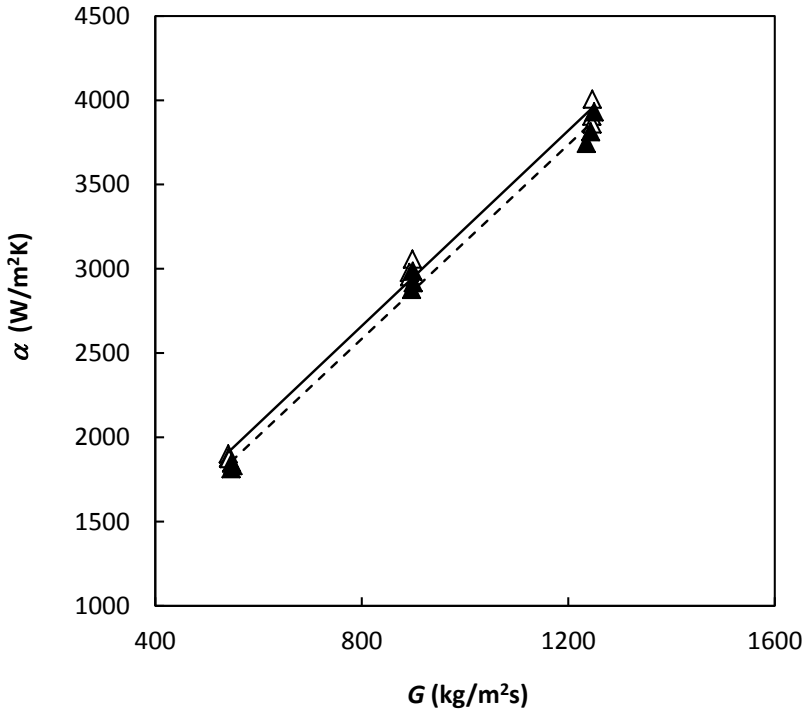

Figures 12.14: Heat transfer coefficient (α) as a function of specific mass flow rate. Water-EG (70:30) (Δ, ─) and water-EG (70:30) nanofluid with 2.5 wt% Ag (▲, - -), at 41°C.

12.6 Comparison with published literature

In literature, few papers deal with silver nanoparticles. Amongst them, in [4], authors found that thermal conductivity of silver in ethylene glycol increased with nanoparticles concentration, as compared to pure ethylene glycol. In [5], a numerical study on Ag-water and Cu-water nanofluids is carried out to study the effects of temperature and viscosity on flow and heat transfer. Authors calculated numerically thermal conductivity using equation 3.15 and dynamic viscosity considering equation 3.4. In the paper, conductivity and viscosity data are used to numerically analyse the flow and the heat transfer characteristics. In order to make a comparison, conductivity and viscosity of nanofluids, measured in this chapter, were calculated using the same equations. Experimental conductivity and conductivity estimated by equation 3.15 are shown in Figures 12.3 and 12.4. For water-based nanofluid, maximum deviation is 5.6%, whereas for water-EG-based nanofluid, maximum deviation is 5.3%, both at 70°C. Dynamic viscosity experimental data were compared with data calculated by equation 3.4 obtaining a good agreement for water-based nanofluid (maximum deviation 2.8% at 50°C) and a maximum deviation of 4.6% at 20°C for water-EG-based nanofluid.

Other literature papers studied silver nanoparticles as bactericidal agent [6], as real-time optical sensors [7] and as heat transfer media in heat pipes [8], always finding good improvements in performances.

12.7 Conclusions

In this chapter, nanofluids with Ag nanoparticles were studied. Both water-based and water and glycol-based nanofluids result very stable nanofluids. For all nanofluids, conductivity increases with temperature. An interesting result was obtained from the measurement on water-based nanofluid at 0.0027 wt%, which conductivity grows up to 12.8% at 70°C, more than the enhancement of the nanofluid at 2.6 wt%, produced differently. This indicates that the presence of a dispersant or the different method of preparation leads to different nanofluids with different properties. For all nanofluids, dynamic viscosity was very similar to that of the base-fluid. Results of heat transfer coefficient measurements reveal that there is not an increase in heat transfer coefficient for these nanofluids at temperatures of 19°C, 31°C and 41°C. This is probably due to the presence of PVP, the polymer used as chemical additive to obtain a stable nanofluid, characterized by very low thermal conductivity. However, at higher temperatures, thermal conductivity enhancement is more evident and, therefore, it could be interesting to measure heat transfer coefficient at 60°C and 70°C. Some modifications to the experimental apparatus are under study to expand the temperature range.

References

[1] E.W. Lemmon, M.L. Huber, M.O. McLinden, NIST Standard Reference Database 23, Reference Fluid Thermodynamic and Transport Properties (REFPROP), version 9.0; National Institute of Standards and Technology (2010).

[2] Å. Melinder, "Properties of Secondary Working Fluids for Indirect Systems. Secondary Refrigerants or Coolants, Heat Transfer Fluids", International Institute of Refrigeration (IIR) (2010).

[3] A.Z. Dakroury, M.B.S. Osman, A.W.A. EI-Sharkawy, "Thermal Properties of Aqueous Solutions of Polyvinylpyrrolidone in the Temperature Range 20-80°C", *International Journal of Thermophysics*, 11, 3, 151-532 (1990).

[4] P. Sharma, I.H. Baek, T. Cho, S. Park, K. B. Lee, "Enhancement of thermal conductivity of ethylene glycol based silver nanofluids", *Powder Technology*, 208, 7–19 (2011).

[5] K. Vajravelu, "The effect of variable viscosity on the flow and heat transfer of a viscous Ag- water and Cu-water nanofluids", Journal of Hydrodynamics, 25, 1-9 (2013).

[6] P. Jain, T. Pradeep, "Potential of silver nanoparticle-coated polyurethane foam as an antibacterial water filter", *Biotechnol Bioeng*, 90, 59-63 (2005).

[7] A.D. McFarland, R.P.V. Duyne, "Single silver nanoparticles as real-time optical sensors with zeptomole sensitivity", *Nano Letters*, 3, 8, 1057-1062 (2003).

[8] L. G. Asirvatham, R. Nimmagadda, S. Wongwises, "Heat transfer performance of screen mesh wick heat pipes using silver–water nanofluid", *International Journal of Heat and Mass Transfer*, 60, 201–209 (2013).

Concluding remarks

Nanofluids were investigated as heat transfer media, considering the high thermal conductivity of solid nanoparticles compared to the inherently poor thermal properties of conventional heat transfer fluids.

An intensive research on the nanofluids behaviour and thermophysical properties was carried out at the Institute of Construction Technologies of the Italian National Research Council. Stability of nanofluids was investigated, and thermal conductivity, dynamic viscosity and convective heat transfer coefficient for promising nanofluids were measured.

- **Nanofluid preparation and stability characterization**

The considered base fluids were water, ethylene glycol (EG) and a mixture water-EG (70 wt% - 30 wt%). The tested nanoparticles are different and can be divided in four classes:

- Oxides (TiO_2, ZnO, Fe_2O_3, SiO_2): they have the lowest thermal conductivity between the considered materials, but they are not very expensive, generally safe in terms of environment and health, and can be dispersed even with the two-step method.
- Metals (Au, Ag): their thermal conductivity is much lower than that of carbon structures, but much higher than that of oxides. However, they are chemically unstable, as they tend to form oxides in contact with air. They are often produced with the single-step method.
- Single-wall carbon nanohorns (SWCNH): they have the highest thermal conductivity and, therefore, they are more promising in terms of heat transfer. However, they are expensive and difficult to produce on a large scale.
- Ceramic material: silicon carbide (SiC) is characterized by high thermal conductivity, but it is expensive and has very high hardness.

Some of the studied nanofluids are commercial fluids and others are non-commercial (prepared by IENI-CNR Padova and ISTEC-CNR Faenza Laboratories).

The stability of nanofluids is a characteristic very difficult to obtain. Because of their high surface energy, the nanoparticles tend to aggregate and to settle, making the nanofluid unstable. To test the average size of the nanoparticles in suspension and ζ potential of the nanofluid, an instrument based on the Dynamic Light Scattering technique was used. Most of

the studied nanofluids reveal the absence of aggregation phenomena and a partial settling of nanoparticles, which return in suspension when simply stirred.

It is important to note that only stable nanofluids should be considered for the measurement of thermophysical properties.

Moreover, in order to avoid particle aggregation, chemical additives (surfactants, tensioactives) are used and often they are crucial. These substances, distributing around the nanoparticle, neutralize the surface reactivity, but also change the thermophysical properties. For this reason, the choice of the proper stabilizer is essential and the amount of additive must be controlled.

- **Thermal conductivity**

A TPS 2500 S was used for thermal conductivity measurements. The instrument is based on the hot disk technique and can measure thermal conductivity and thermal diffusivity of several materials. To test the instrument and to evaluate its accuracy, preliminary tests were executed on a well-known fluid, *i.e.* water.

Thermal conductivity of nanofluids is generally higher than that of the base fluid, although it is very influenced by the presence of surfactants, which are often polymers. If the additive concentration is high, it could penalize the thermal conductivity enhancement. For example, thermal conductivity of the commercial nanofluid made by ZnO nanoparticles in water, at a mass fraction of 1%, was found to be lower or almost similar to that of water, probably due to the presence of dispersant in the solution. At 5 wt% and 10 wt%, however, thermal conductivity value rises as a function of temperature. For the nanofluid at 10 wt%, it increases up to 13.6% at 70°C.

Additionally, the thermal conductivity of water-Ag nanofluid at 2.6 wt% was measured from 10°C to 70°C. The conductivity increases with temperature, being lower than that of water at 10°C and growing up to 6.5% at 70°C.

It is worth noting a good result has been found with Au-water nanofluid. Au is a very expensive material, but this nanofluid could also be considered for industrial application if the nanofluid is stable and very little quantity of gold are sufficient to have energy efficiency improvements. Thermal conductivity of this nanofluid at 0.02 wt% reaches the maximum value at 70°C, increasing of 21% respect to water. This is a surprising result considering the low nanoparticles concentration.

In general, thermal conductivity enhances with nanoparticle concentration, mostly if there is no surfactants or if their concentrations is very limited. For water-based nanofluids, the enhancement is often more than proportional to the particle concentration. Thermal

conductivity increases also with temperature, reaching the maximum value at 70°C, the maximum measurement temperature at these experimental conditions.

- **Dynamic viscosity**

Dynamic viscosity measurements were performed to verify the influence of nanoparticles on the physical properties of the base fluid. The dynamic viscosity was measured using a rotational rheometer (AR-G2, TA Instruments). Tests were executed on water, a well-known fluid, to evaluate the accuracy of these measurements. It results lower than 1.5% in a temperature range between 10°C and 70°C.

Nanofluids with enhanced thermal properties can be applied in flow devices only if their dynamic viscosity is not excessively high. In fact, high viscosity penalizes the flow and the pressure drop.

In general, for all measured nanofluids, it was observed that:

- with nanoparticles concentrations less than 1 wt%, the variation of viscosity with respect to the base fluid is negligible;
- viscosity decreases with increasing temperature, with the same trend for all the concentrations for a nanofluid and its base fluid;
- as concentration increases, the viscosity increases, but independently from temperature.

Several suspensions were studied and significant enhancements on dynamic viscosity were found for SWCNT-water, SiC-EG, TiO_2-water, SiO_2-water, Fe_2O_3-water, ZnO-water nanofluids respect to the base fluid, at the higher weight concentrations here studied.

Metal-water nanofluids were measured at low concentrations and their viscosity resulted very close to that of water at temperatures between 10°C and 70°C.

For the nanofluids here considered, rheological behaviour was always Newtonian except for SiC-GE nanofluids at 5 wt%, which seems to present a shear-thinning behaviour.

- **Heat transfer coefficient**

With the aim to understand the heat transfer capability of nanofluid, an apparatus for convective heat transfer measurements was built. Before measuring nanofluids, preliminary tests using pure water as reference fluid were made in order to verify the accuracy of the measurements and to achieve the value of heat transfer coefficient of water for the subsequent comparison between water-based nanofluid and the base fluid. All the measurements were performed in a heat flow rate range from 200 to 600 W and the thermal balance was always within 4%.

Experimental thermal conductivity and dynamic viscosity data were used to calculate the convective heat transfer coefficient. Nanofluid density ρ_{nf} and nanofluid heat capacity $c_{p,nf}$ were calculated as weighted averages.

The heat transfer coefficient of the nanofluid composed of ZnO in water, in concentration of 5 wt% and 10 wt%, did not reveal an increase of the coefficient in a temperature range between 19°C and 40°C. Also for nanofluids with SiC nanoparticles dispersed in ethylene glycol at concentration of 0.1 wt% and 1 wt% there was not an increase of the heat transfer coefficient at temperatures of 32°C and 50°C. The same result was obtained for the nanofluid with Ag nanoparticles dispersed in water at a concentration of 2.6 wt% and for the nanofluid with Ag nanoparticles dispersed in water and ethylene glycol at a concentration of 2.5 wt% and temperatures of 19°C, 31°C and 41°C.

On the contrary, heat transfer coefficient measurements on Au-water nanofluid at 0.02 wt% at Re ranging from 4000 to 17000, revealed different behaviour. The fluid showed an enhancement, compared with pure water, up to approximately 5-6% in the temperature range between 19°C and 41°C. Considering the strong dependence of thermal conductivity enhancements on temperature, obtaining small heat transfer enhancements within this range of temperatures promises much higher improvements at higher temperatures. In the future, heat transfer measurements at higher temperatures will be performed. Moreover, the production of stable nanofluids at higher metal nanoparticles concentration is ongoing.

- **In conclusions**

Despite an exponential increase in recent years of theoretical and experimental analyses on nanofluids, further studies are needed to fully understand their behaviour. Literature data are often controversial and nanofluids with a good stability are very difficult to obtain. In fact, an important issue is the production of stable and safe nanofluids, through the development of the most suitable methods of production, possibly on large-scale. Thermal conductivity, dynamic viscosity and heat transfer coefficient experimental data, obtained in various laboratories, are still scarce and often inconsistent. The study of the influence of size, shape, concentration and nanoparticles material, both from the experimental and theoretical point of view, must be deepened. Nanofluids are so complex that it seems to be necessary that they have to be tailor-made to be successful. However, they are also very promising for several technical applications. Nanofluids can be used as heat transfer fluids in high heat flux systems such as electronic cooling systems, chillers, solar applications and heat pipes.

Therefore, each contribute on properties measurement, heat transfer applications characterization, or theoretical analysis is very important, especially at this stage of research, in which many questions must to be solved.

List of publications

Part of the results presented in this thesis has been published on international journals or conference proceedings.

- F. Agresti, S. Barison, S. Battiston, C. Pagura, L. Colla, L. Fedele, M. Fabrizio, "Tuning the thermal diffusivity of silver-based nanofluids by controlling nanoparticle aggregation", *Nanotechnology*, 2013 Sep 13;24(36):365601. doi: 10.1088/0957-4484/24/36/365601.
- L. Colla, L. Fedele, M. Scattolini, S. Bobbo, "Water-based Fe_2O_3 nanofluid characterization. Thermal conductivity and viscosity measurements and correlation", *Advances in Mechanical Engineering*, art. no. 674947 (2012).
- L. Fedele, L. Colla, S. Bobbo, "Viscosity and Thermal Conductivity Measurements of Water-Based Nanofluids Containing Titanium Oxide Nanoparticles", *International Journal of Refrigeration*, 35, 5, 1359-366 (2012).
- S. Bobbo, L. Fedele, A. Benetti, L. Colla, M. Fabrizio, C. Pagura, S. Barison, "Viscosity of water based SWCNH and TiO_2 nanofluids", *Experimental Thermal and Fluid Science*, 36, 65-71 (2012).
- L. Fedele, L. Colla, S. Bobbo, S. Barison, F. Agresti, "Experimental stability analysis of different water-based nanofluids", *Nanoscale Research Letters*, 6, 300 (2011).
- L. Colla, "Investigation on thermophysical properties of nanofluids", published on the proceedings of "*Convegno annuale dell'A.I.P.T.*", Bologna (2013).
- S. Bobbo, L. Colla, M. Securo, L. Fedele, "The potential HVAC&R applications of nanofluids" presented to "15th European Conference IIR-United Nations UNEP - ATF – CSG on the Latest technologies in refrigeration and air conditioning", Milano, Italy (2013).
- L. Colla, M. Blosi, M. Scattolini, S. Bobbo, L. Fedele, "Investigation on stability and properties of water−based gold nanofluids", published on the proceedings of "*Fourth IIR Conference on Thermophysical Properties and Transfer Processes of Refrigerants*", June 17-19, 2013 Delft, The Netherlands, Paper No. TP-042.
- F. Agresti, S. Barison, S. Battiston, C. Pagura, L. Colla, L. Fedele, M. Fabrizio, "Influence of molecular weight of PVP on aggregation and thermal diffusivity of silver-based nanofluids", published on the proceedings of "Nanotech Conference&Expo 2013", 2013, Washington, DC (USA).
- S. Bobbo, L. Colla, M. Scattolini, L. Fedele, "Study on the heat transfer capability of silicon carbide - Ethylene glycol nanofluid", published on the proceedings of "2012 NSTI Nanotechnology Conference and Expo", NSTI-Nanotech 2012 , pp. 345-348.
- S. Bobbo, L. Colla, L. Fedele, M. Scattolini, "Characterization of the Heat Transfer Potentiality of Water-Based ZnO Nanofluids", published on the proceedings of "*Eighteenth Symposium on Thermophysical Properties*", Boulder, CO, USA, 2012.
- S. Barison, F. Agresti, S. Bobbo, L. Colla, L. Fedele, L. Mercatelli, E. Sani, C. Pagura, M. Fabrizio, "Nanofluids as Energy Vectors: Synthesis Methods, Stability and Functional Characterization", poster at TICME - 2011 "Trento Innovation Conferences On Materials Engineering - 2nd Meeting: Advances in Materials for Energy and Environment", 2011, Trento.

- S. Bobbo, L. Colla, M. Scattolini, F. Agresti, S. Barison, C. Pagura, L. Fedele, "Thermal Conductivity and Viscosity Measurements of Water-Based Silica Nanofluids", published on the proceedings of "Nanotechnology Conference&Expo" NSTI-Nanotech, 2011, Boston, MA (USA), 2011, 2 , pp. 478-481.
- S. Bobbo, L. Colla, L. Fedele, "Nanofluids: a new generation of high efficiency fluids", presentato al "14th European Conference IIR-United Nations UNEP - ATF – CSG on Technological Innovations in Refrigeration and in Air Conditioning", 2011, Milano, Italy.

Summary

Nanofluids are formed by solid particles with nano-sized dimension (1-200 nm) dispersed into common fluids. From the beginning, they have been proposed as heat transfer media, considering the high thermal conductivity of solid nanoparticles compared to the inherently poor thermal properties of conventional heat transfer fluids. In the last years, an exponential increase of publications on nanofluids is occurred. However, nanofluids are complex fluids, literature experimental works are often controversial and theoretical investigations must to be deepened. A big issue concerns the production of stable and reliable fluids, since different nanoparticles can be prepared with different methods and, also, different nanofluids derive from different preparation techniques.

In this work, several nanofluids were analysed. The stability of the suspension was evaluated considering the mean size distribution of nanoparticles in suspension using the DLS technique. In addition, the ζ potential and the pH of the nanofluids were measured for the stability analysis. For stable nanofluids, the study of the thermophysical properties is necessary to understand their energy behaviour. Therefore, thermal conductivity was measured by means of the hot disk technique in a temperature range generally between 10°C and 70°C. However, nanofluids can be actually applied in technological systems only if the addition of nanoparticles does not determine a significant viscosity enhancement. For this reason, dynamic viscosity was determined experimentally, using a rotational rheometer. All the measurements were performed at constant temperature and variable shear rate, generally starting from 80 1/s to 1200 1/s, at constant step of about 124 1/s, in a temperature range generally between 10°C and 70°C. Other nanofluids properties, density and heat capacity, are calculated from weighted averages.

The final objective of this work is to investigate the convective heat transfer capabilities of nanofluids. For this purpose, an experimental apparatus was built in order to measure the convective, single phase heat transfer coefficient of nanofluids, at constant wall heat flux. A constant heat flux condition was imposed through the wall of a straight copper tube in which the measured fluid flows. Heated test section is 2 meter long, inner diameter measures 8 mm and the heat flux is generated by heating electrical resistance wires winded continuously around the pipe. At the inlet and outlet of the measurement section 2 Platinum resistance

thermometers (Pt100) measure fluid bulk temperatures. 32 thermocouples measure the wall temperature along the heated pipe. They are inserted into cavities, which are dug in the tube wall thickness to enable the sensors to be as close as possible to the internal pipe surface. Other components are a gear pump, a Coriolis mass flow meter and a chiller. The circuit was tested with water in order to verify the operation using a fluid of known properties. Results confirm that the circuit is suitable for heat transfer coefficient measurements.

In this thesis, nine nanofluids have been considered.

Water-based nanofluid containing TiO_2 nanoparticles was studied at four different nanoparticle concentrations (1 wt%, 10 wt%, 20 wt% and 35 wt%). All the fluids resulted quite stable, even after 30 days, in a static situation and completely stable after sonication for one hour. The average particle diameter was 76 nm and no aggregations were found. The measured thermal conductivity increases with mass concentration and with temperature. The effect of increasing conductivity is more evident at higher temperatures. All the nanofluids exhibited a Newtonian rheological behaviour. The viscosity enhancement, related to pure water, was independent from temperature for all the concentrations here analysed. The nanofluid at 1 wt% shows a water like behaviour and a variation, with respect to water, within the experimental error, but at the higher concentrations the viscosity enhancement is not proportional and surprisingly excessive (+243% for 35 wt% at 70°C).

Nanofluids based on water and SWCNH, with the addition of SDS as dispersant, were studied at different concentrations, *i.e.* 0.01%, 0.1%, 1% by mass. Nanofluids showed a good stability and a Newtonian behaviour at each composition. Negligible variations on the viscosity of the nanofluids in relation to water are observed at nanoparticles concentrations up to 0.1 wt%. On the contrary, a significant increase is measured for nanoparticles concentration of 1 wt%. Part of this increment is due to the addition of the dispersants. Few theoretical models were applied to predict the experimental data, but they were found able to represent only nanofluids with nanoparticle concentrations lower than 1% wt. Then, a new correlation was proposed to represent the experimental data for the SWCNH/water nanofluids. Moreover, thermal conductivity was measured for the nanofluid at 0.1 wt% and the nanofluid behaviour was very similar to that of water, probably due to the presence of SDS.

Stability, viscosity and thermal conductivity for nanofluids formed by water and SiO_2 nanoparticles with concentration from 1% to 54% by mass were measured. Nanofluids were stable and the thermal conductivity, at ambient temperature for the nanofluid at 54 wt%, was compared with a benchmark study result, finding a good agreement. Thermal conductivity clearly enhances with reference to water, but only at the higher concentrations with a weak

dependence on temperature. At the same time, viscosity increases even more significantly and, for this reason, water-based nanofluids with silica nanoparticles should not be suitable for thermal applications.

Another interesting water-based nanofluid, with Fe_2O_3 nanoparticles, was investigated, at a mass concentration ranging between 5 and 20%. It has long time stability, also at high concentration as 20 wt%. Thermal conductivity increases with mass fraction and with temperature. Thermal conductivity ratio is greater at the highest concentrations. The rheological behaviour of the nanofluids is Newtonian and the dynamic viscosity increases considerably in respect of water, mainly at mass fraction of 20%. Therefore, the increment in thermal conductivity is combined with a rising in dynamic viscosity. For this reason, Fe_2O_3 water-based nanofluid, studied in this work, is not energetically convenient for technical applications.

ZnO-water nanofluid was studied at 1, 5, 10 wt%, resulting very stable during the analysis lasting for one month. Thermal conductivity is similar to that of water at the lower concentration, while for nanofluids at 5 wt% and 10 wt% there are enhancements of 12% and 15% at 70°C, respectively. The dynamic viscosity of the nanofluids at 1 wt% is very similar to water viscosity, while it increases of about 5% for the nanofluid at 5 wt% and 12% for the nanofluid at 10 wt%. The nanofluids heat transfer coefficient at 5 wt% and 10 wt% was measured. Results do not show an increase on the heat transfer coefficient for these suspensions.

Ethylene glycol-based nanofluids, containing silicon carbide in the concentrations 0.1, 1 and 5 wt%, were characterized. Ethylene glycol can be used as a heat-transfer fluid in heat transfer applications with maximum operating temperatures higher than water boiling temperature or minimum operating temperatures lower than water freezing temperature. Silicon carbide is characterized by high thermal conductivity, *i.e*. 490 W/mK, and it is supposed to enhance the thermal properties of ethylene glycol more than other common materials, such as metal oxides. Experimental results indicate that thermal conductivity enhancement is relatively high at all the concentrations and is increasing with temperature up to more than 20% for the 5 wt% nanofluid. The viscosity enhancement is negligible at concentrations up to 1 wt%. Vice versa, it is quite significant for the 5 wt% nanofluid, with a strong increase at temperatures higher than 50°C, suggesting aggregation of the nanoparticles. The results of heat transfer measurements indicate EG-SiC nanofluids here studied are not promising as heat transfer media.

Stability, dynamic viscosity, thermal conductivity and heat transfer coefficient for nanofluids formed by water and Au nanoparticles were studied at 0.02 wt%, 0.05 wt% and

0.1 wt%. Fluids were prepared with a one-step "eco-friendly" method. The thermal conductivity of the nanofluid at 0.02 wt% showed significant enhancement (up to 21%) compared to water. The nanofluid at 0.1 wt% was completely unstable and also the nanofluid at 0.05 wt% was too unstable during the measurement. The dynamic viscosity of the nanofluids was found to be very similar to water, thus not penalizing flow performance. The heat transfer coefficient of the nanofluid at 0.02 wt% shows an enhancement, compared with pure water, up to approximately 5-6% in the temperature range between 19°C and 41°C. This is a promising result and it will be interesting, for future works, to optimize a chemical synthesis able to produce nanofluids with higher nanoparticles concentration. In fact, increasing the amount of nanoparticles, thermophysical properties could be improved and nanofluids could result promising for many industrial applications.

Finally, two different nanofluids containing silver nanoparticles were analysed. The first one is water-based, composed of 2.6 wt% and 0.0027 wt% of Ag nanoparticles and the second one is 2.5 wt% Ag nanoparticles in a mixture water-ethylene glycol at a mass fraction (70:30). All nanofluids were very stable and, for all nanofluids, conductivity increases with temperature. An interesting result was obtained from the measurement on water-based nanofluid at 0.0027 wt%, which conductivity grows up to 12.8% at 70°C, more than the enhancement of the nanofluid at 2.6 wt%, produced differently. This indicates that the presence of a dispersant or the different method of preparation leads to different nanofluids with different properties. For all nanofluids, dynamic viscosity was very similar to that of the base-fluid. Results of heat transfer coefficient measurements reveal that there is not an increase in heat transfer coefficient for these nanofluids at temperatures of 19°C, 31°C and 41°C. This is probably due to the presence of PVP, the polymer used as chemical additive to obtain a stable nanofluid, characterized by very low thermal conductivity. However, at higher temperatures, thermal conductivity enhancement is more evident and it could be interesting to measure heat transfer coefficient at 60°C and 70°C, therefore, some modifications to the experimental apparatus are under study.

In conclusion, after an intense work of experimental measurement on several nanofluids, a nanofluid with extraordinary thermophysical properties was not found, in spite of some results published in the literature. However, nanofluids are really complex and it seems they should be tailor-made to be successful. It is worth noting that, at this stage, literature on nanofluids is really inconsistent, giving different and opposite results and many questions on nanofluids must be solved. For this reason, each contribute on properties measurement or theoretical analysis is very important.

Starting from the present results, future works will be done on the experimental apparatus for the heat transfer coefficient measurement to increase the temperature range, to study nanofluids for high temperature applications.

Moreover, amongst all the studied suspensions, it seems metal nanoparticles are the most promising. More concentrated nanofluids, with the proper surfactants, are under study.

Riassunto

I nanofluidi sono costituiti da particelle solide di dimensione nanometrica (1-200 nm) disperse all'interno di fluidi comuni. Considerata l'elevata conduttività termica delle nanoparticelle solide rispetto alle proprietà termiche intrinsecamente scarse dei fluidi convenzionalmente usati per lo scambio termico, i nanofluidi sono stati inizialmente proposti come fluidi termovettori caratterizzati da interessanti proprietà termiche. Negli ultimi anni, il numero di pubblicazioni sui nanofluidi ha avuto una crescita esponenziale. Tuttavia, i nanofluidi sono fluidi complessi e i lavori sperimentali che si trovano in letteratura presentano spesso risultati tra loro discordanti e imprecisi, non supportati da valutazioni teoriche che devono essere approfondite. Uno dei principali problemi riguarda la produzione di sospensioni stabili, affidabili e riproducibili. Infatti, pur partendo da fluidi base e nanoparticelle dello stesso tipo, differenti metodi di preparazione possono portare a nanofluidi diversi e, quindi, con caratteristiche differenti.

In questo lavoro, sono stati presi in considerazione diversi nanofluidi, in acqua o glicole e con nanoparticelle di ossidi, metalli o carbonio, per valutare le possibili differenze tra i fluidi risultanti. Ogni fluido è stato attentamente caratterizzato.

Per ogni nanofluido, la stabilità della sospensione è stata valutata considerando la distribuzione della dimensione media delle nanoparticelle in sospensione, utilizzando la tecnica DLS (*Dynamic Light Scattering*). Inoltre, per l'analisi di stabilità, sono stati misurati anche il potenziale ζ ed il pH dei nanofluidi.

Per i nanofluidi che sono risultati stabili, si è proceduti con lo studio delle proprietà termofisiche, necessario per comprendere il loro potenziale impiego energeticamente favorevole in applicazioni specifiche. Per questo motivo, prima è stata misurata la conduttività termica, utilizzando la tecnica *hot disk* in un intervallo di temperatura in genere compresa tra 10°C e 70°C. Tuttavia, è importante considerare che i nanofluidi possono essere effettivamente utilizzati negli impianti solo se l'aggiunta di nanoparticelle non determina un significativo aumento della viscosità. Pertanto, la viscosità dinamica dei nanofluidi considerati è stata determinata sperimentalmente, utilizzando un reometro rotazionale. Tutte le misure sono state eseguite a temperatura costante e *shear rate* variabile, generalmente tra 80 1/s e 1200 1/s, a passo costante di circa 124 1/s, in un intervallo di

temperatura in genere compresa tra 10°C e 70°C. Altre proprietà dei nanofluidi, come densità e calore specifico, sono state calcolate come medie pesate considerando la composizione di nanoparticelle.

L'obiettivo finale di questo lavoro è stato quello di indagare le capacità di scambio termico convettivo dei nanofluidi. A questo scopo, è stato costruito un apparato sperimentale per misurare il coefficiente di scambio termico monofase convettivo, in condizione di flusso termico di parete costante. La parte principale dell'apparato è costituito da un tubo di rame, in cui viene fatto scorrere il fluido considerato, a cui viene imposto un flusso termico costante. La sezione di misura riscaldata ha una lunghezza di 2 m e diametro interno di 8 mm. Il flusso termico è generato da resistenze elettriche avvolte con continuità attorno al tubo. 2 termoresistenze al platino (Pt100) misurano la temperatura del fluido all'ingresso e all'uscita della sezione di misura, mentre 32 termocoppie misurano la temperatura di parete lungo il tubo riscaldato. Le termocoppie sono inserite all'interno di cavità, scavate nello spessore del tubo, per consentire ai sensori di essere il più vicino possibile alla superficie interna del tubo. Gli altri componenti sono una pompa ad ingranaggi, un misuratore di portata ad effetto Coriolis ed un *chiller*. Il circuito è stato testato con acqua, al fine di verificarne il funzionamento utilizzando un fluido di proprietà note e i risultati confermano che il circuito è idoneo a misure di coefficiente di scambio termico.

In questa tesi, sono stati considerati nove nanofluidi.

Il nanofluido a base d'acqua, contenente nanoparticelle di TiO_2, è stato studiato a quattro diverse concentrazioni di nanoparticelle (1%, 10%, 20% e 35% in massa). Tutti i fluidi sono risultati abbastanza stabili, anche dopo 30 giorni, quando non agitati, e completamente stabili dopo un'ora di sonicazione. Il diametro medio delle particelle è 76 nm e non si sono formati aggregati. La conduttività termica misurata aumenta all'aumentare della frazione di nanoparticelle e della temperatura. Tale aumento è più evidente alle temperature più elevate. Tutti i nanofluidi mostrato un comportamento reologico Newtoniano. L'aumento di viscosità, rispetto all'acqua pura, è indipendente dalla temperatura per tutte le concentrazioni qui analizzate. Il nanofluido all'1% in massa ha una viscosità molto simile a quella dell'acqua, essendo la variazione all'interno dell'errore sperimentale. Tuttavia, a concentrazioni più alte l'aumento di viscosità non risulta proporzionale, ma sorprendentemente eccessivo (+243% al 35% in massa a 70°C).

Il nanofluido a base di acqua e SWCNH, con l'aggiunta di SDS come disperdente, è stato studiato a diverse concentrazioni, 0.01%, 0.1%, 1% in massa. Tali nanofluidi mostrato una buona stabilità ed un comportamento Newtoniano ad ogni composizione. Sono state osservate variazioni trascurabili della viscosità dei nanofluidi rispetto all'acqua per

concentrazioni di nanoparticelle fino allo 0.1% in massa. Al contrario, è stato misurato un aumento significativo di viscosità per la concentrazione di nanoparticelle 1% in massa. Parte di questo incremento è dovuto all'aggiunta del disperdente. Inoltre, sono stati applicati alcuni modelli teorici per prevedere i valori sperimentali, risultando rappresentativi solo per i nanofluidi con concentrazioni di nanoparticelle inferiori all'1% in massa. Quindi, è stata proposta una nuova correlazione, adatta a rappresentare i dati sperimentali per i nanofluidi formati da SWCNH e acqua. In seguito, è stata misurata la conduttività termica del il nanofluido allo 0.1% in massa ed il comportamento è risultato molto simile a quello del fluido base, probabilmente a causa della presenza di SDS.

Per nanofluidi formati da acqua e nanoparticelle SiO_2 in concentrazione da 1% a 54% in massa, sono state misurate la stabilità, la viscosità dinamica e la conduttività termica. Queste sospensioni sono risultate stabili fino a concentrazioni del 27% in massa (purtroppo, non è stato possibile analizzare al DLS il nanofluido al 54%). La conduttività termica del nanofluido al 54% in massa, a temperatura ambiente, è stata confrontata con il risultato fornito da uno studio di riferimento, ottenendo un ottimo accordo, entro lo 0.1%. Per tutte le concentrazioni, la conduttività termica è stata misurata a diverse temperature, osservando, alle concentrazioni più elevate, un chiaro incremento rispetto all'acqua, con una debole dipendenza dalla temperatura. Allo stesso tempo, però, la viscosità aumenta molto più significativamente con la concentrazione, rendendo i nanofluidi SiO_2-acqua poco adatti per le applicazioni termiche.

Un altro interessante nanofluido a base d'acqua, con nanoparticelle di Fe_2O_3, è stato studiato ad una concentrazione in massa compresa tra 5 e 20%. La stabilità è risultata buona per lungo tempo, anche alla concentrazione più elevata. La conduttività termica aumenta con la frazione di massa e con la temperatura ed il rapporto della conduttività rispetto a quella dell'acqua è maggiore alle concentrazioni più elevate. Il comportamento reologico dei nanofluidi è Newtoniano e gli aumenti di viscosità dinamica rispetto al fluido base, sono notevoli, soprattutto a frazioni di massa del 20%. È evidente, quindi, che l'incremento della conduttività termica è associato ad un aumento della viscosità dinamica. Per questo motivo, l'applicazione energeticamente favorevole del fluido deve essere attentamente valutata con riferimento alla particolare applicazione.

Il nanofluido ZnO-acqua è stato studiato a concentrazioni di 1, 5, 10% in massa, risultando molto stabile durante l'analisi al DLS, per la durata di un mese. La conduttività termica del nanofluido alla concentrazione più bassa è simile a quella dell'acqua, mentre per nanofluidi al 5% e 10% in massa, sono stati misurati incrementi del 12% e del 15% a 70°C, rispettivamente. La viscosità dinamica del nanofluido all'1% in massa è molto simile alla

viscosità del fluido base, mentre aumenta di circa il 5% per la nanofluido al 5% in massa e del 12% per il nanofluido al 10% in massa. Inoltre, per i nanofluidi al 5% e 10% in massa, è stato misurato il coefficiente di scambio termico, senza averne osservato alcun incremento.

Sono stati, inoltre, caratterizzati nanofluidi a base di glicole etilenico, contenenti carburo di silicio alle concentrazioni di 0.1, 1 e 5% in massa. Il glicole etilenico può essere utilizzato come fluido termovettore in applicazioni di scambio termico, con temperature massime superiori alla temperatura di ebollizione dell'acqua o minime inferiori alla temperatura di solidificazione dell'acqua. Il carburo di silicio è caratterizzato da elevata conduttività termica, 490 W/mK, e si suppone che consenta di migliorare le proprietà termiche del glicole etilenico più di altri materiali comuni, come gli ossidi metallici. I risultati sperimentali indicano che l'incremento di conduttività termica è relativamente elevato a tutte le concentrazioni e che aumenta con la temperatura, fino a oltre il 20% per il nanofluido al 5% in massa. L'aumento di viscosità è risultato trascurabile o negativo per concentrazioni fino a 1% in massa. Viceversa, è risultato abbastanza significativo per la nanofluido al 5% in massa, con un forte incremento a temperature superiori a 50°C, suggerendo che possa essersi verificata un'aggregazione delle nanoparticelle. I risultati delle misure di coefficiente di scambio termico indicano che i nanofluidi EG-SiC, qui studiati, non sono promettenti come sostitutivi termovettori.

Sono state studiate la stabilità, la viscosità dinamica, la conduttività termica ed il coefficiente di scambio termico dei nanofluidi composti da acqua e nanoparticelle di oro alle concentrazioni 0.02, 0.05 e 0.1% in massa. I fluidi sono stati preparati con un metodo *eco-friendly* a *single-step*. La conduttività termica del nanofluido allo 0.02% ha mostrato un incremento significativo (fino al 21%), rispetto all'acqua. Il nanofluido allo 0.1% è risultato completamente instabile ed anche il nanofluido allo 0.05% è risultato visivamente instabile durante la misura. La viscosità dinamica dei nanofluidi è risultata essere molto simile a quella del fluido base, quindi non penalizzante le prestazioni di flusso. Il coefficiente di scambio termico del nanofluido allo 0.02% ha mostrato un incremento rispetto all'acqua pura, fino a circa 5-6% nell'intervallo di temperatura tra 19°C e 41°C. Questo risultato sembra promettente e sarà interessante, per lavori futuri, ottimizzare una sintesi chimica in grado di produrre nanofluidi con concentrazione di nanoparticelle di oro superiore. Infatti, aumentando la quantità di nanoparticelle, le proprietà termofisiche potrebbero migliorare ed i nanofluidi potrebbero risultare adatti per molte applicazioni industriali.

Infine, sono stati analizzati due diversi nanofluidi contenenti nanoparticelle di argento (Ag). Il primo è a base di acqua, composto da 2.6% e 0.0027% in massa di nanoparticelle di Ag, mentre il secondo è formato da 2.5% in massa di nanoparticelle di Ag in una miscela di

acqua e glicole etilenico ad una frazione di massa (70:30). Tutti i nanofluidi sono risultati molto stabili e, per tutti nanofluidi, la conduttività aumenta con la temperatura. Un risultato interessante è stato ottenuto dalla misura di un nanofluido a base di acqua, allo 0.0027% in massa, la cui conduttività cresce fino al 12.8% a 70°C, aumento più elevato di quello ottenuto dal nanofluido al 2.6% in massa, prodotto in modo diverso. Questo indica che la presenza di un disperdente o il diverso metodo di preparazione porta a nanofluidi differenti, con proprietà differenti. Per tutti i nanofluidi, la viscosità dinamica è risultata molto simile a quella del fluido base. I risultati delle misure del coefficiente di scambio termico indicano che non vi è un aumento nel coefficiente per questi nanofluidi alle temperature di 19°C, 31°C e 41°C. La causa principale è probabilmente la presenza del PVP, il polimero usato come additivo chimico per ottenere un nanofluido stabile, il quale è caratterizzato da bassa conduttività termica. Tuttavia, potrebbe essere interessante misurare il coefficiente di scambio termico a 60°C e 70°C, temperature alle quali l'aumento di conduttività termica è più evidente. Alcune modifiche dell'apparato sperimentale sono in fase di studio, per ampliare l'intervallo di temperatura misurabile che attualmente si ferma a 50°C.

In conclusione, dopo un intenso lavoro di misura sperimentale su più nanofluidi, non è stato trovato alcun nanofluido con straordinarie proprietà termofisiche, nonostante alcuni risultati pubblicati in letteratura che avevano posto le basi iniziali per questa tesi. Tuttavia, i nanofluidi sono fluidi molto complessi e, dai risultati ottenuti, è evidente che si debba portare molta attenzione alla loro preparazione affinché risultino stabili e con proprietà interessanti. È necessario notare, inoltre, che in questa fase la letteratura sui nanofluidi è particolarmente discordante e incompleta, poiché fornisce risultati diversi e opposti, e che molte questioni teoriche alla base del comportamento termofisico dei nanofluidi devono essere ancora risolte. Per questo motivo, ogni contributo scientifico alle misure di proprietà o alle analisi teoriche è molto importante.

Partendo dai risultati attuali, in futuro saranno apportate modifiche all'apparato sperimentale per la misura coefficiente di scambio termico, allo scopo di aumentare l'intervallo di temperatura misurabile, per studiare nanofluidi adatti ad applicazioni ad alta temperatura.

Inoltre, tra tutte le sospensioni studiate, quelle con nanoparticelle metalliche sembrano le più promettenti. Per questo motivo, nanofluidi più concentrati, con surfattanti adatti, sono in fase di studio.

Ringraziamenti

Non avrei potuto svolgere questo lavoro senza l'aiuto di molte persone. Desidero quindi ringraziare il mio supervisore, il Professor Claudio Zilio per i preziosi suggerimenti che spesso hanno migliorato la mia ricerca e gli amici dello IENI e dell'ISTEC, Simona, Filippo e Magda per aver preparato i nanofluidi.

Questo periodo di dottorato è stato per me particolarmente formativo, professionalmente ma anche umanamente, e per questo i miei ringraziamenti vanno a Mauro, Sergio e Laura, con i quali è sempre un piacere lavorare.

La professionalità e l'aiuto costante di Mauro sono stati molte volte fondamentali per il proseguimento della mia attività. Sono grata a Sergio per avermi permesso di partecipare a questo progetto e per il suo supporto scientifico.

In particolare, desidero ringraziare Laura, con la quale ho condiviso molti momenti e che per me è un punto di riferimento molto importante. A lei va il mio "grazie" per avermi sempre seguita, guidata, incoraggiata e per aver creduto in me, durante tutto il periodo del dottorato e della stesura della tesi.

Infine, ringrazio Marco, che è sempre al mio fianco.